Synchronization in Networks of Bistable Systems

A thesis
submitted by

Pranay Deep Rungta

in partial fulfillment of
the requirements for the degree of
Doctor of Philosophy

Indian Institute of Science Education and Research (IISER) Mohali

March 2018

Certificate of Examination

This is to certify that the dissertation titled *Synchronization in Networks of Bistable Systems* submitted by **Mr. Pranay Deep Rungta** (Reg. No. PH15021) for the partial fulfillment of Doctor of Philosophy programme of the Institute, has been examined by the thesis committee duly appointed by the Institute. The committee finds the work done by the candidate satisfactory and recommends that the report be accepted.

Dr. Kamal P. Singh Dr. Rajeev Kapri Professor Sudeshna Sinha

(Supervisor)

Declaration

The work presented in this dissertation has been carried out by me under the guidance of Prof. Sudeshna Sinha at the Indian Institute of Science Education and Research Mohali.

This work has not been submitted in part or in full for a degree, a diploma, or a fellowship to any other university or institute. Whenever contributions of others are involved, every effort is made to indicate this clearly, with due acknowledgment of collaborative research and discussions. This thesis is a bona-fide record of original work done by me and all sources listed within have been detailed in the bibliography.

Pranay Deep Rungta

(Candidate)

In my capacity as the supervisor of the candidate's doctoral thesis, I certify that the above statements by the candidate are true to the best of my knowledge.

Professor Sudeshna Sinha

(Supervisor)

Acknowledgements

"No duty is more urgent than that of returning thanks"

James Allen

I have been lucky to have my PhD guide as Prof Sudeshna Sinha who have always encouraged me and guided me in every step of research work at Indian Institute of Science Education and Research, Mohali. Her approach towards every problem has been a great source of motivation for me. I will always be very grateful to her for this.

I am thankful to my doctoral committee members, Dr. Rajeev Kapri and Dr. Kamal P. Singh for helping me throughout the PhD and for sharing their invaluable time and knowledge.

I am deeply thankful to my dear friends and collaborators: Chandrakala Meena, Anshul Choudhary, Manoj, Promit, Sudhanshu, Archana, Karishma, Hema, Harshita, Manisha, Tj, Ashish, Sandeep, Haseeb for the moral support and for making life at IISER lively and happy going.

Finally, I would like to thank Shweta and my parents for always believing in me and making my journey a really smooth ride. I express my thanks to one and all who have contributed to the completion of my Ph.D.

Above all, my deepest gratitude to Almighty for his mercies and blessings.

Preface

The central focus of this thesis is the emergence of synchronization and collective dynamics in networks of bistable dynamical elements. Specifically, we study different classes of networks, and identify the properties that are most crucial for the stability of the synchronized state in these networks.

In the first part of this thesis we focus on the sensitivity of networks to heterogeneity in small world networks. Here we investigate in detail the dynamics of networks of bistable elements with varying degrees of randomness in connections through extensive numerics. We consider both static random links and time-varying random links. We explore how the presence of a few dissimilar elements affects the collective features of this system, and find that a network with random links is hyper-sensitive to heterogeneity. Namely, counter-intuitively, even a small number of distinct elements manages to drastically influence the collective dynamics of the network, with the mean-field swinging to the steady state of the minority elements.

We find that the transition in the collective field gets sharper as the fraction of random links increases, for both static and time-varying links. We also demonstrate that networks where the links are switched more frequently, synchronize faster. Lastly, we show that as global bias tends to a critical value, even a single different element manages to drag the entire system to the natural stable state of the minority element. So it is evident that when coupling connections are random, a network with even a very small number of links per node, has the ability to become ultra-sensitive to heterogeneity.

The results mentioned above raised further pertinent questions, such as the following: Which networks are more conducive to synchronization? What properties in a network influence synchronization most significantly? So in the second research problem in this thesis, we investigate the collective dynamics of bistable elements connected in different network topologies, ranging from rings and small-world networks, to random and deterministic scale-free networks. We focus on the correlation between network properties and global stability measures of the synchronized state, in particular the average critical coupling strength $\langle \epsilon_c \rangle$ yielding transition to synchronization. Further we estimate the robustness of the synchronized state by finding the minimal fraction of nodes f_c that need to be perturbed in order to lose synchronization.

Our central result from these synchronization features is the following: while networks properties can provide indicators of synchronization within a network class, they

fail to provide consistent indicators across network classes. For instance, the heterogeneity of degree does not consistently impact synchronization, as evident through the stark difference in the synchronizability of rings vis-a-vis small-world and star networks, all of which have same average degree and deviation around the mean degree in the limit of large networks. Further we demonstrate that clustering coefficient is also not a consistent feature in determining synchronization. This is clear through the similarity of synchronization properties in rings with significantly different clustering coefficients, and the striking difference in synchronization of a star network and a ring having the same clustering coefficient. Even characteristic path length, which is of paramount importance in determining synchronization, does not provide a one-to-one correspondence with synchronization properties across classes. Namely, synchronization is significantly favoured in networks with low path lengths within a network class. However, the same characteristic path length in different types of networks yields very different $\langle \epsilon_c \rangle$ and f_c.

The next research problem addresses the following important question: Which nodes have the greatest influence on the stability of synchronized state in the network? In order to address this question, we investigate the collective dynamics of bistable elements connected in different network topologies, ranging from rings and small-world networks, to scale-free networks and stars. We estimate the dynamical robustness of such networks by introducing a variant of the concept of multi-node basin stability, which allows us to gauge the global stability of the dynamics of the network in response to local perturbations affecting a certain class of nodes of a system.

We show that perturbing nodes with high closeness and betweeness-centrality significantly reduces the capacity of the system to return to the desired state. This effect is very pronounced for a star network which has one hub node with significantly different closeness/betweeness-centrality than all the peripheral nodes. In such a network, perturbation of the single hub node has the capacity to destroy the collective state. On the other hand, even when a majority of the peripheral nodes are strongly perturbed, the hub manages to restore the system to its original state, demonstrating the drastic effect of the centrality of the perturbed node on the dynamics of the network.

Further, we explore Random Scale-Free Networks of bistable dynamical elements. We exploit the difference in the distribution of betweeness centralities, closeness centralities and degrees of the nodes in Random Scale-Free Networks with $m = 1$ and $m = 2$, to probe which centrality property most influences the robustness of the collective dynamics in these heterogeneous networks. Significantly, we find clear evidence that the betweeness centrality of the perturbed node is more crucial for dynamical robustness, than closeness

centrality or degree of the node. This result is important in deciding which nodes to safeguard in order to maintain the collective state of this network against targetted localized attacks.

In conclusion, in this thesis we explore the phenomena of synchronization across wide classes of networks and we identify the network properties that exert significant influence on the global stability of the synchronized state. So our results shed light on the collective dynamics of networks of bistable systems, and may indicate trends for complex dynamical networks in general.

List of Publications

1. Random links enhance the sensitivity of networks to heterogeneity.
   Pranay Deep Rungta and Sudeshna Sinha.
   Europhysics Letters, **112.6** (2016): 60004.

2. Are network properties consistent indicators of synchronization?
   Pranay Deep Rungta, Anshul Choudhary, Chandrakala Meena Sudeshna Sinha
   Europhysics Letters, **117.2** (2017): 20003.

3. Threshold-activated transport stabilizes chaotic populations to steady states.
   Chandrakala Meena, **Pranay Deep Rungta** and Sudeshna Sinha
   PLoS ONE 12(8): e0183251 (2017).

4. Identifying nodal properties that are crucial for the dynamical robustness of multi-stable networks
   Pranay Deep Rungta, Chandrakala Meena and Sudeshna Sinha
   arXiv preprint arXiv : 1801.02409 (2018).

Contents

Chapter 1

Introduction

In this work, we have studied collective dynamics of a group of coupled bistable elements. Bistable systems are relevant in a variety of fields, ranging from relaxation oscillators and multi-vibrators, to light switches and Schmitt triggers. Further it is of utmost importance in digital electronics, where binary data is stored using bistable elements.

1.1 Bistable system

Throughout this study we have considered three different bistable systems. The most general one is the following first order differential equation:

$$\dot{x} = F(x) = x - x^3 \tag{1.1}$$

We chose this particular function, because it has the simplest nonlinear polynomial form in one variable, which gives rise to two stable fixed points (see fig. 1.3).

Another bistable system taken in consideration was the piece-wise continuous function given as following:

$$F(x) = \begin{cases} \beta x_l^* - \alpha x & \text{if } x < x_l^* \\ (\beta - \alpha)x & \text{if } x_l^* \leq x \leq x_u^* \\ \beta x_u^* - \alpha x & \text{if } x > x_u^* \end{cases} \tag{1.2}$$

where x_u^* and x_l^* are the upper and lower thresholds respectively (see fig. 1.1). This dynamical equation can be realized efficiently in electronic circuits [39].

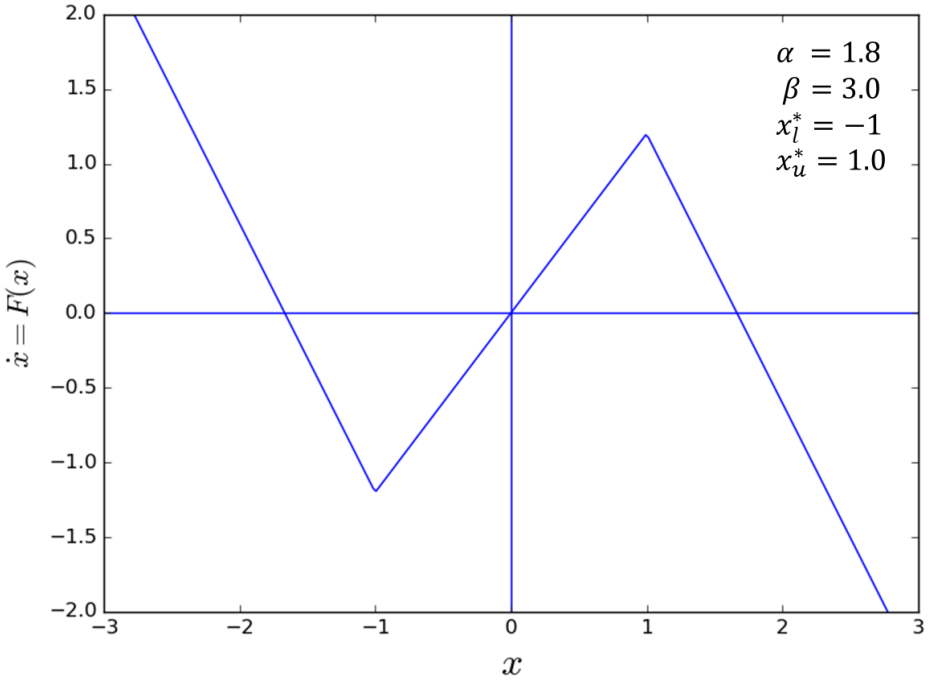

Figure 1.1: Plot of function $F(x)$ given by equation 1.2.

We also explored different networks of bistable *synthetic genetic networks*, where the nodal dynamics was given by [18, 19, 20]:

$$F(x) = \frac{m(1 + x^2 + \alpha\sigma_1 x^4)}{1 + x^2 + \sigma_1 x^4 + \sigma_1\sigma_2 x^6} - \gamma_x x \tag{1.3}$$

where x is the concentration of the repressor. The nonlinearity in this $F(x)$ leads to a double well potential, and different γ introduces varying degrees of asymmetry in the potential (see fig.1.2).

In order to demonstrate the generality of the results presented in this thesis, and to show that they hold for a large class of bistable systems, we have verified all results for all three types of local dynamics described by the equations 1.1,1.2 and 1.3 above.

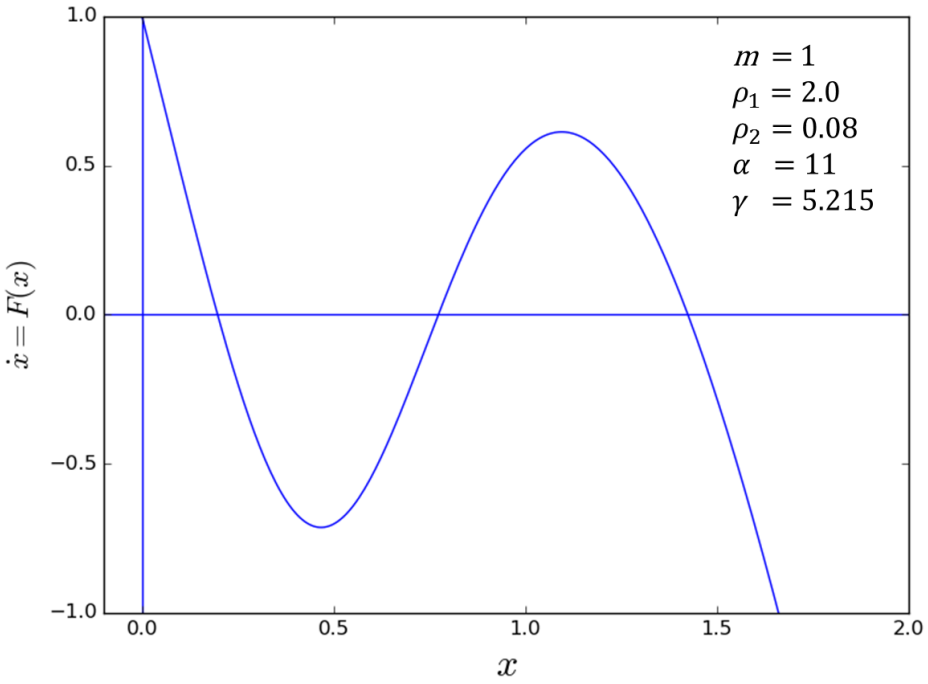

Figure 1.2: Plot of function $F(x)$ given by equation 1.3.

Analysis

Now we choose the first system, which is the most general one, in order to illustrate different features of a bistable system. Note that the analysis here is applicable to all three systems mentioned above. First we look at the vector field (flow) generated by the equation 1.1 in one dimension, as shown in fig. 1.3.

We can analytically find the fixed points $x^\star$ by setting $\dot{x} = 0$ in equation 1.1.

$$\dot{x} = F(x) = 0 \tag{1.4}$$
$$\implies \quad x - x^3 = 0 \tag{1.5}$$
$$\implies \quad x(1-x)(1+x) = 0 \tag{1.6}$$
$$\implies \quad x = 0, +1, -1 \tag{1.7}$$

To find the stability of these equations we differentiate equation 1.1 and check the sign of $F'(x)$, evaluated at the fixed points $x^\star$ determined by 1.7.

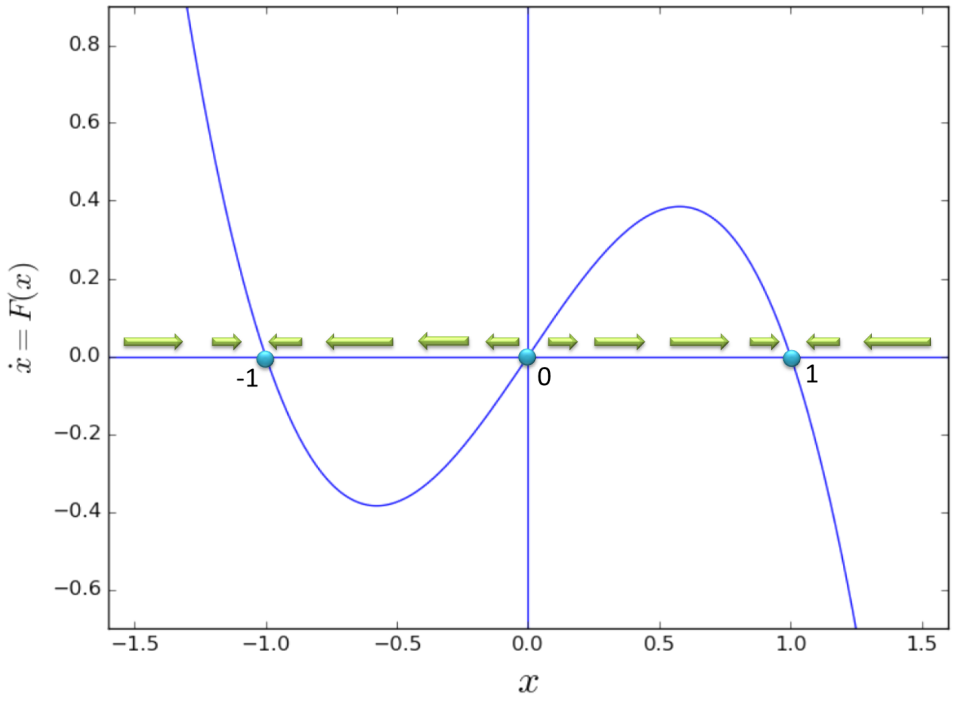

Figure 1.3: Flow(vector field) generated by force function $\dot{x} = x - x^3$ in one dimension.

$$F(x) = x - x^3 \tag{1.8}$$

$$\implies \quad F'(x) = 1 - 3x^2 \tag{1.9}$$

$$\therefore \quad F'(0) = 1 \tag{1.10}$$

$$and \quad F'(1) = F'(-1) = -2 \tag{1.11}$$

Since $F'(0) > 0$, $x^\star = 0$ is an *unstable* fixed point, while $F'(1) = F'(-1) < 0$ implies that $x^\star = -1, 1$ are *stable* fixed points

Potential Function

Another way of understanding the above system is by defining a quantity analogous to a potential function, given as:

$$V(x) = -\int F(x)dx \tag{1.12}$$

Thus, the above equation yields

$$V(x) = \frac{x^4}{4} - \frac{x^2}{2} \tag{1.13}$$

Fig. 1.4 shows this potential function and marks the stable and unstable points. Thus for any given initial condition $x_0 > 0$ and $x_0 < 0$ the system is bound to settle to the stable states $x^\star = +1$ and $x^\star = -1$ respectively.

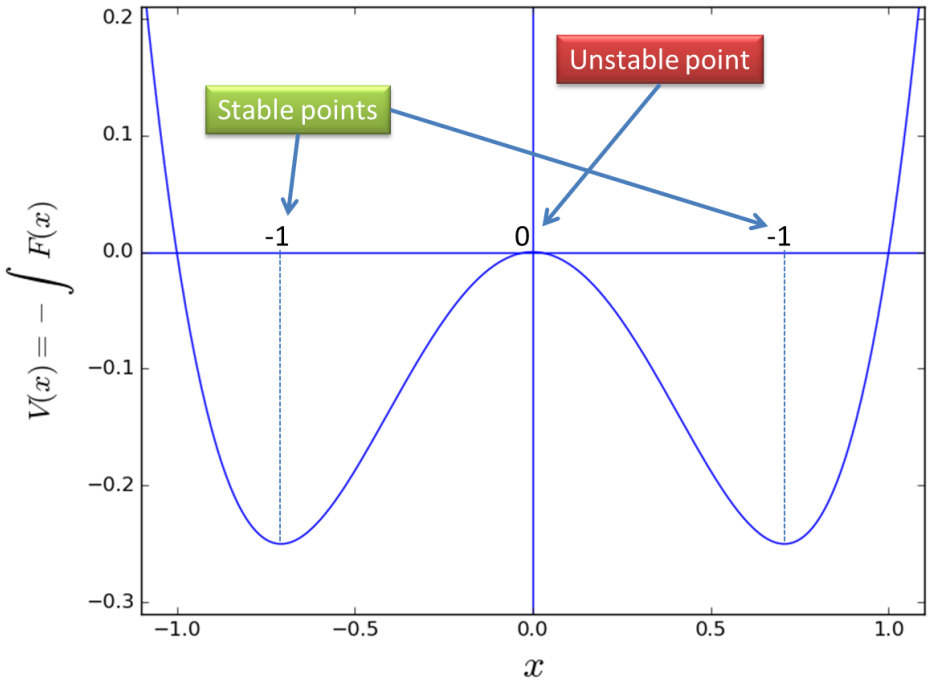

Figure 1.4: Flow (vector field) generated by $F(x) = x - x^3$ in one dimension.

Synchronization

Synchronization of complex networks has attracted wide research interest, from fields as diverse as ecology and sociology to power grids and climatology [25, 26, 16, 27]. Collective spatiotemporal patterns emerging in dynamical networks are determined by the interplay of the dynamics of the nodes and the nature of the interactions among the nodes.

The concept of synchronization provides a general approach to the understanding of the collective behavior of coupled dynamical systems, and the term has expanded in usage to include several types of correlated collective behaviour. Some of the widely used terms relating to synchronization are following:

1. Complete synchronization: The systems are said to be completely synchronized when there is a set of initial conditions so that the systems eventually evolve identically in time.

2. Generalized synchronization: This type of synchronization occurs mainly when the coupled chaotic oscillators are different. Given the dynamical variables $(x_1, x_2, ..., x_n)$ and $(y_1, y_2, ..., y_m)$ that determine the state of the oscillators, generalized synchronization occurs when there is a functional, ϕ, such that, after a transitory evolution from appropriate initial conditions, the following condition holds:

$$[y_1(t), y_2(t), ..., y_m(t)] = \phi[x_1(t), x_2(t), ..., x_n(t)]$$

.

3. Phase synchronization: Phase synchronization occurs when the coupled chaotic oscillators keep their phase difference bounded while their amplitudes remain uncorrelated.

4. Anticipated synchronization: This type occurs between chaotic oscillators whose dynamics is described by delay differential equations, coupled in a drive-response configuration. The response anticipates the dynamics of the drive.

5. Lag synchronization: This type of synchronization is similar to anticipated synchronization(i.e. the dynamics of these oscillators is described by delay differential equations, coupled in a drive-response configuration). This occurs when the strength of the coupling between phase-synchronized oscillators is increased.

The unifying thread in all the different types of synchronization is the emergence of a consistent relationship between the variables of a set of dynamical systems, and this can arise in contexts ranging from simple first-order phase oscillators to complex chaotic systems. Further, these types of synchronization apply to both mono-stable, as well as multi-stable systems [33].

In this thesis, a synchronized state refers to a state where all nodes in the network evolve to the same stable state after transients. That is, all the dynamical elements comprising the network evolve to the same well of the double-well potential function describing the system.

1.2 Networks

The principal focus of this thesis is the collective dynamics of a group of bistable elements connected in different network topologies, ranging from regular rings and small-world networks on one hand, to deterministic scale-free and random scale-free networks on the other. So we first present a brief summary of the properties of these networks.

1. Ring: Here each node has degree K (K even) and is connected to $K/2$ nearest neighbors on either side (see fig. 1.5). There are two independent parameters which completely determine the topology, namely system size (denoted by N), number of neighbors of each node (denoted by k).

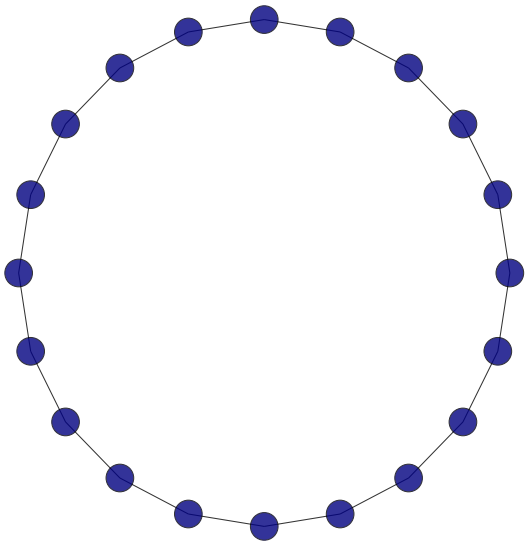

Figure 1.5: Construction of a Ring Network of size $N = 20$ and $k = 2$.

2. Star network: here all the peripheral nodes are attached to one hub(see fig.1.6). It has only one independent parameter namely system size (denoted by N).

3. Deterministic scale free network: this has the particular hierarchical structure generated iteratively for different orders (denoted by g) [37] (see fig.1.7). Here the order g, which is the only relevant network parameter, determines the number of nodes in the network, with $N = 3^g$.

4. Random Scale-Free: this is constructed via the Barabasi-Albert preferential attachment algorithm, with the number of links of each new node denoted by parameter

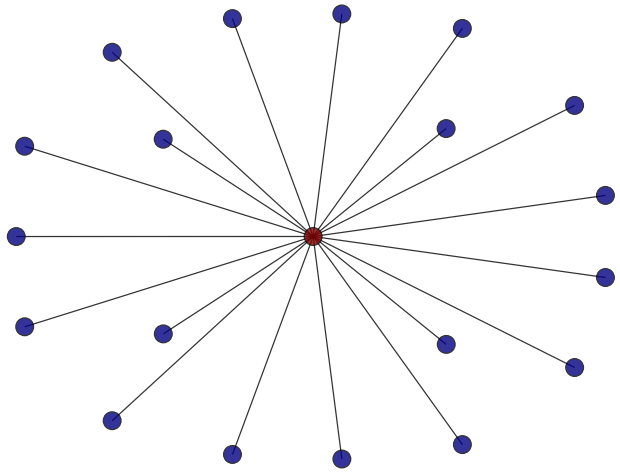

Figure 1.6: Construction of a Star Network of size $N = 20$.

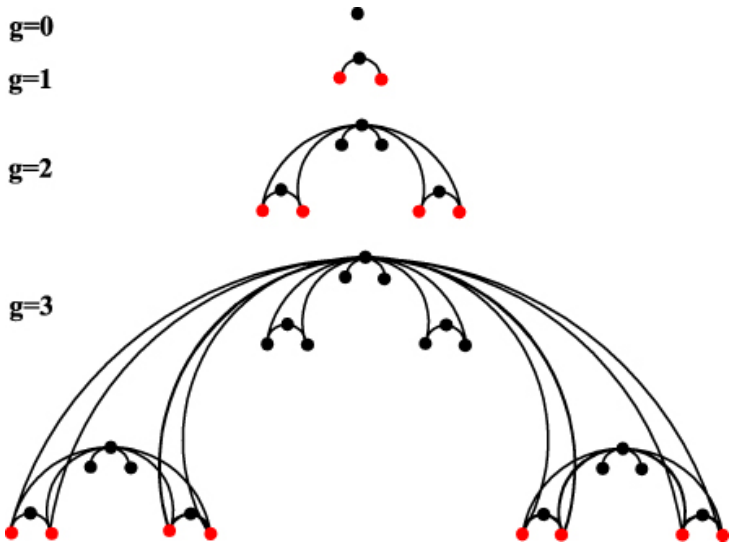

Figure 1.7: Construction of a Deterministic Scale-Free Network (adapted from Ref. [37]).

m [36](see fig. 1.8, 1.9). Thus, there are two independent parameters which completely determine the topology, namely system size (denoted by N), number of links of each new node (denoted by m).

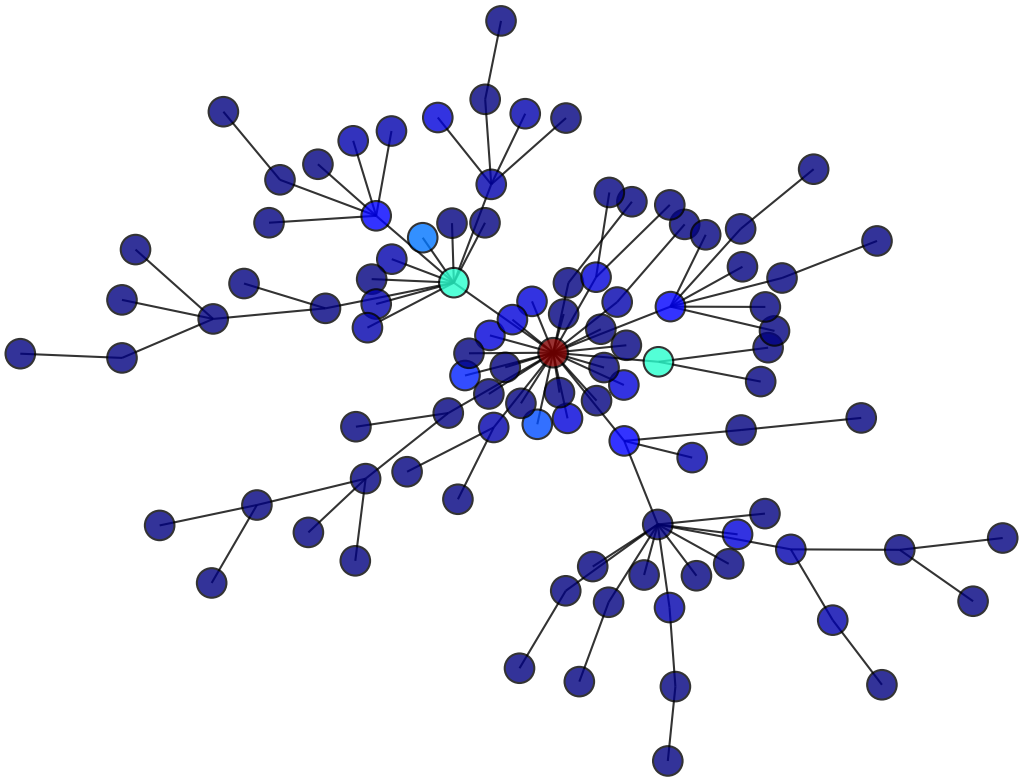

Figure 1.8: Construction of a Scale-Free Network (adapted from Ref. [36]) of size $N = 100$ with $m = 1$.

5. Small-World network: This is constructed via the Watts-Strogatz algorithm [6]. Namely, we start from a ring with vertices having degree k (as in 1 above), and then rewire links to random non-local nodes with probability p (see fig. 1.10). Thus, there are three independent parameters which completely determine the topology, namely system size (N), number of neighbors of each node (k) and the probability p with which we rewire links to random non-local nodes. So p can be roughly interpreted as fraction of random links in the network.

Outline of the thesis: The thesis is broadly divided into three parts. In the first part (Chapter 2), we study synchronization in small world networks and we show that they exhibit the interesting phenomena of hypersensitivity. Specifically we demonstrate

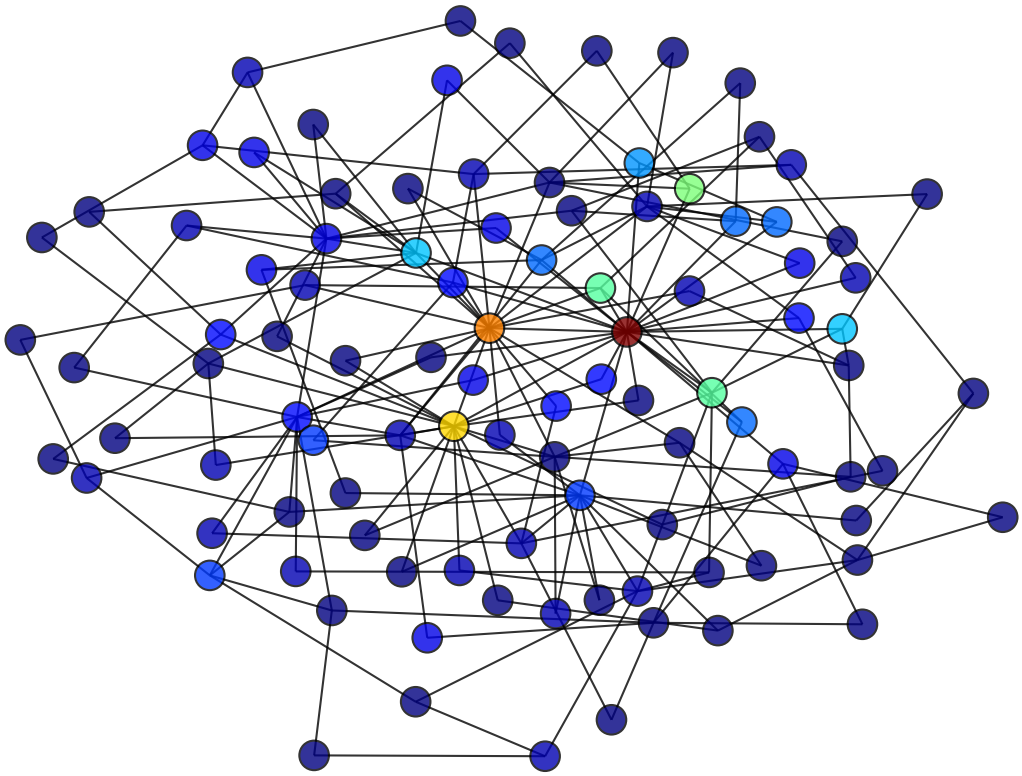

Figure 1.9: Construction of a Scale-Free Network (adapted from Ref. [36]) of size $N = 100$ with $m = 2$.

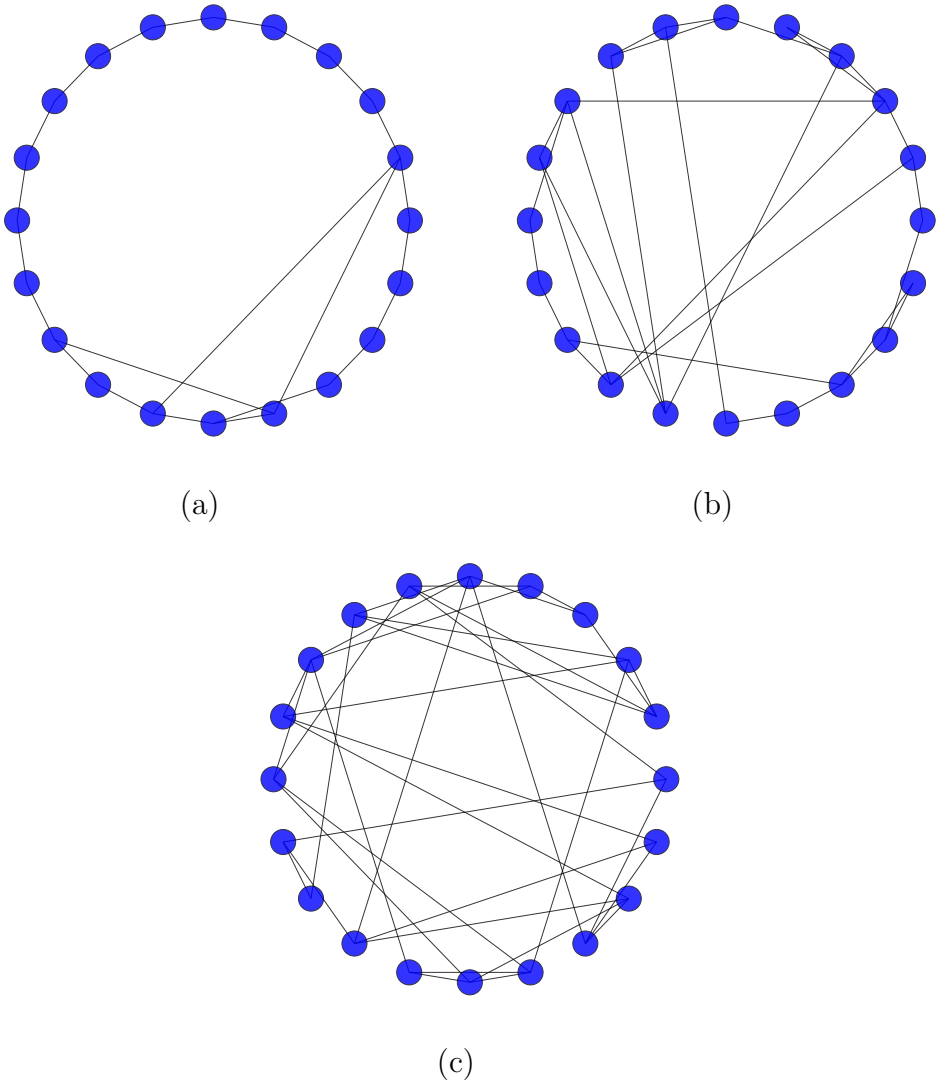

Figure 1.10: Construction of a Small world Network (adapted from Ref. [6]) of size $N = 20$ for different fractions of random links: (a) $p = 0.1$, (b) $p = 0.5$, and (c) $p = 0.9$.

that as the fraction p of random links increases, the system readily synchronizes, as well as becomes more sensitive to heterogeneity, unlike bistable elements coupled in the well structured ring topology. In the second part (Chapter 3), we study five different classes of networks and identify the ones that synchronize most readily and those that are difficult to synchronize. We then attempt to uncover underlying network patterns that may be correlated with the propensity (or lack thereof) of synchronization in those networks. In the third part (Chapter 4), we study the ability of a network to recover from large localized perturbations. In this part we address the question of identifying the nodal properties that render a network most vulnerable to targetted attacks. We conclude in Chapter 5 with a summary of our principal results, and indicate some future directions that arise from the work in this thesis.

Chapter 2

Random links enhance the sensitivity of networks to heterogeneity

Adapted from the work published in :

P. D. Rungta and S. Sinha EPL, **112** (2015) 60004 .

2.1 Introduction

The study of large interactive nonlinear systems has been a very active area of research in recent years [1]. In this chapter we will focus on a network of coupled bistable elements and explore the role of heterogeneity in the emergent spatio-temporal patterns [2, 3]. Now, in the context of the response of coupled bistable systems to heterogeneity, some counter-intuitive results were obtained recently for the case of global coupling [4, 5]. Specifically, Ref. [4] considered a collection of N nonlinear dynamical elements with two distinct stable states x_+^* and x_-^*, with the equation governing the temporal evolution of element i given by:

$$\dot{x}_i = G(x_i) + a_i + C(\langle x \rangle - x_i) + b \tag{2.1}$$

where element (node) index $i = 1, 2, \ldots, N$, with N being system size. The elements are coupled through the *mean field* $\langle x \rangle = \frac{1}{N}\sum_{i=1}^{N} x_i$, with C being the strength of coupling. The local dynamics is determined by $G(x_i)$ which is a generic nonlinear function giving rise to a bistable potential, with two steady states at x_-^* (lower well) and x_+^* (upper well). The local parameter a_i may differ from element to element, leading to heterogeneity in the system. This local parameter determines the location and depth of the stable states of the nodal dynamics in the uncoupled case. Parameter b is a *global bias*, common to the elements, and can be used as a "control lever" to tip the collective behaviour of the system to different patterns.

Consider a heterogeneous system comprised of two distinct types of elements, with N_0 number of elements having $a_i = 0$ in Eqn. 2.1, and the rest of the elements $N_1 = N - N_0$ having $a_i = 1$. When uncoupled the collective field is naturally just the weighted average of the steady states of the elements. When coupled, since the contribution of each node is of the order of $O(1/N)$, one expects that the dynamics of system should be dominated by the majority set. Very interestingly however, it was found that under certain conditions all the elements in the system evolved to the stable state of the minority population [4]. Namely, the entire system was driven to the natural state of the set with a much smaller number of elements. The underlying reason for this counter-intuitive behavior was the interplay of the relative depths of the different local steady states due to heterogeneity, and the *strong global coupling* of the system which leads to synchronization.

Further it was observed that for suitable global bias b this system could be made *ultra-sensitive* to heterogeneity in the system. That is, the collective field reflected the

presence of the smallest deviation from uniformity in the local parameter a_i. In fact it was found that in certain systems, even a *single* element with a different a_i, could lead the entire system to its natural state. Thus, in these conditions the collective field of the system is any extremely sensitive detector of non-homogeneity.

2.2 Model

In this chapter we will investigate the following important issues regarding this remarkable phenomena: First, we will attempt to ascertain if global coupling is indeed necessary to observe this phenomena, or if such hyper-sensitivity can arise in systems where the coupling range is restricted to much smaller neighbourhoods. Further, we will also seek to uncover if *randomizing connections aids or hinders this sensitivity to heterogeneity.* We will address the pertinent question of the *minimal degree of coupling necessay to allow the minority set to determine the collective behaviour of the system.* To probe the above questions, we study the evolution of N bistable elements, coupled to k neighbours, given by:

$$\dot{x_i} = G(x_i) + a_i + C\left[\frac{1}{k}\Sigma_{j=1}^{k}(x_j - x_i)\right] + b \tag{2.2}$$

for $i = 1, \ldots N$. In the interaction term, $\Sigma(x_j - x_i)$ is a sum over the k neighbors of the i^{th} node, and gives the *local field* experienced by each element. When the underlying connections are regular, we have $j = i \pm m$, with m ranging from 1 to $k/2$ (with k considered an even integer in this work).

Specifically we consider the widely studied case of $k = 2$ (namely two neighbours) and the nonlinear function $G(x_i) = x_i - x_i^3$ at the the nodes of the network, yielding two steady states $x_-^* = -1$ (lower well) and $x_+^* = 1$ (upper well). The parameter a_i is 1 for N_1 randomly selected nodes and 0 for others. The important thing to note is that different a_i gives rise to different potential functions as displayed by different curves in Fig. 2.1-a.

Further, the parameter b is the global bias and is used to tilt the potential wells on one side. In this study we consider bias $b < 0$, which tilts and thus makes the negative well more probable. Fig 2.1 a-c shows the trend of increasing negative bias on potential wells for both nodes, namely ones with $a_i = 0$ and ones with $a_i = 1$.

The coupling is strong, with coupling constant $C = 1$. We explored the behavior of the system arising from a large sample of initial conditions, with the initial state of the elements drawn randomly from a uniform distribution $[-2 : 2]$. We also ascertained that

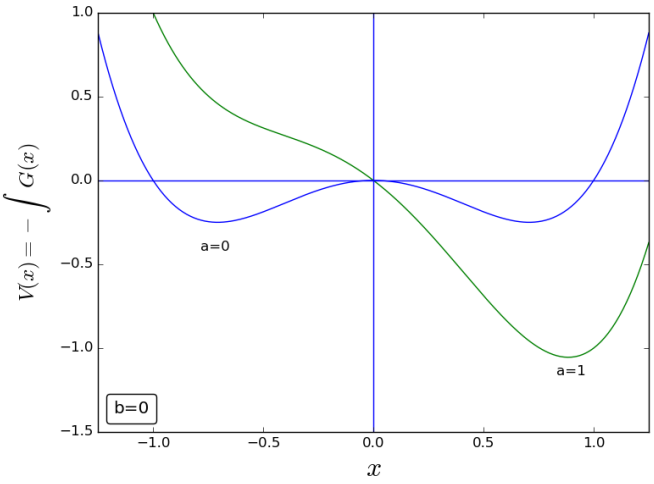

(a)

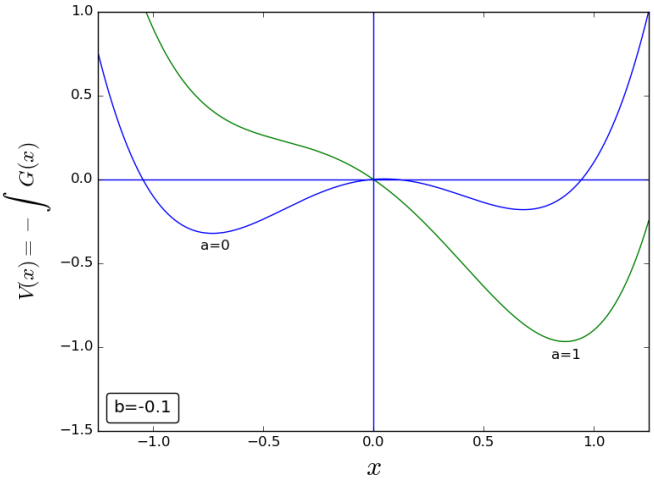

(b)

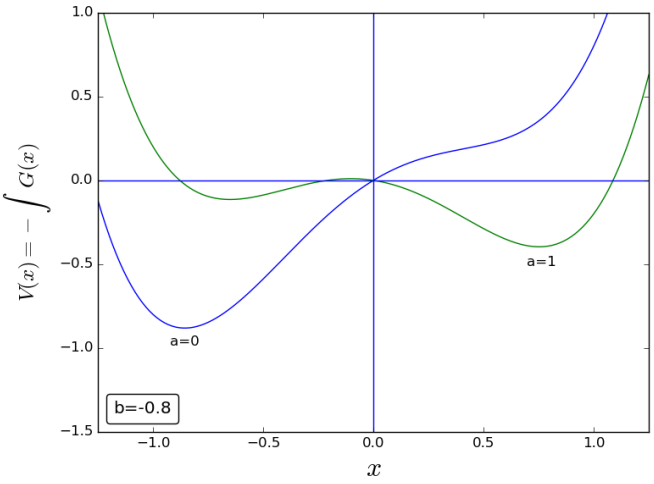

(c)

Figure 2.1: Plot of potential wells underlying the system $\dot{x} = (x_i - x_i^3) + a + b$ with $a = 0$ and with $a = 1$. Figure a-b-c displays the trend of increasing bias.

the results were robust with respect to the time-step in the numerical simulations, over orders of magnitude.

To explore the effect of random connections on the collective behaviour of the system, we study wide-ranging degree-preserving connection topologies, with varying fractions of random links. We will use the well-known Watts-Strogatz small-world network framework to interpolate between the completely regular lattice [1] and a completely random network [6]. Our connection network will consist of a regular graph of nodes, with a fraction p of the links randomized(see 2.2). In particular we investigate networks of these bistable systems, with p ranging from 0 (regular lattice) to 1 (random networks). So the local field is determined by a set of elements, ranging from k nearest neighbours on a ring, to k random non-local sites, depending on the topology of the underlying network of connections. Additionally, we consider two classes of connections: (a) *static networks*, where the connections remain unchanged, namely the case of frozen or quenched links; (b) *time-varying or dynamically changing networks*, where the links switch periodically, namely the connectivity matrix changes at regular intervals [7, 8, 9, 10, 11, 12, 13, 14]. Generally speaking, these random links provide shortcut paths for the spatial flow of information, leading to more efficient synchronization [15, 16] and more efficient control to fixed states [7, 8], as well as suppression of blow-ups in complex networks [9, 10].

In order to probe the effect of local heterogeneity, we consider the network with N_0 nodes with $a_i = 0$, and $N_1 = N - N_0$ nodes with $a_i = 1$. Figs. 2.3-2.5 show representative space-time patterns for $k = 2$. For the case of the regular ring (i.e. $p = 0$) displayed in Fig. 2.3 we show three illustrative cases: (a) a homogeneous ring with all elements having $a_i = 0$; (b) a ring with just a single element having $a_i = 1$ while the rest have $a_i = 0$ (namely $N_1 = 1$ and $N_0 = N - 1 >> N_1$); (c) a ring with a reasonably large set of elements with $a_i = 1$, e.g. $N_1 = 30$ in a lattice of size $N = 100$. It is clearly evident that there is no synchronization in the regular ring when N_1 is small, and typically different elements i evolve to different steady states depending on their individual a_i and the initial state.

In Fig. 2.4 and Fig. 2.5 we show representative spatiotemporal patterns for a ring with a large number of links randomized, namely a fraction p of nearest neighbour connections are rewired to random sites in the network. In Fig. 2.4 the connections are static, while in Fig. 2.5 the links are switched periodically. It is clearly evident that when there is a sufficiently large fraction of random links, either static or time-varying, global synchronization emerges. When the system is homogeneous and all the elements have $a_i = 0$ then all the elements in the system go to the lower state. However remarkably, just a *single*

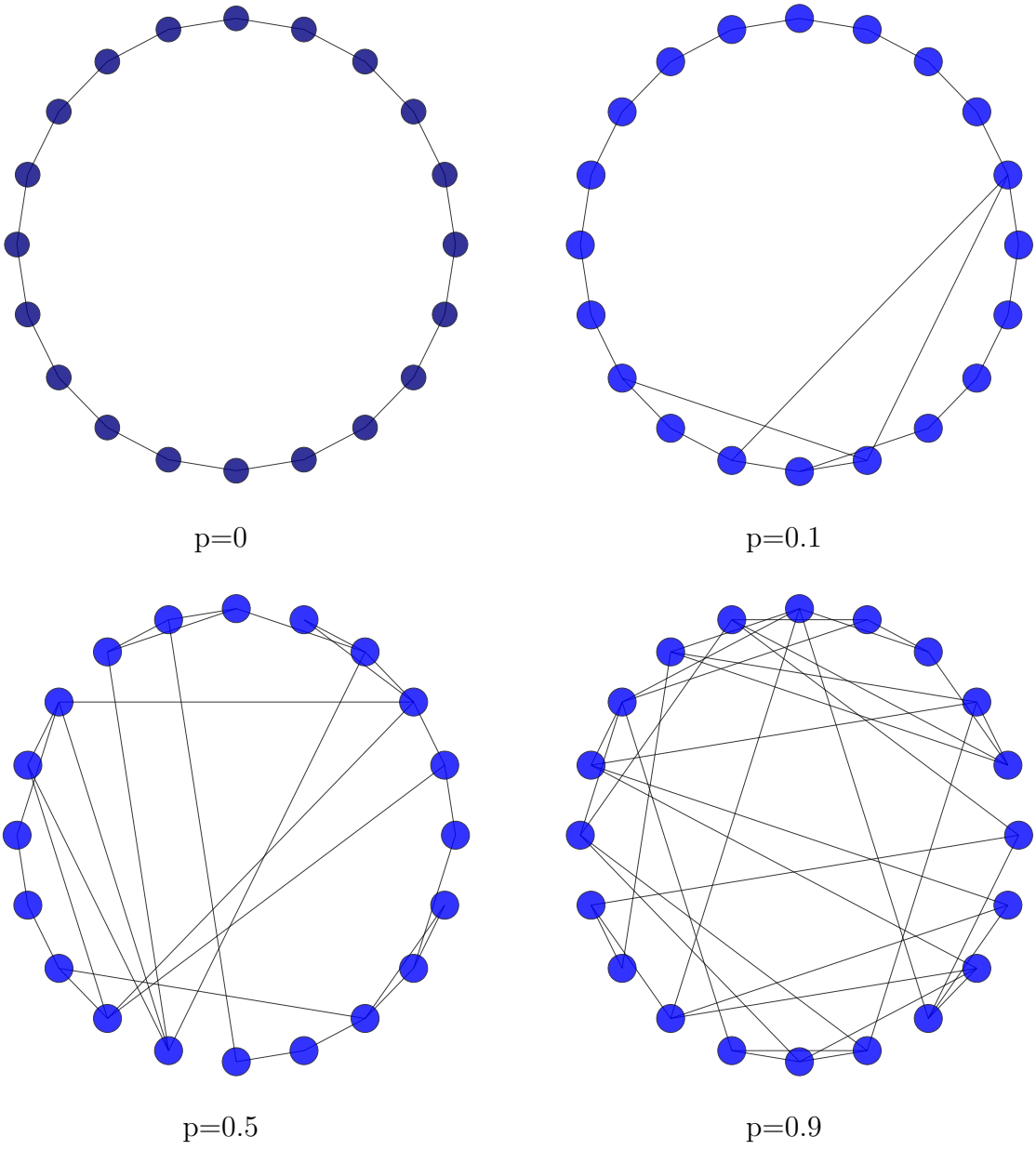

Figure 2.2: Small world network with increasing fraction of random links p.

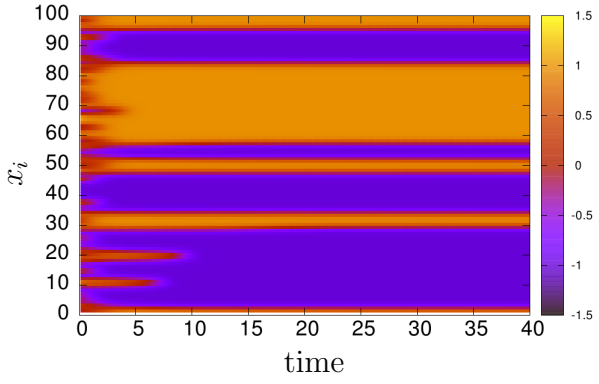

(a)

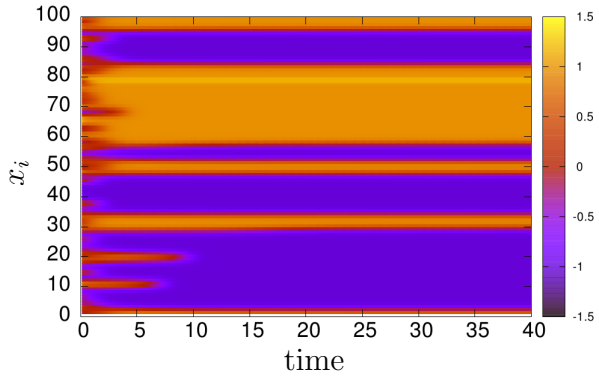

(b)

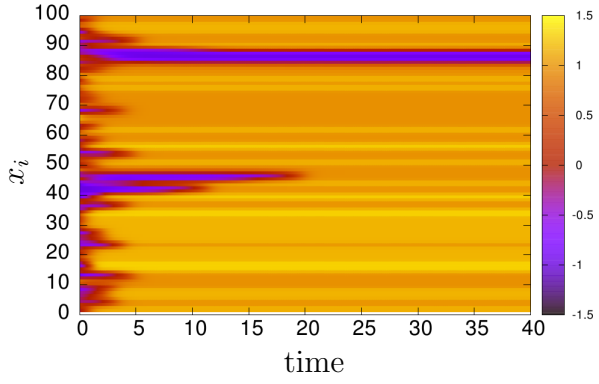

(c)

Figure 2.3: Time evolution of coupled bistable elements x^i ($i = 1, \ldots, N$, with $N = 100$) governed by Eqn. 2.2, with $k = 2$, where the number of sites N_1 with $a_i = 1$ is (a) 0, (b) 1 and (c) 30. Here the network is completely regular, without any random links, namely $p = 0$, and the global bias $b = -0.035$. In this figure, as well as in Figs. 2.4 and 3, time runs along the x-axis, the index i of the elements ($i = 1, \ldots, 100$) is given along the y-axis, and the colors represent the value of state x_i of element i at a particular point in time (with the yellow end of the spectrum representing 1.5 and the indigo end representing -1.5.

.

different element in the system can swing the system to the upper state. So the system with random links is ultra-sensitive to the presence of even the smallest heterogeniety.

In order to quantify this behaviour further, we have probed the time evolution of the mean field $\langle x \rangle = \frac{1}{N}\sum_{i=1}^{N} x_i$ where N is the system size, namely we track how the average value of the state of the elements changes in time, starting from generic initial conditions. When the asymptotic mean field is close to -1, it implies that most elements have evolved to the lower well and almost none are in the upper well. However when the mean field is close to 1, it is signifies that most elements are in the upper well. So the asymptotic mean field indicates the fraction of elements in the network that have evolved to the upper well.

Fig. 2.6 shows how the mean field in a network with a large fraction of random links swings around 1 from -1 when just one of the elements in the network is different. In contrast, notice that the mean field is effected very little by this in the case of the regular ring. We will quantify this remarkably strong response to non-uniformity below.

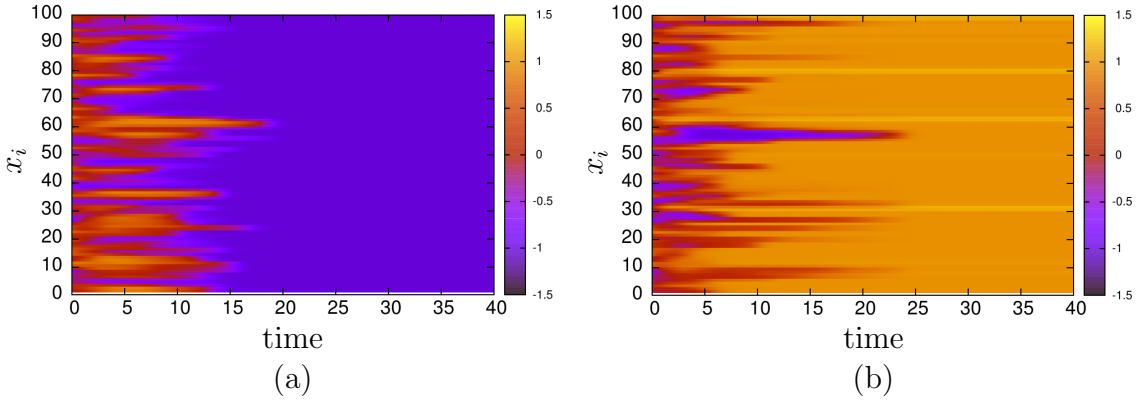

Figure 2.4: Time evolution of coupled bistable elements x^i ($i = 1, \ldots, N$, with $N = 100$) governed by Eqn. 2.2, with $k = 2$, where the number of sites N_1 with $a_i = 1$ is (a) 0 and (b) 1. Here the fraction of random links is $p = 0.8$, and the links are static. The global bias $b = -0.035$.Again, as in the last figure, time runs along the x-axis, the positions of the elements are shown along the y-axis, and the colors represent the value of state x_i of element i at a particular point in time. Clearly the presence of just 1 distinct element in a network of size 100 drastically changes the outcome of the evolution of network.

2.3 Effect of varying heterogeneity

In order to quantitatively examine how collective features, as exemplified by the mean field $\langle x \rangle$, are affected by the majority and the minority elements, we calculate the asymptotic

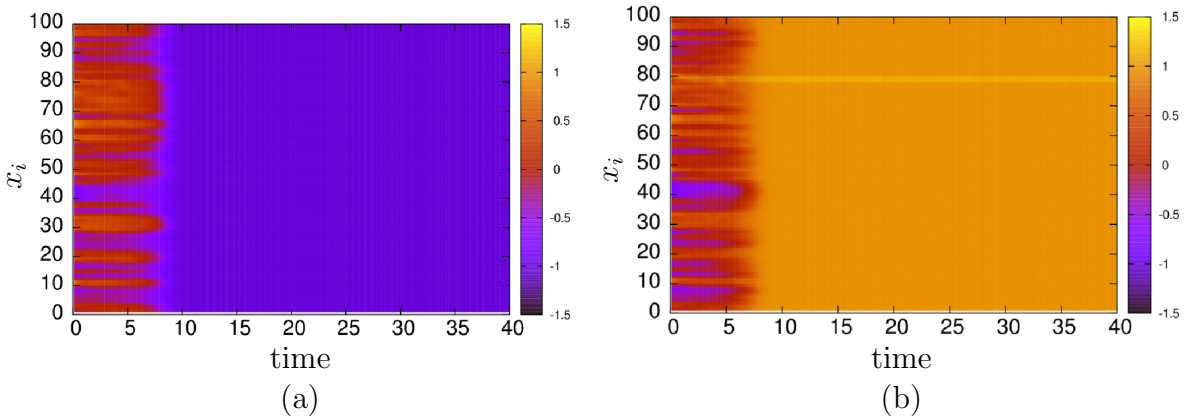

Figure 2.5: Time evolution of coupled bistable elements x^i ($i = 1, \ldots, N$, with $N = 100$) governed by Eqn. 2.2, with $k = 2$, where the number of sites N_1 with $a_i = 1$ is (a) 0 and (b) 1. Here the fraction of random links is $p = 0.8$, and the links are time-varying (with the periodicity of switching links being 0.1). The global bias $b = -0.035$. Again, as in the last figure, time runs along the x-axis, the positions of the elements are shown along the y-axis, and the colors represent the value of state x_i of element i at a particular point in time. Clearly the presence of just 1 distinct element in a network of size 100 drastically changes the outcome of the evolution of network.

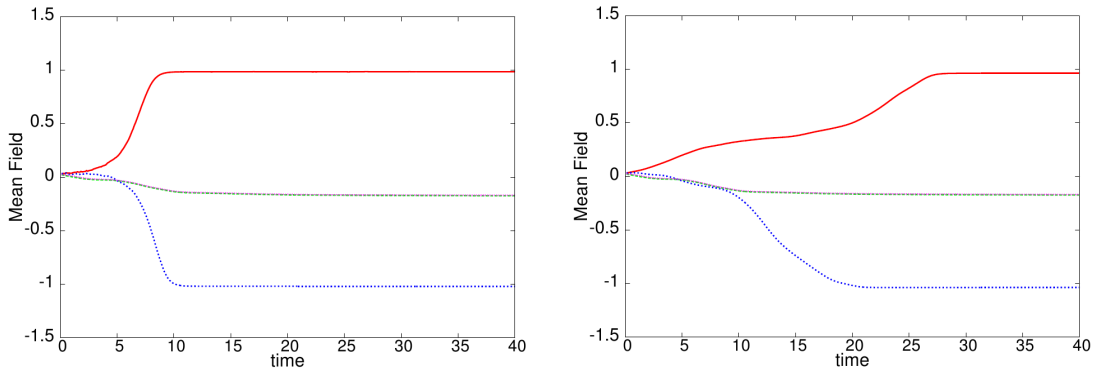

Figure 2.6: Time evolution of the mean field of the coupled system of bistable elements, governed by Eqn. 2.2, with $k = 2$ and fraction of random links $p = 0.8$, for (a) dynamically changing links (with $b = -0.035$) and (b) static links (with $b = -0.075$). The number of sites N_1 with $a_i = 1$ is equal to 0 (blue) and 1 (red). The case of $p = 0$, with $N_1 = 0$ and $N_1 = 1$ is shown by the nearly overlapping green and magenta curves respectively. Note that all curves evolve from the same initial state. Clearly for the case of random links the presence of just *one* distinct element in a network of size 100 swings the collective field from around -1 to 1, while for a regular ring of bistable elements the presence of 1 distinct element changes the mean field incrementally.

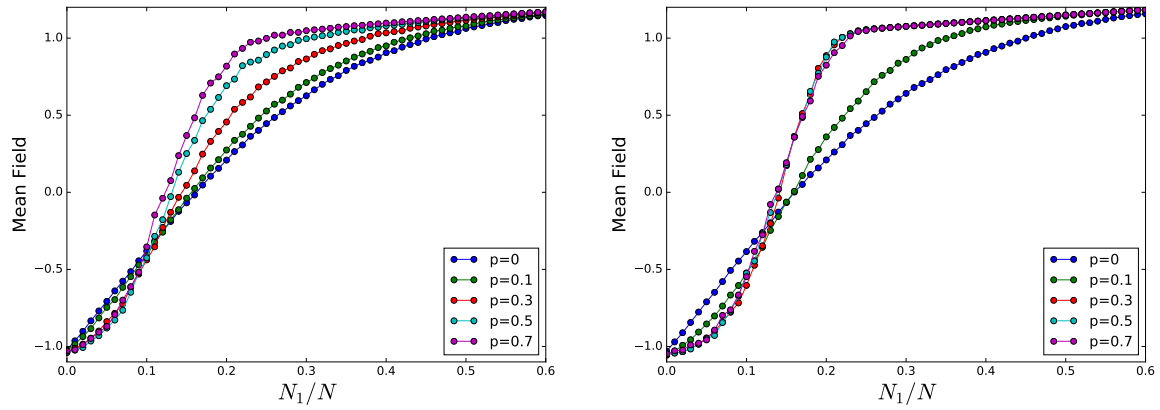

(a) (b)

Figure 2.7: Average mean field in a network as a function of N_1/N (i.e. fraction of elements with $a_i = 1$), with different fractions of random links p. Here network size $N = 100$, and global bias is $b = -0.1$. Note that both static random connections(a) and time-varying random links(b) yield similar results.

mean field, averaged over a large number of initial states. This quantity helps us to systematically gauge the effect of the relative magnitudes of N_0 and N_1 on the collective behaviour of heterogeneous networks.

Figs. 2.7-2.9 shows the transition in the average mean field with increasing heterogeneity, indicating sharp change in collective behaviour as N_1 increases. It is evident from the figures that there is a transition from the case where all elements are in the lower well to a situation where the entire system is in the upper well, i.e. the mean field swings from approximately x^*_- to x^*_+.

First, notice how the degree of randomness in spatial connections makes a crucial difference to the transition in the collective field under increasing heterogenity. The influence of random links on the sensitivity of collective properties on local non-uniformity is apparent in Figure 2.7. It is clearly seen that increasing the fraction of random links p results in a sharper transition. So when the links are increasingly random, one obtains synchronization of the dynamics of the entire system to the stable state of the minority group, in response to increasingly small number of elements that are distinct.

Fig. 2.8a demonstrates the trends with changing system size N. It is evident that larger system sizes give rise to sharper transitions in the collective field under increasing heterogeneity, with the transition occuring at the same critical N_1. This illustrates that the size of the coupling neighbourhood, relative to the size of system, does not influence the sensitivity of the network to heterogeneity. In order to infer the trend in the ther-

modynamic limit, we use finite size scaling. As shown in Fig. 2.8b for a given bias b and fraction of random links p, the form

$$\mathcal{F}((N_1 - N_1^{critical})/\sqrt{N})$$

yields good data collapse.

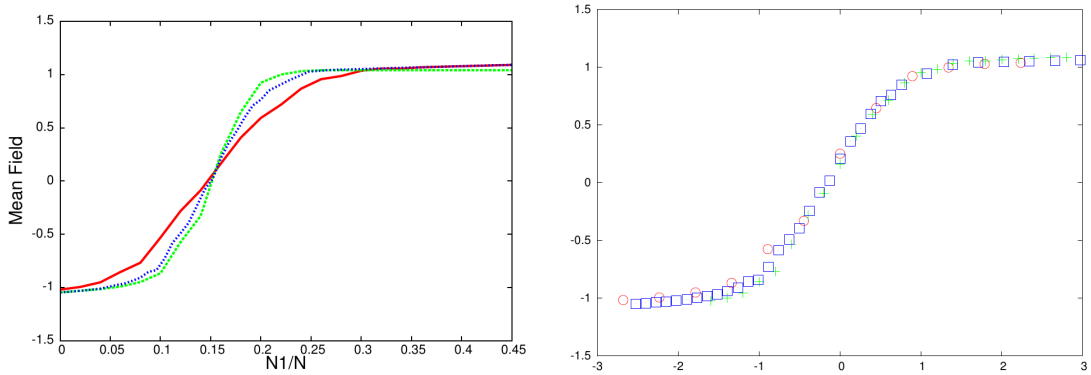

(a) (b)

Figure 2.8: (a) Average mean field as a function of N_1/N (i.e. fraction of elements with $a_i = 1$ in a network of size N), for networks with $N = 100$ (red), 250 (green) and 500 (blue); (b) mean field of the networks of different sizes on the y-axis, with respect to scaled size $(N_1 - N_1^{critical})/\sqrt{N}$ on the x-axis, yielding a good data collapse. Here the global bias $b = -0.1$, fraction of dynamically varying random links $p = 0.8$, and $N_1^{critical}/N = 0.16$. Similar results are obtained for the case of static links.

2.4 Effect of global bias on sensitivity

Fig. 2.9 shows the effect of changing global bias on the collective behaviour of the network. It is evident from the figure that for negative global bias tending to zero, namely $b \to 0^-$, this transition shifts towards $N_1 \to 1$ limit, when p is large. So the collective field of the network reflects even the smallest degree of non-uniformity in the system when there are sufficient number of random links in the network. Thus the system at the appropriate global bias is ultra-sensitive to heterogeneity, with the collective field displaying a remarkably large swing in response to just one element with $a_i = 1$. So the transition tends to the $N_1 = 1$ limit, indicating that typically the collective field is capable of reflecting the presence of even a single different element in a network with random links, as illustrated for particular examples in Figs. 2.4 and 2.5.

Remarkably then, we observe that the network exhibits sensitivity to heterogeneity even when each node is coupled to only two other nodes. This is a significant difference from earlier results where the system exhibited ultra-sensitivity under mean field coupling. So even when the information flow is constrained to just two other sites, and not the entire system as in the case of global coupling, the majority elements can synchronize to the natural state of the minority set if the links are sufficiently random. This result is potentially very significant for systems where connections are sparse. It is also potentially pertinent for engineered systems where one would like to reduce the cost of adding coupling connections in order to achieve this effect.

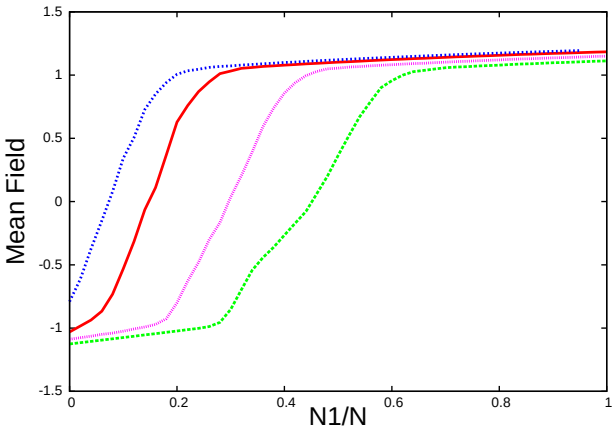

Figure 2.9: Average mean field as a function of N_1/N (i.e. fraction of elements with $a_i = 1$ in a network of size N), evolving under different values of global bias b equal to -0.05 (blue), -0.1 (red), -0.2 (magenta) and -0.3 (green). Here network size $N = 100$, and fraction of random links $p = 0.8$. Note that both static random connections and time-varying random links yield similar results.

2.5 Synchronization

We now focus more on the emergence of synchronization in the network. In order to probe the degree of synchronization we find the synchronization error (after transience) given as the root mean square deviation of the local state of the nodes, averaged over time and different initial conditions, which can be mathematically expressed as:

$$Z_{sync} = \frac{1}{S}\sum_{S}\left\{\frac{1}{T}\sum_{T}\left\{\frac{1}{N}\sum_{i=1}^{N}\left[x_i(t) - \langle x(t)\rangle\right]^2\right\}^{1/2}\right\} \tag{2.3}$$

When this measure tends to zero, the system tends to *complete synchronization*.

Fig. 2.10 shows the average synchronization error as a function of the coupling strength C in Eqn. 2.2. It is clear that as coupling strength increases, the network gets more synchronized, as is intuitively expected [16]. Further it is evident that for networks with random links (i.e. $p > 0$), after a critical coupling strength complete synchronization is obtained. This holds true for both static links and dynamically varying links. However, for a regular ring (namely $p = 0$) the system never attains complete synchronization, as corroborated by the space-time patterns in Fig. 2.3. The emergence of synchronization under random connections is in accordance with earlier results on small-world networks [17].

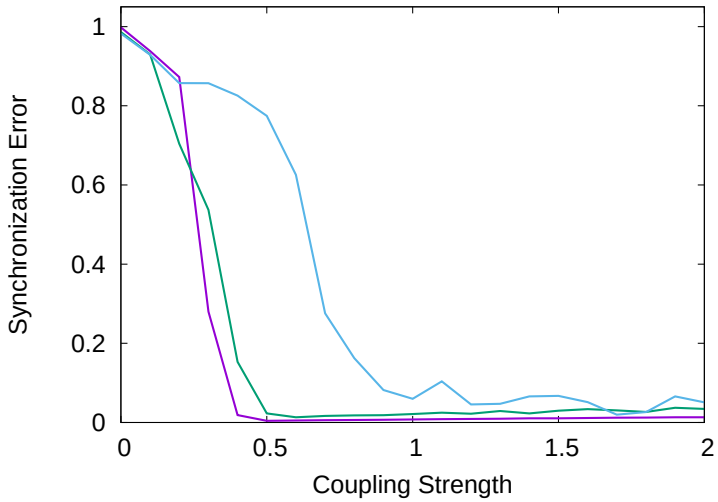

Figure 2.10: Synchronization error (averaged over 1000 random initial conditions) as a function of coupling strength C, for $p = 0$ (blue), and for $p = 0.8$ with static links (green) and dynamically varying links (purple). Here network size $N = 100$, global bias is $b = -0.1$ and $N_1 = 0$. Notice that both static random connections and time-varying random links yield similar results.

2.6 Fast synchronization in networks with time varying connections

We also consider the *efficiency of synchronization* in different kinds of networks. Comparison between Figs. 2.4 and 2.5 shows that synchronization occurs faster when the network has time-varying links rather than static links. This observation is corroborated quantitatively by studying the average time taken by a random initial network to reach the synchronized steady state, and it is clear from Fig. 2.11 that as the switching of links

becomes more frequent, the time taken to synchronize decreases. The underlying reason for this fast approach to the asymptotic state is the more efficient flow of information in a dynamically changing network, as many distant nodes get connected over a short period of time. So a network with rapidly varying links yields very fast synchronization.

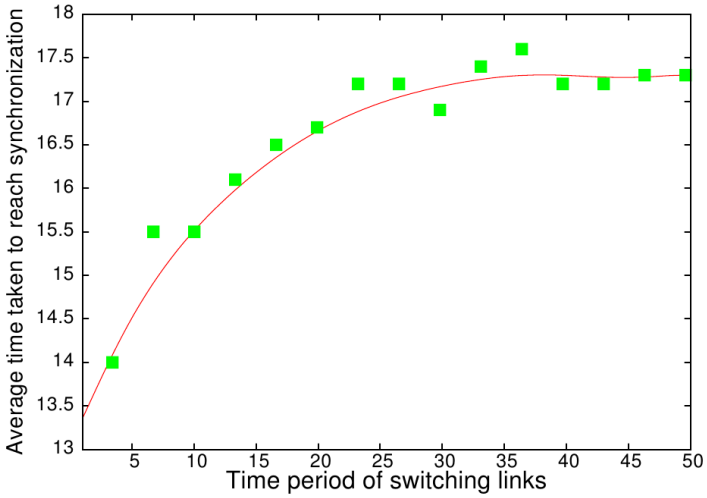

Figure 2.11: Average time taken by a network to reach the synchronized steady state, for different values of rewiring time period ranging from 0.1 to 50, with fraction of random links $p = 0.8$. Here $N_1 = 1$ and global bias $b = -0.1$ and system size $N = 100$.

So sufficient number of random links leads to synchronization of all elements in the network even when there is heterogeneity in the system. Further, when the connections are switched periodically this synchronization occurs more efficiently, and the time taken to reach the synchronized state is significantly smaller for dynamically changing connectivity.

2.7 Varying local dynamics and coupling range

Lastly, in order to gauge the generality of our observed phenomena under variation of the nodal dynamics, we investigated a coupled network where the local bistable system was given by:

$$\dot{x} = \begin{cases} \beta x_l^* - \alpha x & \text{if } x < x_l^* \\ (\beta - \alpha)x & \text{if } x_l^* \leq x \leq x_u^* \\ \beta x_u^* - \alpha x & \text{if } x > x_u^* \end{cases} \tag{2.4}$$

where x_u^* and x_l^* are the upper and lower thresholds respectively. This system also displays ultra-sensitivity when the coupling connections are sufficiently random. Since this piecewise-linear system has a simple and efficient circuit realization, it can potentially help one verify ultrasensitivity in experiments. Further, we investigated networks with larger coupling range, such as $k = 4$, and found similar behaviour, indicating the generality of the results(see Fig. 2.12 for some representative results).

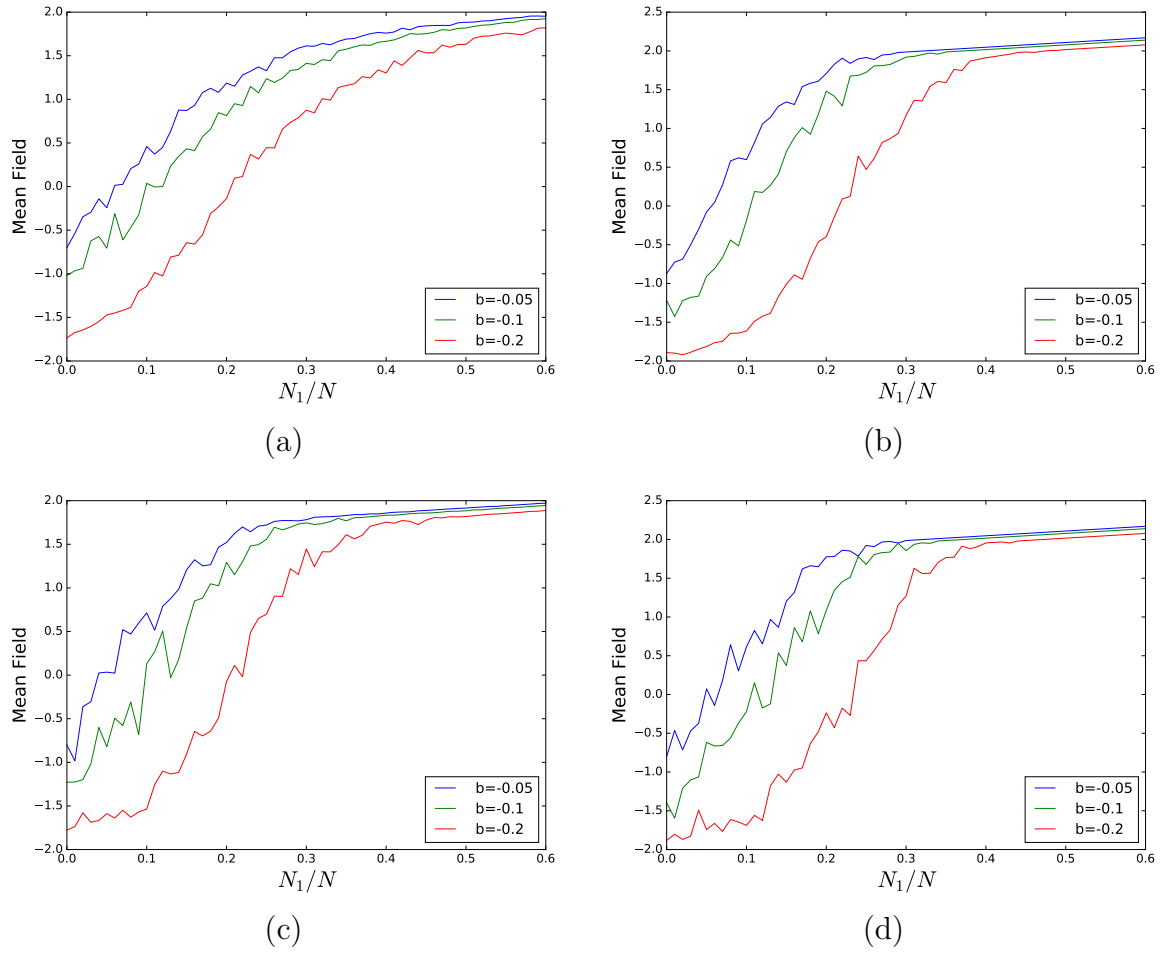

Figure 2.12: Average mean field as a function of N_1/N (i.e. fraction of elements with $a_i = 1$ in a network of size N), evolving for different values of global bias b. Here network size $N = 100$, and fraction of random links $p = 0.3$(a,b) and $p = 0.7$(c,d). Note that both static random connections(a,c) and time-varying random links(b,d) yield similar results.

Further, in order to demonstrate the generality of these observations, we also explored different networks of bistable *synthetic genetic networks*, where the nodal dynamics was given by [18, 19, 20]:

$$F(x) = \frac{m(1 + x^2 + \alpha\sigma_1 x^4)}{1 + x^2 + \sigma_1 x^4 + \sigma_1\sigma_2 x^6} - \gamma_x x \tag{2.5}$$

where x is the concentration of the repressor. The nonlinearity in this $F(x)$ leads to a double well potential, and different γ introduces varying degrees of asymmetry in the potential. We find that the qualitative trends in both these bistable systems is similar to that described above, indicating the generality of the central results presented here(see Fig. 2.13).

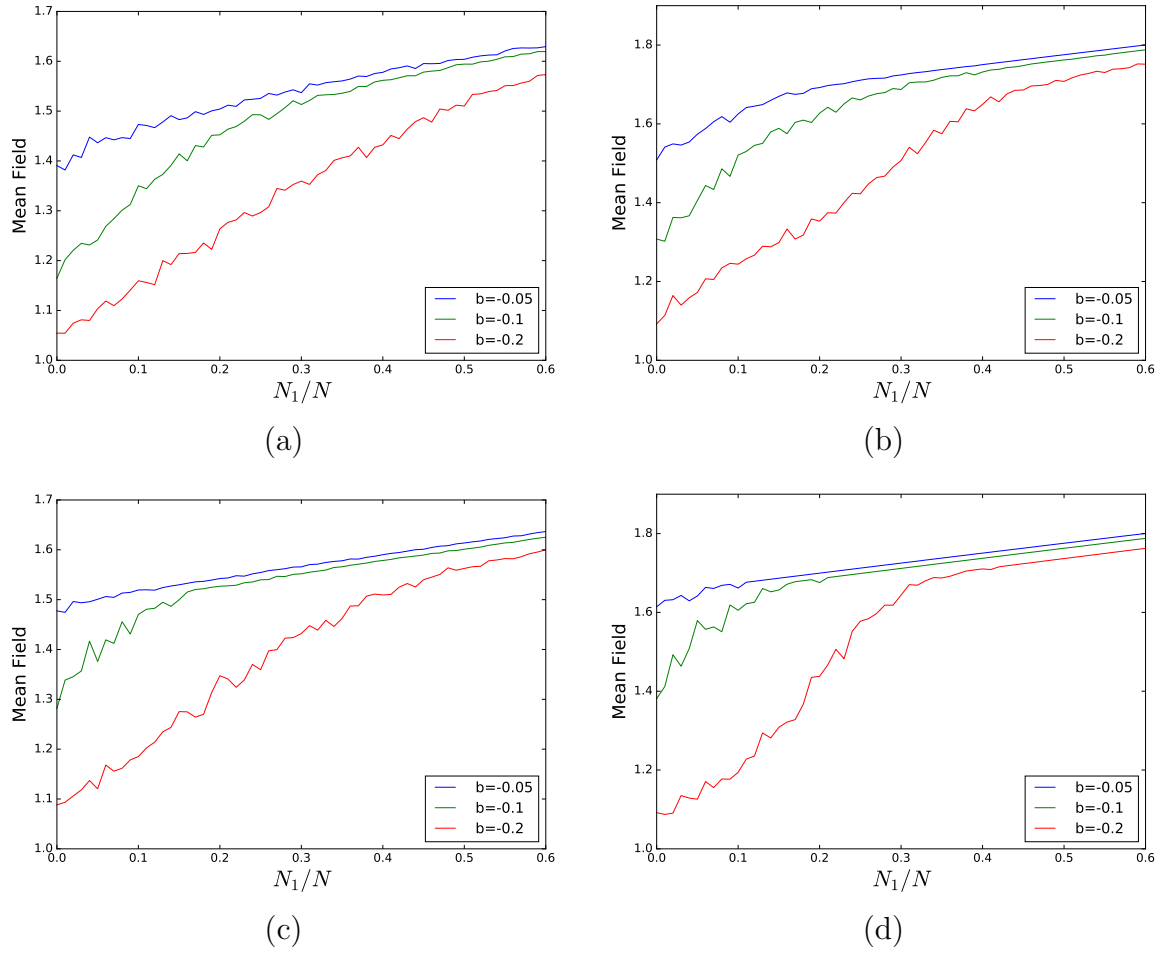

Figure 2.13: Average mean field as a function of N_1/N (i.e. fraction of elements with $a_i = 1$ in a network of size N), evolving for different values of global bias b. Here network size $N = 100$, and fraction of random links $p = 0.3$(a,b) and $p = 0.7$(c,d). Note that both static random connections(a,c) and time-varying random links(b,d) yield similar results.

2.8 Effect of noise

Additionally, we checked that the qualitative trends are not degraded by the presence of weak noise. This is indicative of the robustness of the phenomena. Thus we added noise

to the dynamical equation given by:

$$\dot{x_i} = G(x_i) + a_i + C\left[\frac{1}{k}\Sigma_{j=1}^{k}(x_j - x_i)\right] + b + D\eta \tag{2.6}$$

where η is obtained from a Gaussian distribution(mean 0, variance 1) and D is the strength of the noise. All other terms are as before(refer equation 2.1). We numerically integrated the above equation using the EulerMaruyama method.

Fig. 2.14 shows the results of our simulation. Clearly, we can observe that the qualitative trends of the phenomena is stable and persistent under low noise. Thus, we can guarantee the validity of hypersensitivity in practical applications.

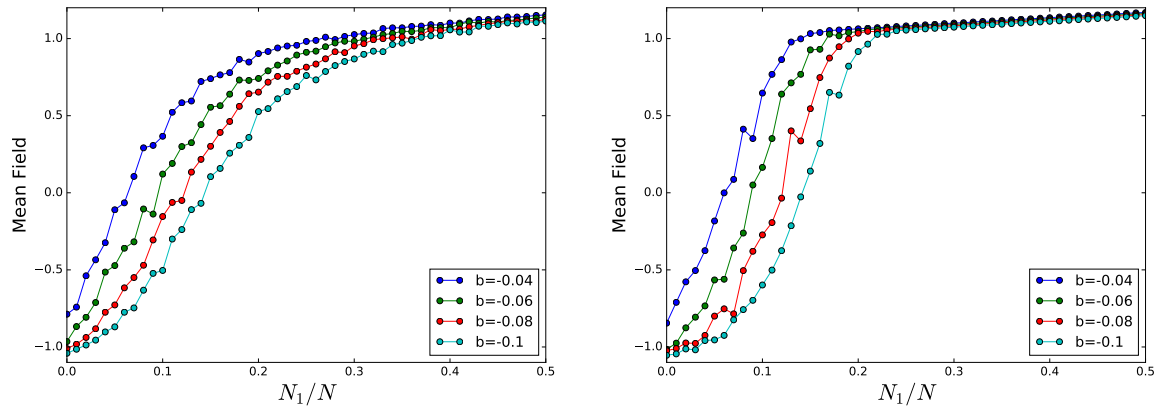

(a) (b)

Figure 2.14: Average mean field as a function of N_1/N (i.e. fraction of elements with $a_i = 1$ in a network of size N), evolving under the influence of low noise(D=0.1) for different values of global bias b. Here network size $N = 100$, and fraction of random links $p = 0.3$. Note that both static random connections(a) and time-varying random links(b) yield similar results.

2.9 Potential application

Without loss of generality, we use the bistable elements to stably encode N binary items (0 or 1) by setting a_i $(i = 1, \ldots N)$ to take values 0 or 1, respectively [see Fig.1(a)]. This creates a (unsorted) binary database. Then, using the scalable ultra-sensitivity demonstrated above, one can search this arbitrarily large database for the existence of a single different bit (say a single 1 in a string of 0's) by making just one measurement of the evolved mean field of the whole array. That is, a single global operation can determine

the existence of very few special items in a given, arbitrarily large, unsorted database of general items.

Lastly, we suggest this ultra-sensitivity may find application in handling problems involving a large number of variables, such as the important and difficult problem of designing search engines for large unsorted databases [4], which can be posed in layman's language as "finding a needle in a haystack". So a query such as the existence (or not) of any different bits in a collection of items, can be addressed without measuring the entire system item by item,. Rather, by using the ultra-sensitive response to heterogeneity, one can gauge the presence of a different element by just one mean field measurement.

2.10 Conclusion

In summary, in this work we have investigated the dynamics of networks of bistable elements with varying degrees of randomness in connections, considering both static random connections and time-varying random links. We probed how the presence of a few dissimilar elements affects the collective features of this system, and find that a network with random links is hyper-sensitive to heterogeneity. Namely, even a small number of distinct elements manages to drastically influences the collective dynamics of the network, with the mean-field swinging to the stable value of the minority elements. We find that the transition in the collective field gets sharper as the fraction of random links increases, for both static and time-varying links. We also demonstrated that networks where the links are switched more frequently, synchronize faster. Lastly, we showed that as global bias tends to a critical value, even a single different element manages to drag the entire system to the natural stable state of the minority element. So it is evident that when coupling connections are random, a network with even a very small number of links per node, has the ability to become ultra-sensitive to heterogeneity. This phenomenon can potentially be observed in social and biological networks [21], and implemented in experiments such as coupled nano-mechanical resonators [22, 23] and coupled laser arrays [24].

Chapter 3

Are network properties consistent indicators of synchronization?

Adapted from the work published in :

P. D. Rungta, A. Choudhary, C. Meena and S. Sinha EPL, **117** (2017) 20003 .

3.1 Introduction

Synchronization of complex networks has attracted wide research interest, from fields as diverse as ecology and sociology to power grids and climatology [25, 26, 16, 27]. Collective spatiotemporal patterns emerging in dynamical networks are determined by the interplay of the dynamics of the nodes and the nature of the interactions among the nodes. So it is of utmost relevance to ascertain how connection properties impact synchronization, and this important issue has attracted much research effort, though still not attained clarity yet [28, 29, 30, 31, 32].

In broad terms, the concept of synchronization provides a general approach to the understanding of the collective behavior of coupled dynamical systems, and the term has expanded in usage to include several types of correlated collective behaviour, such as complete synchronization, generalized synchronization, phase synchronization, lag synchronization, and anticipated synchronization. The unifying thread in all the different types of synchronization is the emergence of a consistent relationship between the variables of a set of dynamical systems, and this can arise in contexts ranging from simple first-order phase oscillators to complex chaotic systems. Further, these types of synchronization apply to both mono-stable, as well as multi-stable systems [33]. However, while synchronization in mono-stable systems is commonly studied, synchronization of multi-stable systems is still not that well explored. One underlying reason for this, is that the concept of a linearly stable synchronized state is inadequate to capture the collective dynamics of multi-stable systems, and consequently even the simple phenomenon of complete synchronization necessitates global measures in order to adequately understand the collective behaviour in systems with co-existing attractors [34, 35].

In this chapter, we consider the collective dynamics of a group of bistable elements connected in different network topologies, ranging from regular rings and small-world networks on one hand, to deterministic scale-free and random scale-free networks on the other. Bistable systems are relevant in a variety of fields, ranging from relaxation oscillators and multivibrators, to light switches and Schmitt triggers. The basic question we will address is the following: are there features of the underlying connection network that provide *consistent markers* for the emergence of *complete synchronization* and the robustness of the synchronized state? Specifically, complete or identical synchronization is the phenomena where the difference between the dynamical variables of the constituent dynamical systems in the network is zero. Since we consider bistable systems, complete synchronization here naturally implies that all nodes in the network evolve to the same

well.

In particular, we consider the system of N coupled bistable elements given as:

$$\dot{x_i} = F(x_i) + \epsilon \frac{1}{k_i} \sum_j (x_j - x_i) \tag{3.1}$$

Here i is the node index ($i = 1, \ldots N$) and ϵ is the coupling constant, reflecting the strength of coupling. The j in Eqn. 3.1 gives the node index of the set of k_i "neighbours" of the i^{th} node, with the set depending on the topology of the underlying connectivity. The function $F(x)$ gives rise to a double well potential, with two stable states x^*_- and x^*_+. For instance one can choose

$$F(x) = x - x^3$$

yielding two stable steady states $x^*_\pm$ at $+1$ and -1, separated by an unstable steady state at 0. So complete synchronization in this network implies that the dynamical variable x_i evolves to the same well, for all i (namely all $x_i > 0$, or all $x_i < 0$, in this particular case).

We explore the behaviour of these bistable dynamical elements coupled in five distinct network classes, namely:

i) Ring: Here each node has degree K (K even) and is connected to $K/2$ nearest neighbors on either side(see fig. 3.1). Namely, $k_i = K$ for all nodes i in Eqn. 3.1, with connections existing between node i and j if $0 < |i-j| \bmod (N - 1 - \frac{K}{2}) \leq \frac{K}{2}$. The clustering coefficient C in a ring is independent of size, and its value for $K = 2$ is zero, while for $K = 4$ it is 0.5. The characteristic path length L is $\frac{N}{2K}$, and it increases linearly with size N.

ii) Star network: here all the peripheral nodes are attached to one hub(see fig.3.2). The clustering coefficient of this network is zero, and its path length tends to 2 for large networks.

iii) Small-World network: This is constructed via the Watts-Strogatz algorithm [6]. Namely, we start from a ring with vertices having degree K (as in 1 above), and then rewire links to random non-local nodes with probability p(see fig. 3.3). Here $k_i = K$ in Eqn. 3.1, with j being nearest neighbours with probability $1 - p$ and random non-local nodes with probability p. For $K = 2$, the clustering coefficient C varies from 0 at $p = 0$, to around 0.02 at $p \sim 1$. The characteristic path length

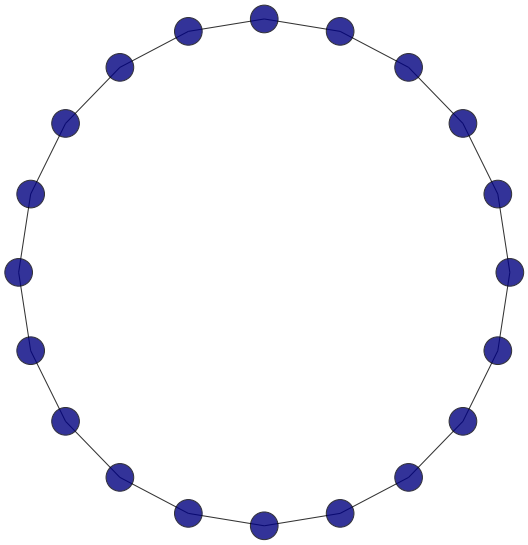

Figure 3.1: Construction of a Ring Network of size $N = 20$ and $k = 2$.

varies from ~ 25 at $p = 0$ to around 5.5 at $p \sim 1$.

iv) Deterministic Scale-Free: this has the particular hierarchical structure, generated iteratively for different orders (denoted by g) [37]. Here the order g, which is the only relevant network parameter, determines the number of nodes in the network, with $N = 3^g$(see fig. 3.4). Here the set of neighbours for node i are all the nodes directly connected by an edge. It can be shown analytically that the degree distribution $P(k)$ is a power-law here, as in the Random Scale-Free case. Namely $P(k) \sim k^{-\gamma}$ with exponent $\gamma = \frac{\ln 3}{\ln 2}$ [37]. In Deterministic Scale-Free networks, the clustering coefficient is zero, and the characteristic path length depends on the order g. Table 3.1 lists the characteristic path lengths L for Deterministic Scale-Free networks with $g = 3, 4, 5, 6$.

Deterministic Scale-Free Network	N	L
$g = 3$	27	2.77
$g = 4$	81	3.51
$g = 5$	243	4.46
$g = 6$	729	5.34

Table 3.1: Mean Path Length L of Deterministic Scale-Free (DSF) networks of different size $N = 3^g$. Here the degree distribution is $P(k) \sim k^{-1.585}$.

v) Random Scale-Free: this is constructed via the Barabasi-Albert preferential attachment algorithm, with the number of links of each new node denoted by parameter m [36](see fig. 3.5,3.6). The network is characterised by a fat-tailed degree

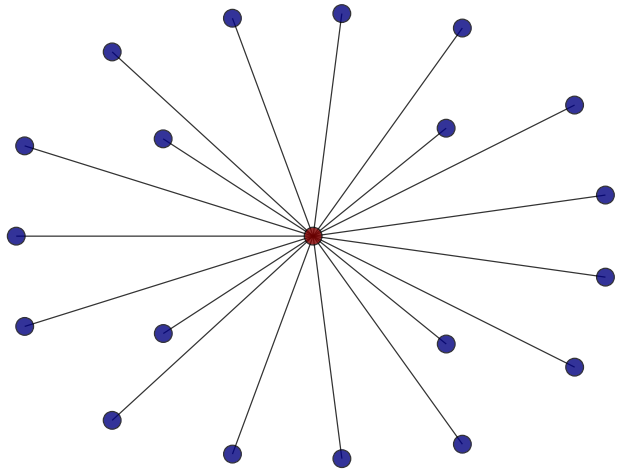

Figure 3.2: Construction of a Star Network of size $N = 20$.

distribution. The clustering coefficients C and characteristic path lengths L, depends on m. Table 3.2 lists the clustering coefficients C and characteristic path lengths L for Random Scale-Free networks with $m = 1, 2, 3, 4$.

Random Scale-Free Network	C	L
$m = 1$	0.00	4.67
$m = 2$	0.14	2.99
$m = 3$	0.16	2.58
$m = 4$	0.19	2.35

Table 3.2: Clustering Coefficient C and Mean Path Length L of Random Scale-Free (RSF) networks with varying m (see text) consisting of 100 nodes. Here the degree distribution of the RSF is $P(k) \sim k^{-3}$, for all m.

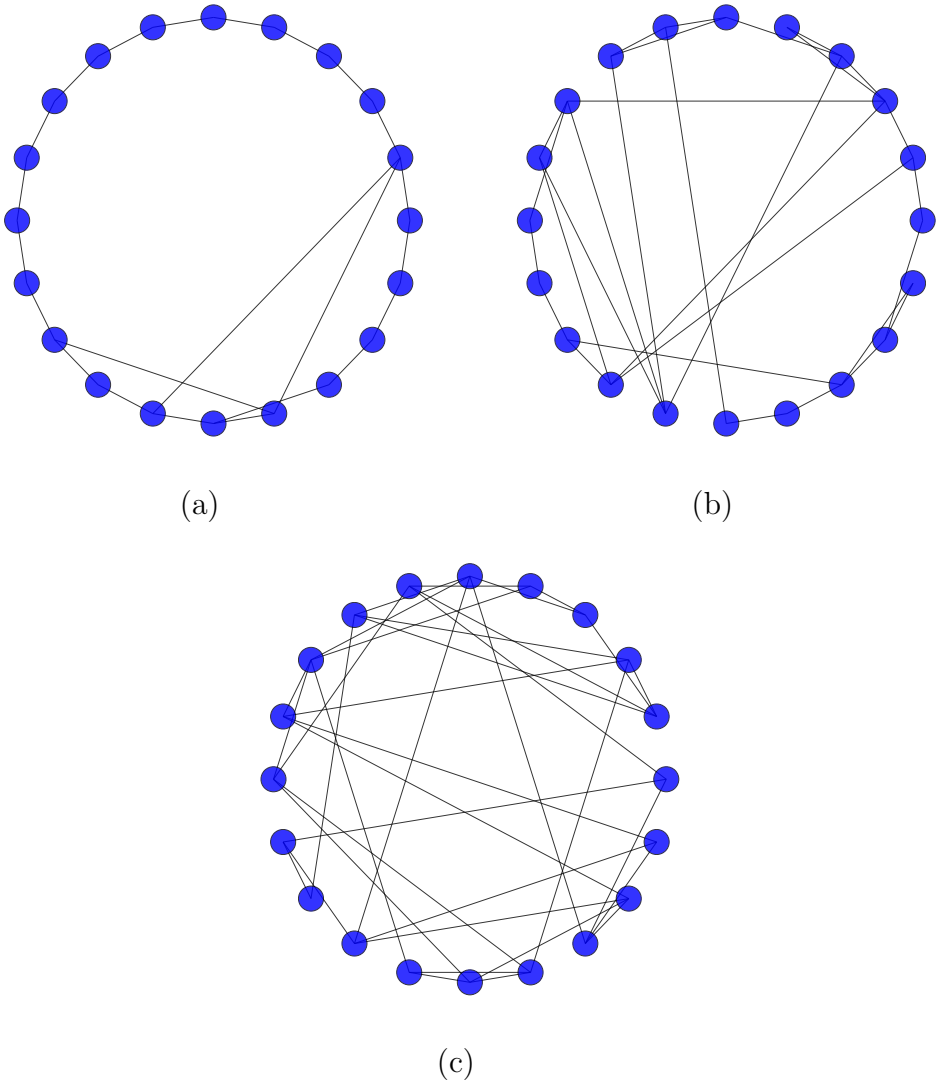

Figure 3.3: Construction of a Small world Network (adapted from Ref. [6]) of size $N = 20$ for different fractions of random link ($p = 0.1$(a), $p = 0.5$(b), $p = 0.9$(c)).

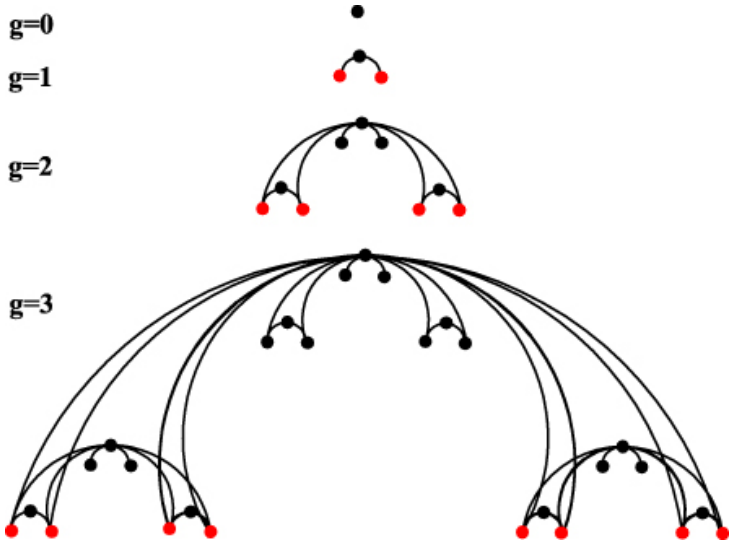

Figure 3.4: Construction of a Deterministic Scale-Free Network (adapted from Ref. [37]).

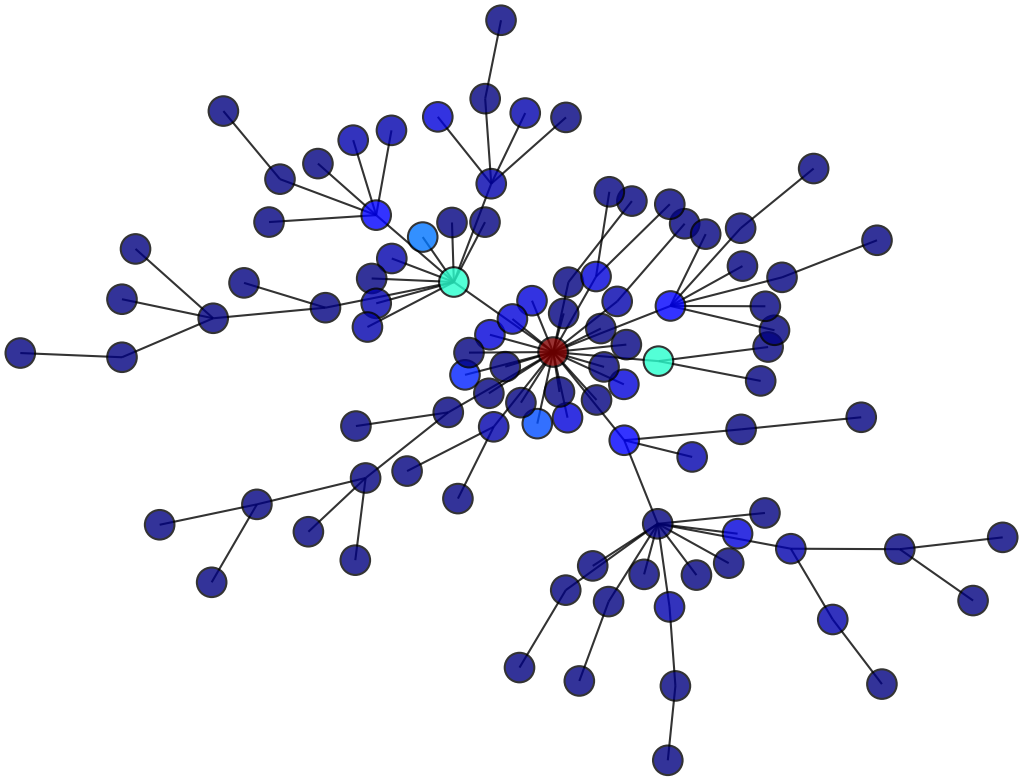

Figure 3.5: Construction of a Scale-Free Network (adapted from Ref. [36]) of size $N = 100$ with $m = 1$.

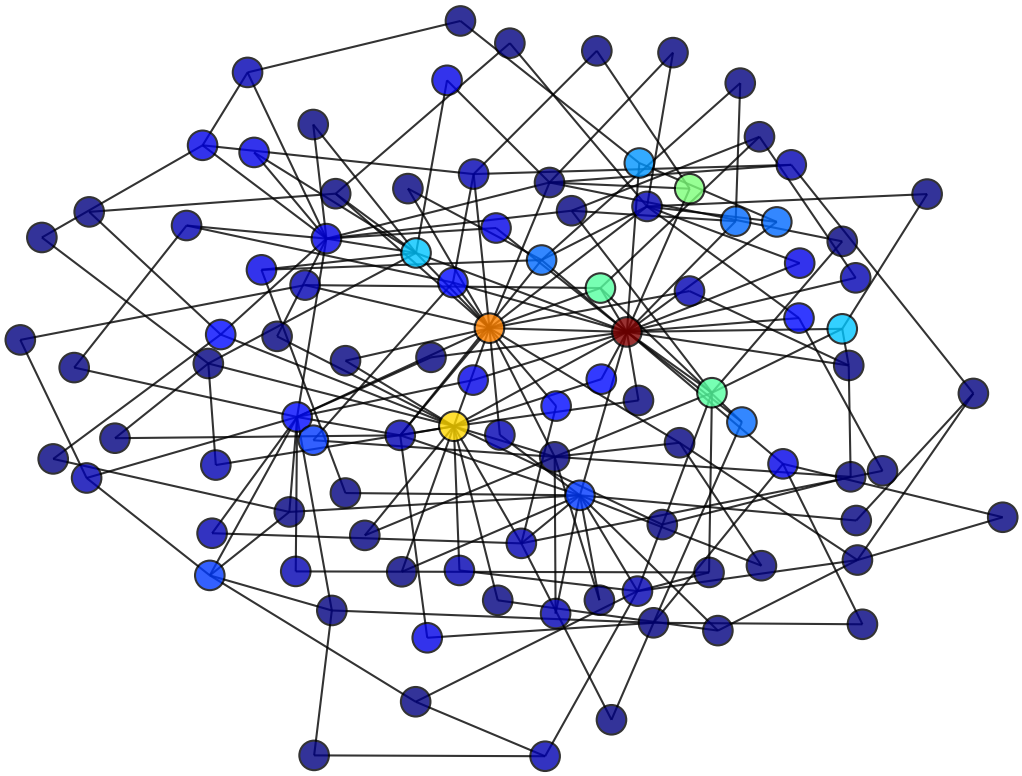

Figure 3.6: Construction of a Scale-Free Network (adapted from Ref. [36]) of size $N = 100$ with $m = 2$.

3.2 Analysis of synchronized state

The focus of our investigation is the asymptotic state of the coupled bistable elements, starting from a random initial state which can be very far from the synchronized state. Our attempt is to *determine which connection topologies, typically, are most conducive to attracting all the elements to the same well.* Note that synchronization of a system depends on the particular realization of the connection network, and so systems with the same network parameters may yield different synchronization transitions [28, 29]. The measure of relevance for a network class would then be some averaged quantity, reflecting the typical behaviour arising from a generic random initial state and network realization.

So, in this work, we estimate the average critical coupling strength characteristic of a network, denoted by $\langle \epsilon_c \rangle$. This is the coupling strength after which synchronization occurs for a specific initial state and a specific realization of the network,averaged over a large range of initial states and network realizations. smaller values of this global averaged quantity $\langle \epsilon_c \rangle$ indicates that the synchronization transition occurs at weaker coupling strengths on average, namely the system is typically more easily synchronized.

Figs. 3.7-3.8 shows the synchronization error, given by the time and ensemble-averaged mean square deviation of the spatial profile, for different network classes: rings, small-world networks, Random Scale-Free networks, Deterministic Scale-Free networks and star networks. The central observations are the following:

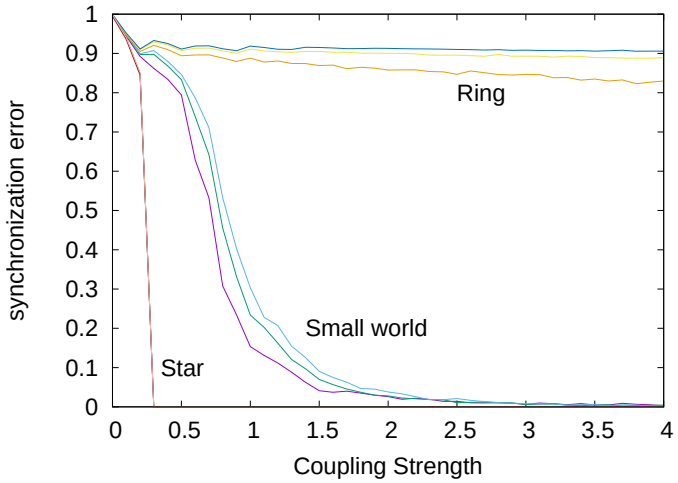

Figure 3.7: Synchronization error for varying coupling strengths, for a system of coupled bistable elements given by Eqn.3.1, with different underlying connection networks: regular Ring with $K = 2$ ($N = 100, 250, 500$ shown in orange, yellow, navy blue respectively), Small-World network with $K = 2$ and $p = 0.5$ ($N = 100, 250, 500$ shown in violet, green, blue respectively) and Star (for $N = 100, 250, 500$ shown in red, black, pink respectively).

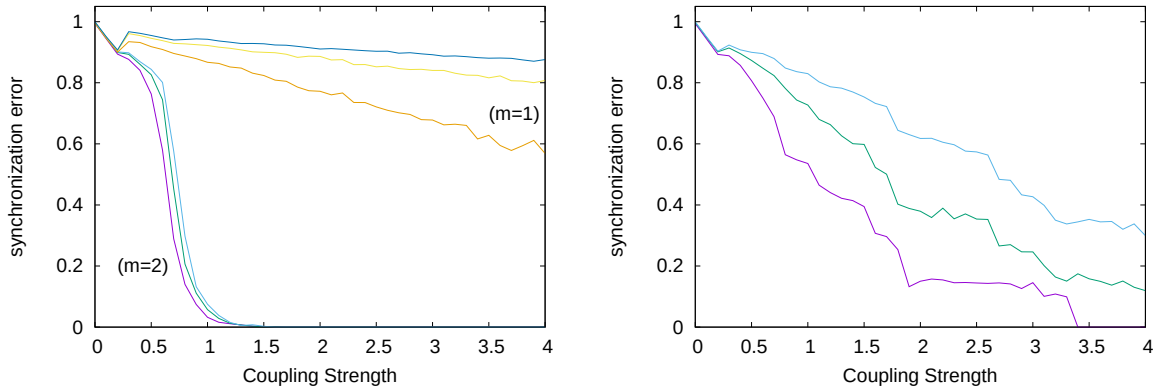

(a) (b)

Figure 3.8: Synchronization error for varying coupling strengths, for a system of coupled bistable elements given by Eqn.3.1, with different underlying connection networks: (a) Random Scale-Free for $N = 100, 250, 500$ shown in violet, green, blue for $m = 1$ and $N = 100, 250, 500$ shown in orange, yellow, navy blue for $m = 2$ respectively, and (b) Deterministic Scale-Free (for $N = 81, 243, 729$ shown in violet, green, blue respectively).

(i) The Star network synchronizes most readily, with the synchronization transition occurring at very low coupling strength, irrespective of the size of the network (cf. Fig. 3.7).

(ii) Small-World networks with high degree of randomness in connections (namely high p) also yield synchronization at low coupling strengths. Fig. 3.9 shows the average synchronization error as a function of coupling strength, for varying fractions of random links p in the Small-World network. It is clearly evident that as p increases, synchronization occurs at increasingly weaker coupling strengths. Namely, the critical coupling $\langle \epsilon_c \rangle$ after which synchronization ensues, decreases with increasing p. So it is clear that a *greater degree of randomness in networks, where characteristic path lengths are significantly shorter, assists synchronization.*

(iii) Rings and Deterministic Scale-Free networks and Random Scale-Free networks with $m = 1$ (namely, where a new node has one link to the existing nodes) *do not yield synchronization* even for very high coupling strengths (cf. Fig. 3.8).

(iv) However, Random Scale-Free networks with $m \geq 2$ (namely, where a new node has two or more links to the existing nodes), allows stable synchronization, even for low coupling strengths (cf. Fig. 3.8).

So the synchronization transition is markedly different in Random Scale-Free networks having the same qualitative degree distribution, but different path lengths, as evident through the lack of synchronization of Random Scale-Free networks with $m = 1$ vis-a-vis

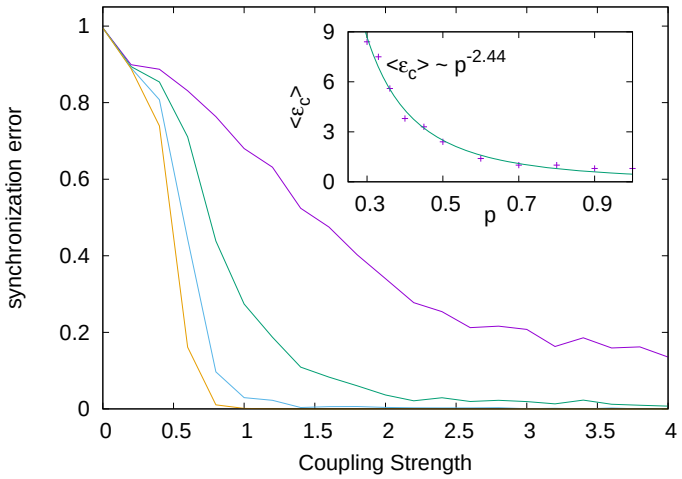

Figure 3.9: Synchronization error as a function of varying coupling strengths, for a system of coupled bistable elements given by Eqn.3.1, in Small-World networks having different fractions of random links p ($p = 0.2, 0.4, 0.6, 0.8$ for violet, green, blue, orange respectively). Here $N = 100$. Inset: Dependence of the average critical coupling strength for the onset of synchronization $\langle \epsilon_c \rangle$, on the fraction of random links p in Small-World networks. The points are obtained from numerical simulations and the solid line displays the best fit curve.

the efficient synchronization of Random Scale-Free networks with $m \geq 2$. This indicates that degree distribution does not influence synchronization [28], though the characteristic path length needs to be sufficiently small in order to give rise to a stable synchronized state.

Additionally there is also very notable difference in the synchronization properties of Deterministic Scale-Free networks and Random Scale-Free networks with higher m, both of which have power-law degree distributions but markedly different characteristic path lengths. This further corroborates that, while *shorter characteristic path lengths assists synchronization*, the *qualitative nature of the degree distribution is not the key feature that determines synchronization.*

Further, the heterogeneity of degree also does not consistently influence synchronization either [30]. This is clearly inferred through the stark difference in the synchronization of Rings and Small-World networks (where the mean square deviation of the degree is zero) and Star networks (where the mean square deviation of the degree tends to zero in the limit of large N).

3.3 Dependence of critical coupling strength on system size

In this section, we estimate the average critical coupling strength characteristic of a network, denoted by $\langle \epsilon_c \rangle$. This is the coupling strength after which synchronization occurs for a specific initial state and a specific realization of the network, averaged over a large range of initial states and network realizations. Smaller values of this global averaged quantity $\langle \epsilon_c \rangle$ indicates that the synchronization transition occurs at weaker coupling strengths on an average, namely the system is typically more easily synchronized. Figure 3.10 show the dependence of critical coupling on system size N in different classes of networks.

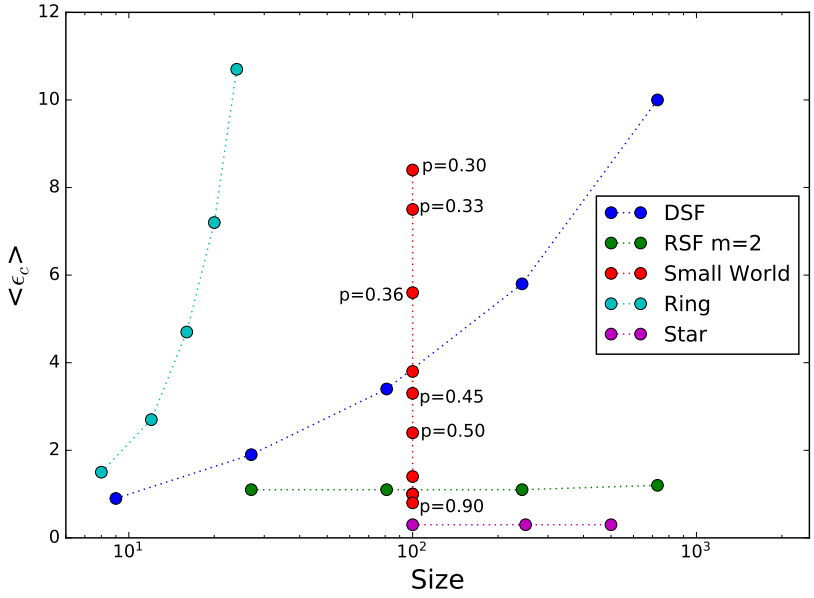

Figure 3.10: Dependence of Critical coupling strength $\langle \epsilon_c \rangle$ on system size N in different classes of networks.

Further, we investigate the variation of critical coupling strength in small world networks for different fractions of random links. Figure. 3.11 shows the average trend and demonstrates the power law fit for the data.

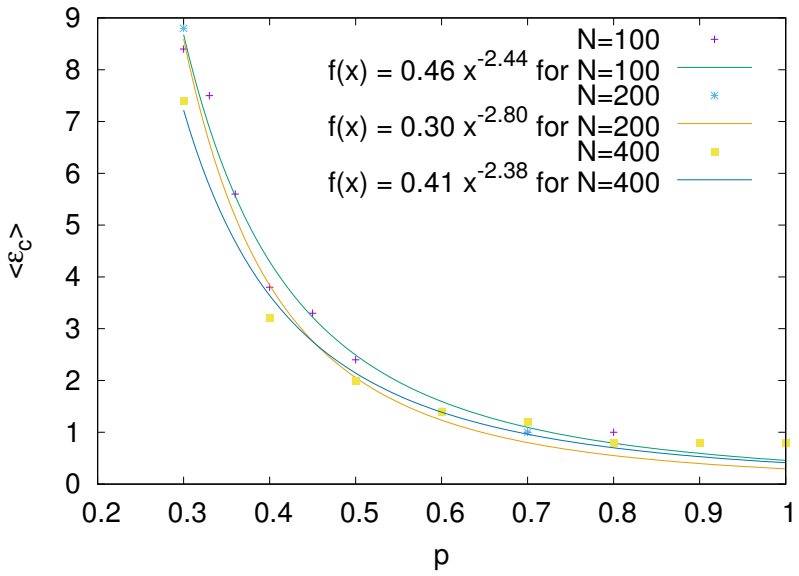

Figure 3.11: Dependence of Critical coupling strength $\langle \epsilon_c \rangle$ on fraction of random links p in small world network for size $N = 100$.

3.4 Comparative synchronizability of different network classes

Inspite of a wide range of studies over the years, no clear picture has emerged on what class of networks synchronize most readily [28, 29, 30, 31, 32]. Here we address this issue by attempting to compare the average critical coupling strength of different network classes (cf. Fig. 3.12). Further, we will try to correlate this with the characteristic path length, which emerged as the network property which most strongly impacts synchronization.

Fig. 3.13 shows the dependence of $\langle \epsilon_c \rangle$ of different classes of networks on characteristic path length [1]. It is clearly evident that, within a particular network class, decreasing path length improves synchronization.It is clear from Fig. 3.7 and Fig. 3.8 that for Star, Random Scale-Free and Small-World networks, changing system size N does not make any appreciable difference. On the other hand, synchronization properties of the Ring is very sensitive to system size. This again is directly related to the sensitivity of the characteristic path length of these networks to size N (cf. Fig. 3.14).

[1] Specifically, the value of critical coupling is given by the minimum ϵ beyond which the time and ensemble-averaged synchronization error is bounded within a prescribed threshold. Note that the qualitative trends reported here are robust under variation of threshold values over orders of magnitude. In a broader context, the critical coupling thus defined is relevant experimentally, as all instruments have finite sensitivity (namely, least count). So in practice the synchronization error cannot be zero with infinite precision and only bounds on the synchronization error are relevant.

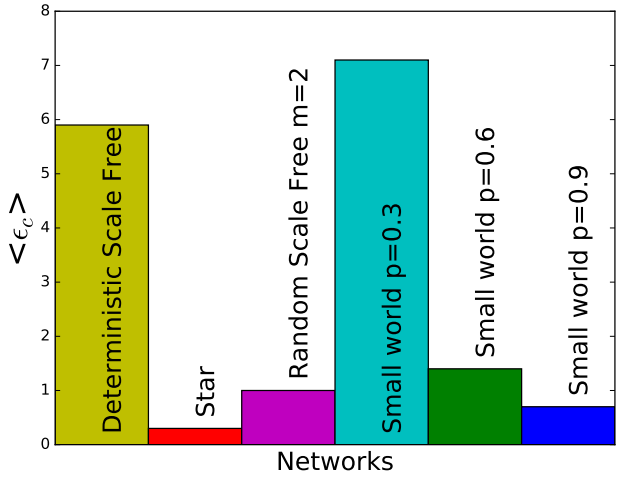

Figure 3.12: Average critical coupling $\langle \epsilon_c \rangle$ for different classes of networks. Ring and Random Scale-Free networks with $m = 1$ do not synchronize at all for $\epsilon \leq 10$, and thus do not appear in the figure. Here system size is $N = 243$ for all networks, and the threshold synchronization error is considered to be 0.02. Low $\langle \epsilon_c \rangle$ (namely, low bars) indicate greater ease of synchronization.

We also probe the commonly used measures of synchronizability obtained through the linear stability analysis to check if it can offer a more consistent indicator of $\langle \epsilon_c \rangle$. Since the average critical coupling strength is obtained by sampling a large set of initial conditions, typically far from the synchronized state, it provides a global indicator of the stability of the synchronized state. So at the outset it is not clear how local measures can capture these global trends. In order to ascertain the correlation of local synchronizability measures and the average critical coupling, we calculated the synchronizability measure obtained through master stability analysis. Following the formalism outlined in Ref. [38], the synchronizability index of a system of size N can be assessed by the spread of eigen-values of the network Laplacian L (defined as $L = D - A$, where D is diagonal of row sums of the network adjacency matrix A). Ordering the eigen-values as: $0 = \lambda_1 < \lambda_2 \leq \lambda_3 \leq \ldots \lambda_N$, where λ_1 has multiplicity 1 and all other eigen-values are strictly positive, the synchronizability index is given by the ratio $\frac{\lambda_2}{\lambda_N}$, with larger values of this ratio implying greater propensity for synchronization.

It can be seen from Fig. 3.15 that a similar trend as observed above is followed from Synchronizability analysis i.e., within a class of network, decreasing path length improves synchronizability.

However there is a caveat: across network classes the comparison does not hold. First, there does not appear to be a critical characteristic path length, below which

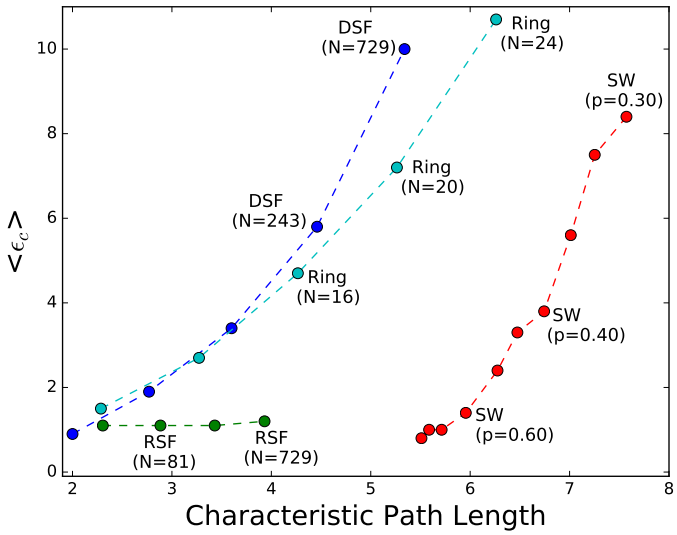

Figure 3.13: Average critical coupling $\langle \epsilon_c \rangle$ vs characteristic path length of different network classes: Deterministic Scale-Free (DSF) in blue, Random Scale-Free (RSF) with $m = 2$ in green, Small-World (SW) in red and Ring with $K = 2$ in cyan. Here the system size of the DSF networks and RSF networks vary from 27 to 729, and the system size of the Ring varies from 8 to 24. SW networks with varying p are shown, for network size $N = 100$.

synchronization is ensured. Nor is there a one-to-one correspondence between path length and ease of synchronization. For example, Small-World networks with high p have greater characteristic path lengths than certain Ring and the Deterministic Scale-Free networks. Yet these Ring and Deterministic Scale-Free networks are much harder to synchronize and consequently have significantly higher $\langle \epsilon_c \rangle$.

Fig. 3.16 shows the dependence of $\langle \epsilon_c \rangle$ of Random Scale Free and Small world network on clustering coefficient. It is observed that within a network class, increasing clustering coefficient aids synchronization. However the sensitivity of synchronization on clustering coefficient in the different network is markedly different. For instance, in Random Scale-Free networks increasing the clustering coefficient has very little effect on the critical coupling strength, while in Small-World networks the effect is stronger. The lack of one-to-one correspondence is very pronounced for the case of clustering coefficient, as evident through the extremely different synchronization properties of Star networks and Rings with nearly same clustering coefficients, and almost same synchronization properties of Rings with very different clustering coefficients. Further that symmetry of the connection graph, as reflected by the order of its automorphism group, is also not a consistent indicator of the synchronization efficiency. This is evident from the fact that the ring which has more symmetry than small-world networks is less synchronizable than small-

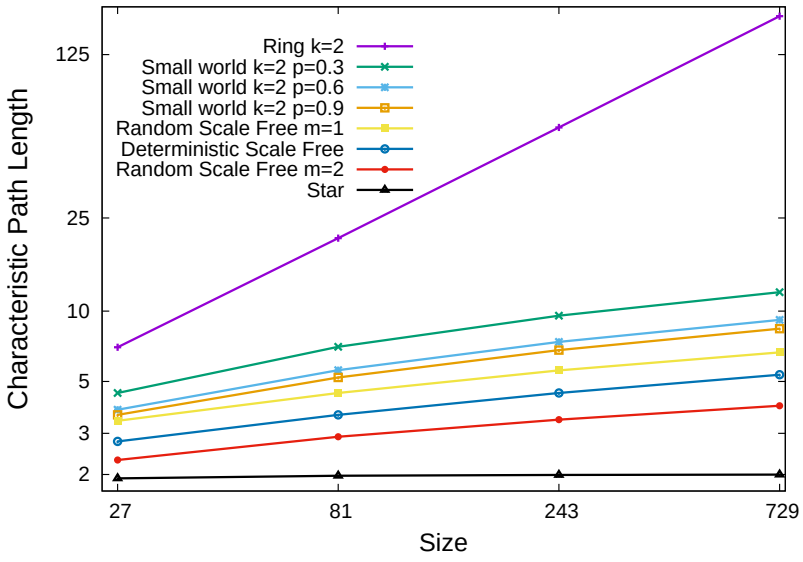

Figure 3.14: Dependence of Characteristic Path Length on system size N in different classes of networks.

world systems, while a star network with much more symmetry than small-world networks is much more synchronizable.

The results are displayed in Fig. 3.17, and it is evident again that there is *no one-to-one correspondence* between synchronizability (as defined above) and the average critical coupling. For instance, we observe that a Small-World network and a ring, with the *same* value of synchronizability have *different* average critical coupling strengths. So the relationship between synchronizability and the average critical coupling strength is not one-to-one, and *same values of synchronizability do not guarantee that the network will synchronize at similar coupling strengths on an average.* Further, the dependence of $\langle \epsilon_c \rangle$ on synchronizability shows different trends for different network classes, with $\langle \epsilon_c \rangle$ decreasing much faster with respect to synchronizability for some networks (such as Small-World networks), and quite slowly for others (such as Deterministic Scale-Free networks).

Lastly, we check if a combination of the two properties clustering coefficient and Characteristic Path Length offers a complete picture of the properties determining synchronization. Fig. 3.18 suggests that there is no such correlation. All this suggests that linear stability approaches, like Master Stability Function analysis, also does not offer a complete picture for global measures of synchronizability.

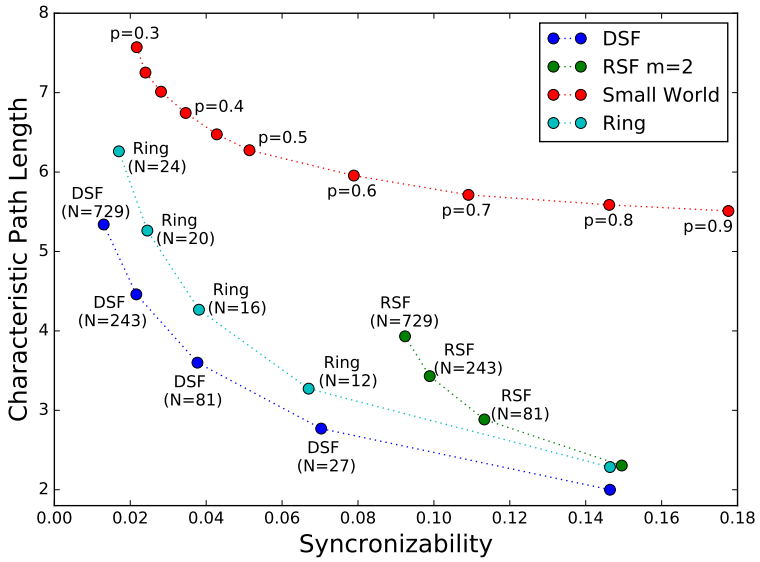

Figure 3.15: Dependence of Characteristic Path Length on Synchronizability in different classes of networks.

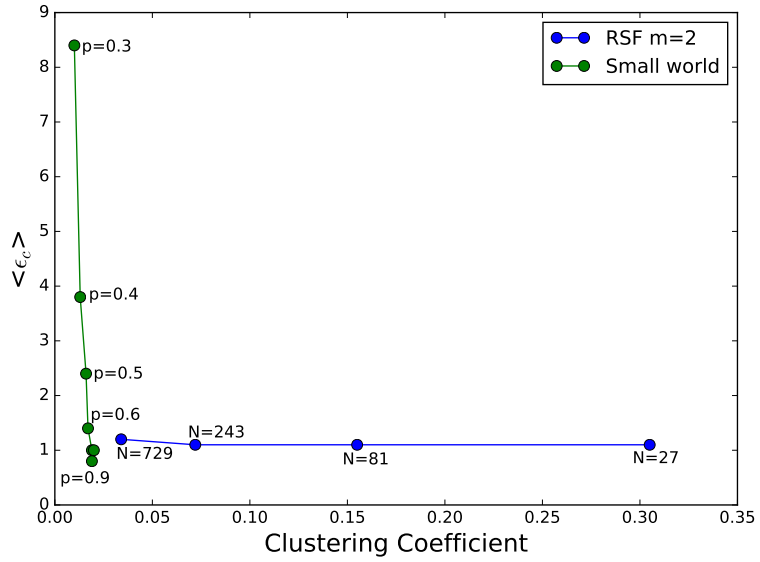

Figure 3.16: Average critical coupling $\langle \epsilon_c \rangle$ vs clustering coefficient for the case of (a) Random Scale-Free (RSF) networks (blue) and (b) Small-World (SW) networks (green).

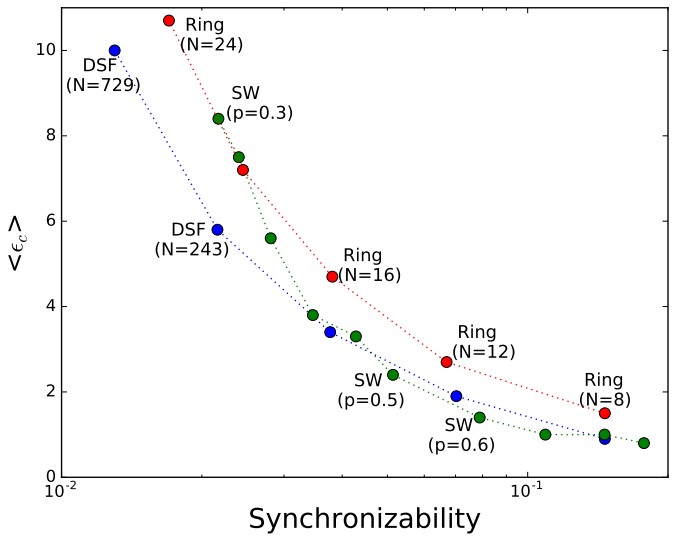

Figure 3.17: Average critical coupling vs Synchronizability ($\frac{\lambda_2}{\lambda_N}$) of different networks: Deterministic Scale-Free (DSF) in blue, Small-World (SW) in green and Ring in red. Here the system size of the DSF network ranges from 81 to 729, the system size of the Ring varies from 8 to 24 and the system size of the SW network is $N = 100$, with varying fractions p of random links ($p \in [0.3 : 0.9]$). Each node has two neighbors in the Ring and the Small-World network.

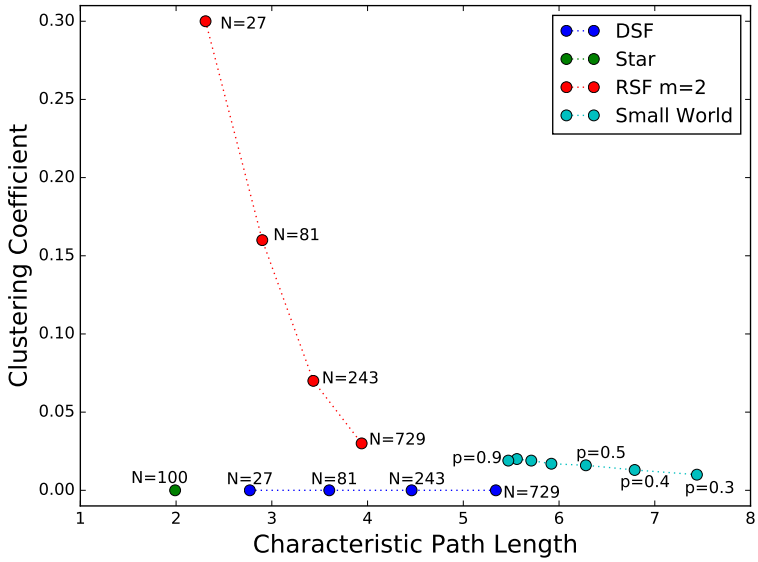

Figure 3.18: Dependence of Characteristic Path Length on Synchronizability in different classes of networks with (i) Deterministic Scale-Free network (DSF) of varying size N ($N = 3^g$) (ii) Star of size $N = 100$ and (iii) Random Scale-Free network (RSF) of varying size N with $m = 2$ (iv) Small-World network (SW) of size $N = 100$ and varying fraction of random links p, .

3.5 Robustness of the Synchronized State

To check the robustness of the synchronized state, we now investigate the number of elements that need to be perturbed in order to push the system away from the synchronized state. In order to gauge this we calculate a measure, denoted as f-node basin stability, given as follows: we initialize the network to its synchronized stable state, with a small spread in the values of x_i, all of which are in the same well. We then perturb f number of randomly chosen nodes such that the values of x_i for these nodes are strongly perturbed and kicked to the basin of attraction of the other well. We then ascertain whether all the elements return to the original well after this perturbation. We repeat this "experiment" over a large sample of perturbed nodes and perturbation strengths, and find the fraction of times the system manages to revert to the synchronized state. This measure is quite analogous to Basin Stability measures [34], and is indicative of the robustness of the synchronized state to localized perturbations in the network.

It can be observed in figure 3.19-3.21 that the synchronized state of bistable elements coupled in a ring is robust if the number of nodes perturbed is less than approximately 10%. Similar robustness holds for bistable elements coupled in a Deterministic Scale-Free network. If the number of nodes perturbed is more than about 15%, one almost never obtains a state where all nodes are in the original well. In contrast, it can be seen that the synchronized state of bistable elements coupled in a Small-World network, or a Random Scale-Free network with $m = 2$, is robust even when the number of nodes perturbed is as high as 40-45%.

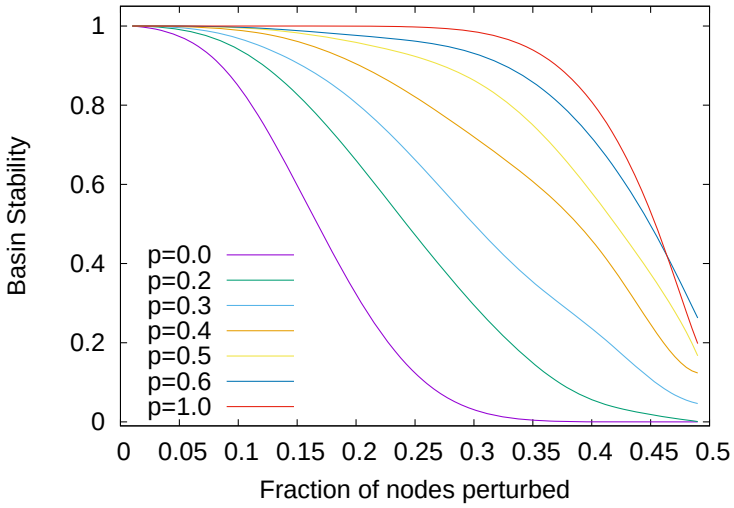

Figure 3.19: Basin Stability (namely, fraction of perturbed systems that remain synchronized) vs fraction of nodes perturbed, in a system of N bistable elements coupled in (a) Small-World (SW) network for different values of fractions of random links.

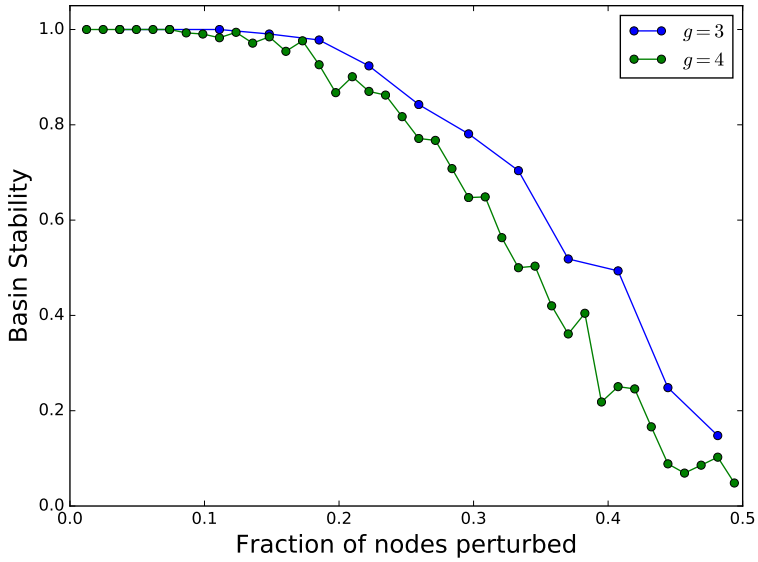

Figure 3.20: Basin Stability (namely, fraction of perturbed systems that remain synchronized) vs fraction of nodes perturbed, in a system of N bistable elements coupled in Deterministic Scale-Free (DSF) network with $g = 3$ and $g = 4$.

Further we can obtain the critical number of nodes f_c needed, on an average, to destroy synchronization, namely the value of f for which the Basin Stability falls below a threshold value (taken to be ≈ 0.9 here). Fig. 3.22 displays this as a function of characteristic path length for the Small-World case. It is apparent that the number of nodes that need to be perturbed increases significantly with decreasing characteristic path length. However, again, across network classes there is no one-to-one correspondence between critical fraction f_c and the characteristic path length. This is clear from the comparison of Random Scale-Free networks and Small-World networks, which have similar f_c, but very different characteristic path lengths. Further, Deterministic Scale-Free networks having shorter characteristic path lengths than Small-World networks have considerably lower f_c, namely less robust synchronized states.

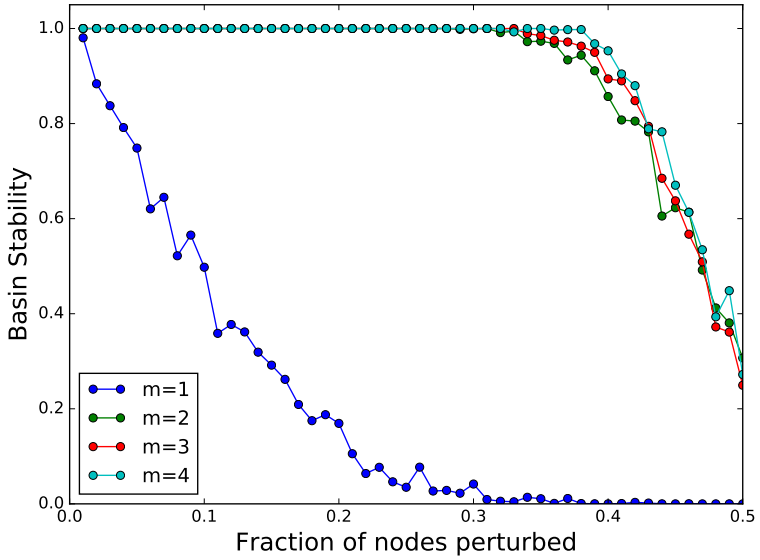

Figure 3.21: Basin Stability (namely, fraction of perturbed systems that remain synchronized) vs fraction of nodes perturbed, in a system of N bistable elements coupled in Random Scale-Free (RSF) network (green) with $m = 1, 2, 3, 4$ and $N = 100$.

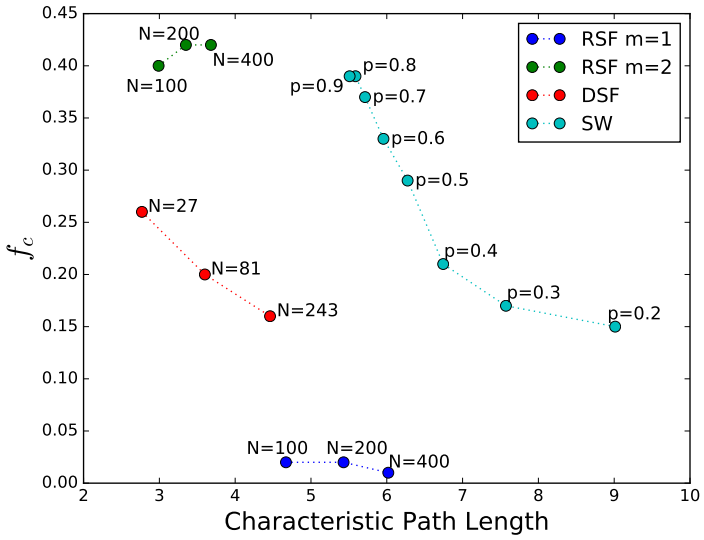

Figure 3.22: Average critical fraction f_c of nodes that need to be perturbed in order to destroy the synchronized state, as a function of characteristic path length, for (i) Small-World network (SW) of size $N = 100$ and varying fraction of random links p, (ii) Random Scale-Free network (RSF) of varying size N with $m = 1$ and $m = 2$ and (iii) Deterministic Scale-Free network (DSF) of varying size N ($N = 3^g$).

3.6 Varying Nodal Dynamics

In order to demonstrate the generality of these observations, we also explored different networks of bistable *synthetic genetic networks*, where the nodal dynamics was given by [18, 19, 20]:

$$F(x) = \frac{m(1 + x^2 + \alpha\sigma_1 x^4)}{1 + x^2 + \sigma_1 x^4 + \sigma_1\sigma_2 x^6} - \gamma_x x \tag{3.2}$$

where x is the concentration of the repressor. The nonlinearity in this $F(x)$ leads to a double well potential, and different γ introduces varying degrees of asymmetry in the potential. Fig. 3.23-3.25 shows some of the representative plots indicating the generality of central results.

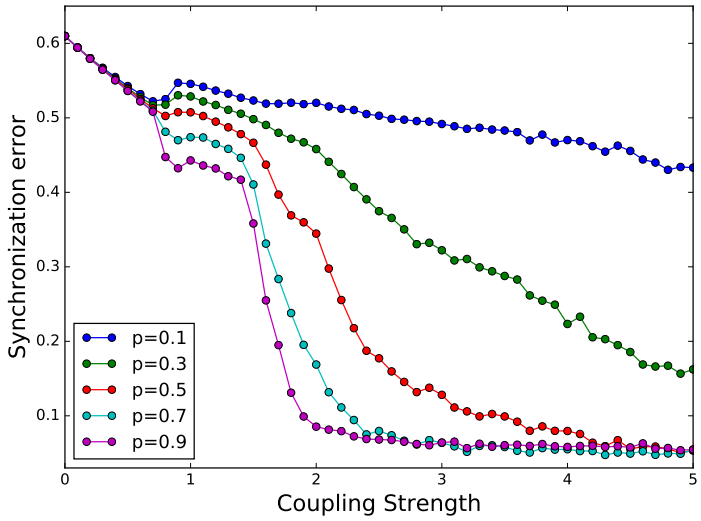

Figure 3.23: Synchronization error for varying coupling strengths, for a system of coupled bistable elements given by Eqn.3.2, with different underlying connection networks: Small-World network with $K = 2$ and $N = 100$ for different values of p.

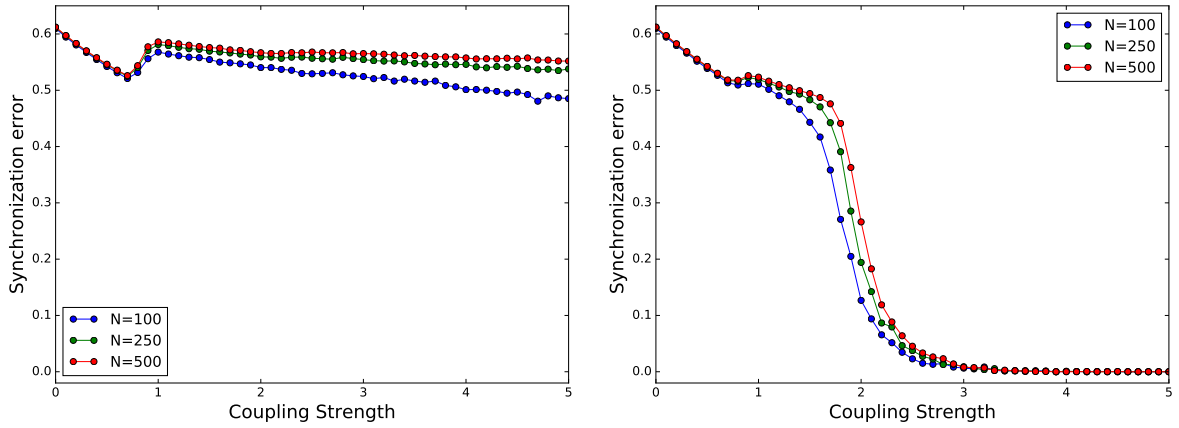

(a) (b)

Figure 3.24: Synchronization error for varying coupling strengths, for a system of coupled bistable elements given by Eqn.3.2, with different underlying connection networks: (a) Random Scale-Free for $N = 100, 250, 500$ for $m = 1$ (b) Random Scale-Free for $N = 100, 250, 500$ for $m = 2$ respectively.

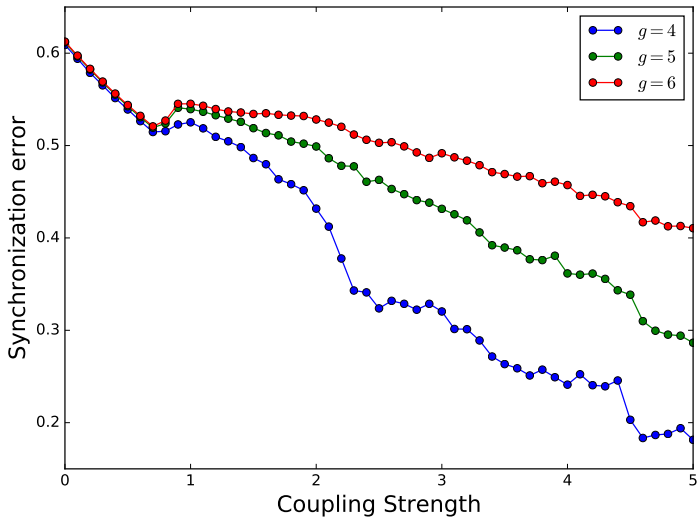

Figure 3.25: Synchronization error as a function of varying coupling strengths, for a system of coupled bistable elements given by Eqn.3.2, in Deterministic scale free network for different values of $g = 4, 5, 6$.

Further we studied different networks of a piece-wise linear bistable system, that can be realized efficiently in electronic circuits [39], given by:

$$F(x) = \begin{cases} \beta x_l^* - \alpha x & \text{if } x < x_l^* \\ (\beta - \alpha)x & \text{if } x_l^* \leq x \leq x_u^* \\ \beta x_u^* - \alpha x & \text{if } x > x_u^* \end{cases} \tag{3.3}$$

where x_u^* and x_l^* are the upper and lower thresholds respectively. We simulated the coupled dynamics of this bistable systems for different network topologies as well. Fig. 3.26-3.28 shows some of the representative plots, again demonstrating that the qualitative trends in this bistable systems is similar to that described above, and thus, indicating the generality of the central results presented here.

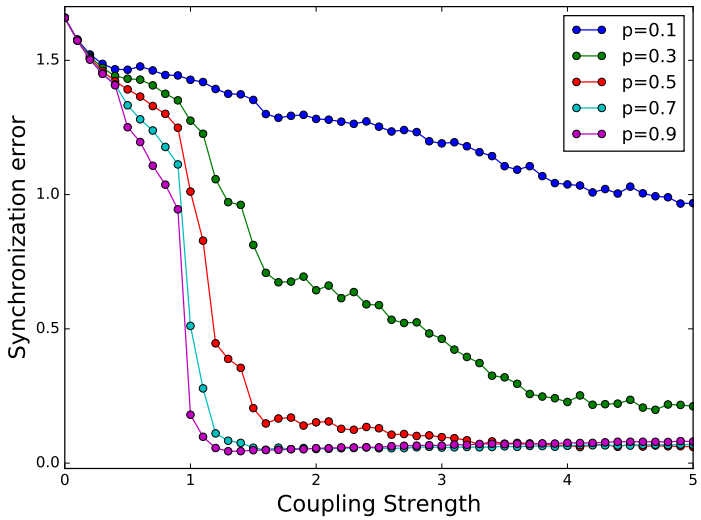

Figure 3.26: Synchronization error for varying coupling strengths, for a system of coupled bistable elements given by Eqn.3.3, with different underlying connection networks: Small-World network with $K = 2$ and $N = 100$ for different values of p.

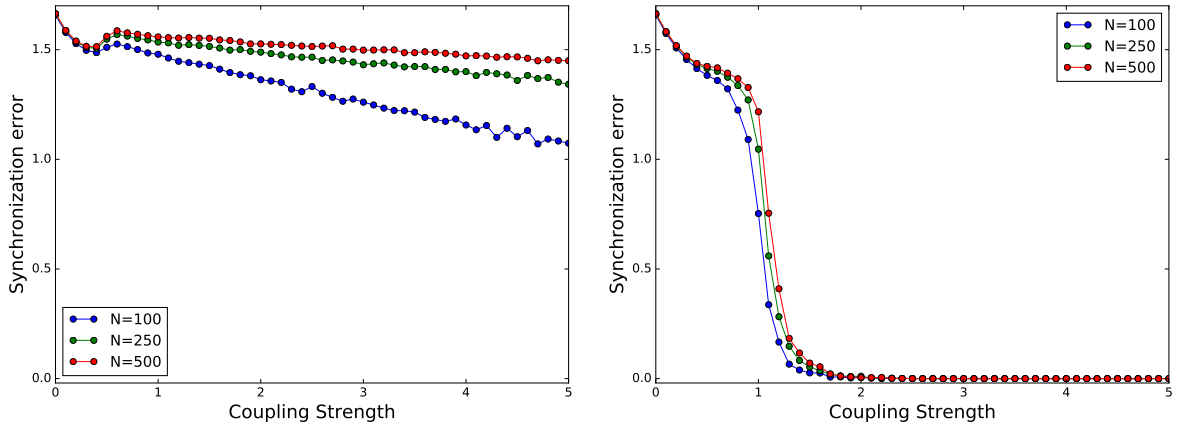

(a) (b)

Figure 3.27: Synchronization error for varying coupling strengths, for a system of coupled bistable elements given by Eqn.3.3, with different underlying connection networks: (a) Random Scale-Free for $N = 100, 250, 500$ for $m = 1$ (b) Random Scale-Free for $N = 100, 250, 500$ for $m = 2$ respectively.

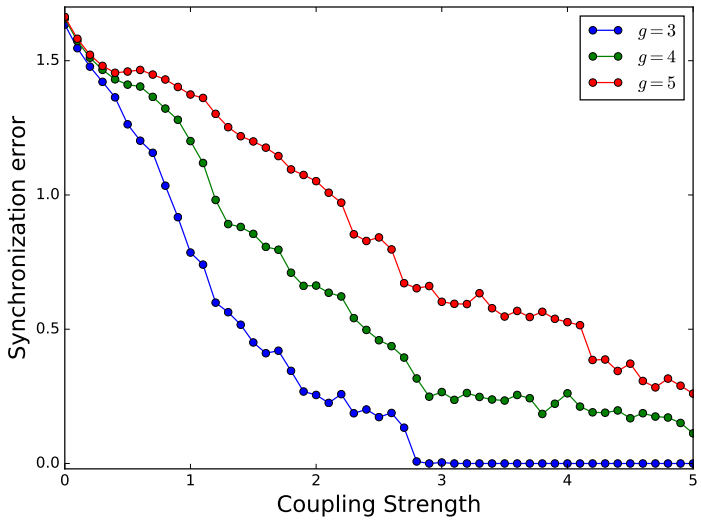

Figure 3.28: Synchronization error as a function of varying coupling strengths, for a system of coupled bistable elements given by Eqn.3.3, in Deterministic scale free network for different values of $g = 4, 5, 6$.

3.7 Conclusions

In summary, we have explored the collective dynamics of bistable elements connected in different network topologies, ranging from rings and small-world networks, to random and deterministic scale-free networks. We have focussed on the correlation between network properties and global synchronization features. In particular, we have estimated the average critical coupling strength yielding transition to synchronization, a quantity indicating the ease of synchronization. Further we estimated the minimal number of nodes that need to be perturbed in order to lose synchronization, and this quantity indicates the robustness of the synchronized state.

Easily synchronizes	**Difficult to synchronize**
Star	Deterministic Scale Free
Random Scale Free $m = 2$	Random Scale Free $m = 1$
Small world (high p)	Ring

Table 3.3: Ability of different network classes to synchronize, as reflected by global measures such as the average critical coupling strength $\langle \epsilon_c \rangle$. As one goes down the columns, $\langle \epsilon_c \rangle$ increases, namely the network synchronizes less easily.

Our central result is that, while networks properties can provide indicators of synchronization within a network class, they fail to provide consistent indicators across network classes (cf. Table 3.3 for a summary). For instance, we demonstrate that clustering coefficient is not a key feature in determining synchronization. This is clear through the similarity of synchronization properties in rings with significantly different clustering coefficients, and the striking difference in synchronization of a star network and a ring having the same clustering coefficient. Even characteristic path length, which is of paramount importance in determining synchronization, does not provide a one-to-one correspondence with synchronization properties across classes. Namely, while synchronization is significantly favoured in networks with low path lengths within a network class, the same characteristic path length in different types of networks yields very different $\langle \epsilon_c \rangle$ and f_c. Further, there appears to be no critical minimal characteristic path length that ensures synchronization from generic random initial states. All this suggests that local properties determined by the connection network does not provide a complete picture of global measures of synchronization.

Our observations then have potential applications. For instance, if one needs to achieve synchronization in a network of bistable elements, such as electronic circuits, constrained by certain connection properties, our analysis can guide the choice of preferred topology [33]. More importantly, in the context of the general understanding of dynamical

networks, our observations suggest important caveats to correlating network features to global dynamical phenomena.

Chapter 4

Identifying nodal properties that are crucial for the dynamical robustness of multi-stable networks

Adapted from the work published in :

P. D. Rungta, C. Meena and S. Sinha
arXiv preprint arXiv, **1801.02409** (2018).

4.1 Introduction

The influence of the interplay of nodal dynamics and the nature of links on the emergent collective patterns in dynamical networks is a broad question of utmost relevance. It has bearing on the basic issue of information flow emanating from nodes in networks, as well as on practical issues such as determination of the nodes to safeguard most stringently in the scenario of targeted attacks on the network. So this aspect of complex networks has attracted much recent research attention [40, 41, 42, 31, 29, 43] as it has considerable import, both from the fundamental, as well as the applied point of view. However inspite of intense research focus, the problem still eludes complete understanding and is still surprisingly open. In fact there exist some mutually contradictory results [41, 31, 44] that make it difficult to obtain clarity on this important problem [45]. There are two key complementary questions here: one involves finding patterns common to networks that allow greater synchronizability; the second question involves identifying common nodal features that render a network most vulnerable to localized perturbations targeting those nodes. In this work we focus on the latter question. Namely, we attempt to identify the nodal property that most significantly influences the global stability of the network.

Lastly note that in a network modeling power grids it had been observed that higher degree nodes which are not adjacent to the end-nodes show higher resilience to perturbations, while perturbations to low degree nodes or end-nodes rendered the network more vulnerable to desynchronization. In the Star network we have the situation where the high degree node is adjacent to the low degree end-nodes. We also find that, in distinct contrast to [42], that the network is significantly more vulnerable to attacks on the hub. So high degree nodes adjacent to low degree nodes display very different response to perturbation as compared to high degree nodes occuring at some distance from the periphery.

As a test-bed for understanding this we consider the collective dynamics of a group of coupled bi-stable elements. Bi-stable systems are relevant in a variety of fields, ranging from relaxation oscillators and multi-vibrators, to light switches and Schmitt triggers. Further it is of utmost importance in digital electronics, where binary data is stored using bi-stable elements. Specifically then, in this work we will explore bi-stable elements, connected in different network topologies, ranging from regular rings to random scale-free and star networks. We focus on the response of this network to localized perturbations on a sub-set of nodes. The central question we will investigate here is the following: *what characteristics of the nodes (if any) significantly affect the global stability?* So we will

search for *consistent* discernable patterns amongst the nodes that aid the maintenance of the stability of the collective dynamics of the network on one hand, and the nodes that rapidly destroy it on the other. In particular, we consider three properties of the nodes: degree, betweenness centrality and closeness centrality. Since these features of a node determine the efficiency of information transfer originating from it, or through it, they are expected to influence the propagation of perturbations emanating from the node.

Normalized degree of a node i in an undirected network is given by the number of neighbors that are directly connected to the node scaled by the total number of nodes N, and is denoted by k_i. So a high degree node indicates that there is direct contact with a larger set of nodes. Normalized betweenness centrality of a node i is given as:

$$b_i = \frac{2}{(N-1)(N-2)} \sum_{s,t \in I} \frac{\sigma(s,t|i)}{\sigma(s,t)}$$

where I is the set of all nodes, $\sigma(s,t)$ is the number of shortest paths between nodes s and t and $\sigma(s,t|i)$ is the number of shortest paths passing through the node i. So if node i has high betweenness-centrality, it implies that it lies on many shortest paths, and thus there is high probability that a communication from s to t will go through it. Normalized Closeness Centrality is defined as:

$$c_i = \frac{N-1}{\sum_j d(j,i)}$$

where $d(j,i)$ is the shortest path between node i and node j in the graph. Namely, it is the inverse of the average length of of the shortest path between the node and all other nodes in the network. So high closeness centrality indicates short communication path to other nodes in the network, as there are minimal number of steps to reach other nodes.

We have seen in ref [29, 31] that some works suggest that betweenness centrality is an important property in determining synchronization in networks. Also, in our previous chapter we have extensively studied synchronization in different classes of network and effect of some network properties that may or may not influence the synchronization. We also studied the effect of these network properties in determining basin stability.

Thereby, an important follow up question that one can ask on the scale of nodes is that how important each node is in determining basin stability. Thus, we have classified nodes based on the betweenness centrality and studied its effects on basin stability.

In this chapter we will explore the extent to which the features of the nodes given

above influence the recovery of a network from large localized perturbations. In order to gauge the global stability and robustness of the collective state of this network, we will *introduce a variant of the recent framework of multi-node basin stability* [34, 35]. In general, the basin stability of a particular attractor of a multi-stable dynamical system is given by the fraction of perturbed states that return to the basin of the attraction of the dynamical state under consideration. In our variant of this measure, we consider an initial state where all the bi-elements in the network are in the same well, and we will refer to this as a 'synchronized state'. So a synchronized state here does not imply complete synchronization. Rather it implies a collective state where the states of the nodes are confined to the neigbourhood of the same attracting stable state, i.e. lies within the basin of attraction of one of the two attracting states. We then perturb a specific number of nodes of a prescribed type, with the perturbations chosen randomly from a given subset of the state space. The multi-node basin stability (BS) is then defined as the fraction of such perturbed states that manage to revert back to the original state from these localized perturbations. Namely, multi-node BS reflects the fraction of the volume of the state space of a sub-set of nodes that belong to the basin of attraction of the synchronized state. So the importance of multi-node BS stems from the fact that it determines the probability of the system to remain in the same well in multi-stable systems when random perturbations throw a specific number of nodes to some other well. This allows us to extract the contributions of individual nodes to the overall stability of the collective behaviour of the dynamical network. Further, since one perturbs subsets of nodes with certain specified features, our variant of the concept of multi-node BS will suggest which nodal properties make the network more vulnerable to attack.

4.2 Model

Specifically we consider the system of N diffusively coupled bi-stable elements, whose dynamics is given as:

$$\dot{x_i} = F(x_i) + C\frac{1}{K_i}\sum_j (x_j - x_i) = F(x_i) + C(\langle x_i^{nbhd}\rangle - x_i) \tag{4.1}$$

where i is the node index ($i = 1, \ldots N$) and C is the coupling constant reflecting the strength of coupling. The set of K_i neighbours of node i depends on the topology of the underlying connectivity, and this form of coupling is equivalent to each site evolving diffusively under the influence of a "local mean field" generated by the coupling neigh-

bourhood of each site i, $\langle x_i^{nbhd} \rangle = \frac{1}{K_i} \sum_j x_j$, where j is the node index of the neighbours of the i^{th} node, with K_i being the total number of neighbours of the node.

The function $F(x)$ gives rise to a double well potential, with two stable states x_-^* and x_+^*. For instance one can choose

$$F(x) = x - x^3$$

yielding two stable steady states $x_\pm^*$ at $+1$ and -1, separated by an unstable steady state at 0. Note that the synchronized state here is a state where x_is for all i are in the same well, i.e. x_i of all the elements in the network are in the neighbourhood of x_-^*, or they are all in the neighbourhood of x_+^*.

We first investigate the two limiting network cases:

1. *Ring*: where all nodes have the same degree, closeness and betweenness centrality(see fig. 4.1).

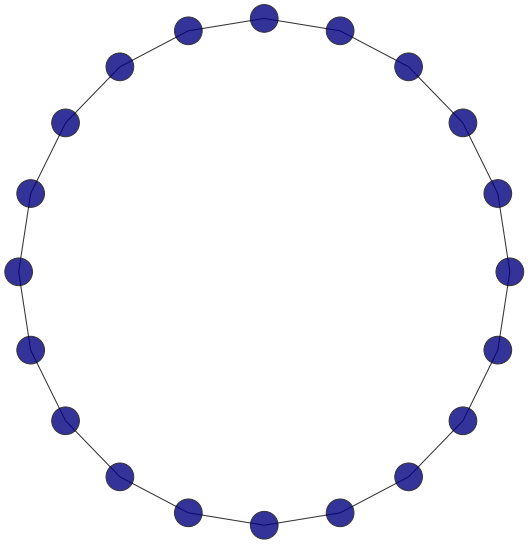

Figure 4.1: Construction of a Ring Network of size $N = 20$ and $k = 2$.

2. *Star network*: where the central (hub) node has the maximum normalized degree ($k_{hub} = 1$), betweenness centrality ($b_{hub} \sim 1$), and closeness centrality ($c_{hub} = 1$), while the rest of the nodes, namely the peripheral nodes ("leaves") have very low degree ($k_{peri} \sim 0$ for large networks), betweenness centrality ($b_{peri} = 0$) and closeness centrality $c_{peri} \sim 0.5$(see fig 4.2).

So on one hand we have the Ring which is completely homogeneous, and on the other

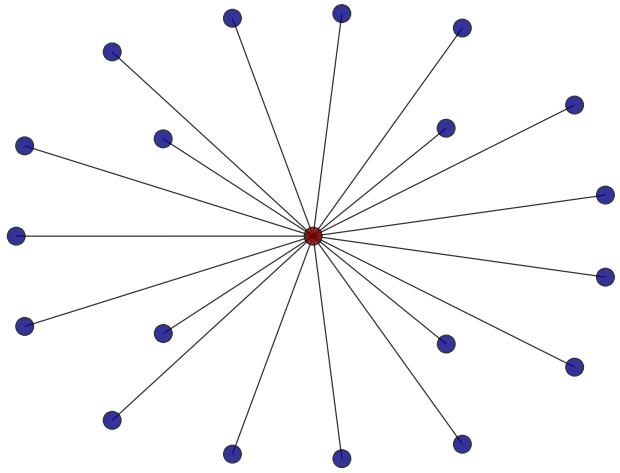

Figure 4.2: Construction of a Star Network of size $N = 20$.

hand we have the Star network where the difference in degree, closeness and betweenness centrality of the hub and the peripheral nodes is extremely large. Exploring these limiting cases allows us to gain understanding of the robustness of the network to large perturbations affecting nodes with different properties.

As indicated earlier, to gauge the effect of different nodal features on the robustness of the dynamical state of the network, we do the following: we first consider a network close to a stable synchronized state, namely one where the states x_i of all the nodes i have a small spread in values centered around x^*_- or x^*_+, i.e. all elements are confined to the same well. We order nodes by some appropriate property, such as increasing or decreasing degree, closeness or betweenness centrality. We then give a *large perturbation* to a small fraction of nodes, denoted by f. This strong perturbation typically kicks the state of the perturbed nodes to the basin of attraction of the other well. We then ascertain whether all the elements return to their original wells after this perturbation, i.e. if the perturbed system recovers completely to the initial state. We repeat this "experiment" over a large sample of perturbed nodes and perturbation strengths, and find the fraction of times the system manages to revert to the original state. This measure of global stability is then a variant of multi-node Basin Stability and it is indicative of the robustness of the collective state to perturbations localized at particular nodes of a certain type in the network.

4.3 Dynamics of a Ring of Bistable Systems

We first investigate the spatiotemporal evolution of a ring of bistable elements, all of whose states are confined to the same well, other than a few nodes that experience a large perturbation which pushes their state to the basin of the other well.

In Fig. 4.3 we show the representative cases of a ring of $N = 100$ elements, with (a) 2 and (b) 4 nodes that are perturbed strongly. It is evident that in case (a) the perturbed nodes recover and return to their original well. However, when the fraction of perturbed nodes is slightly larger, such as in Fig. 4.3b (where the fraction of perturbed nodes is 0.04), the perturbed nodes fail to return to their original well, and remain out of synchronization with the rest of the elements in the ring. This is evident from the switched colors of the asymptotic state of the perturbed nodes in Fig. 4.3b. This suggests that the ring is not robust against such localized perturbations, and even when the fraction of perturbed nodes is very small, these nodes are unable to return to the original well. That is, the elements in the Ring are unable to drag the few perturbed nodes back to the well of the majority of the elements, suggesting that the Ring is not robust against such localized perturbations.

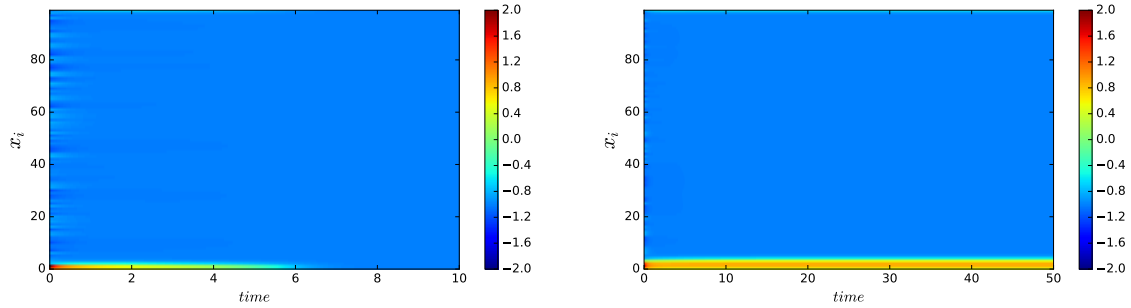

(a) (b)

Figure 4.3: Space-time plot showing the evolution of a ring of bi-stable elements given by Eqn. 4.1. Here system size $N = 100$, $k_i = 2$ for all i, and the coupling strength $C = 1$. The number of nodes perturbed are in clusters (i.e. they are contiguous nodes), and two nodes are perturbed in (a) and four in (b).

Next we attempt to discern the effect of coupling on the robustness of the dynamics. Fig. 4.4 shows the multi-node basin stability for this system, as the coupling strength is increased in the range 0 to 2, for clusters of perturbed nodes with f ranging from 0.01 to 0.08. It is evident from the basin stability of the system, that there is a *sharp transition* from zero basin stability, namely the situation where *no* perturbed state returns to the original state, to basin stability close to one, namely where *all* sampled perturbed states

return to the original state. This indicates that the *system recovers from large localized perturbations more readily if it is strongly coupled*. Further, the figure also demonstrates the extreme sensitivity of basin stability to the number of nodes being perturbed. We find that the system fails to return to the original state, even at very high coupling strengths, when more than 5% of the nodes experience perturbations. For instance, Fig. 4.4 shows the case of a single perturbed node (i.e. $f = 0.01$), where the entire network recovers for coupling strengths stronger than approximately 0.2. In contrast, for $f = 0.08$, where a cluster of 8 nodes are perturbed in the Ring of 100 elements, there is zero basin stability in the entire coupling range. So a Ring loses its ability to return to the original state rapidly with increasing number of perturbed nodes.

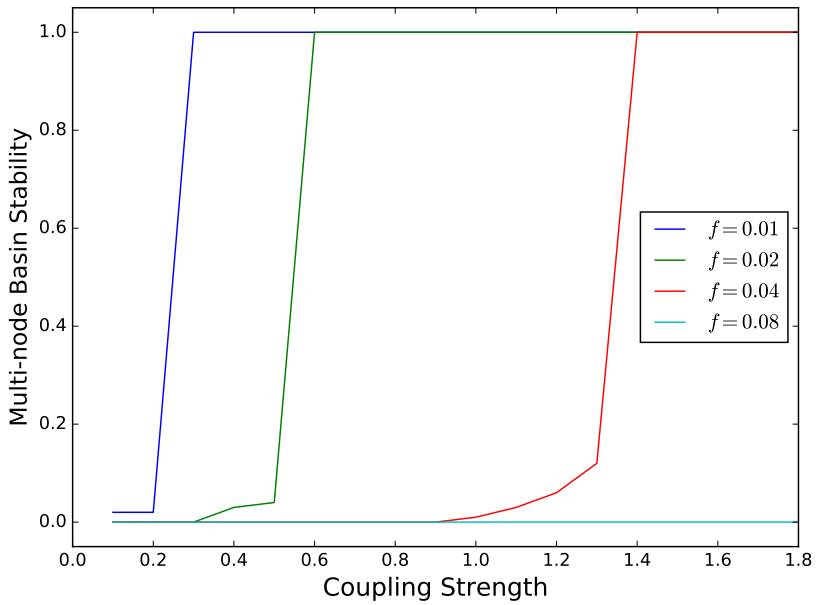

Figure 4.4: Dependence of Multi-Node Basin Stability on coupling strength, for a ring of bistable elements given by Eqn. 4.1, with the number of perturbed nodes. Here the size of the ring is $N = 100$, and size of the coupling neighbourhood is $k = 2$, namely each site couples to its two nearest neighbours. The perturbed nodes f occur in clusters.

For very small f, the entire network returns to its original state, and basin stability is close to 1. On increasing f one observes that there exists a minimum fraction, which we denote as f_{crit}, after which the basin stability sharply declines from 1. So f_{crit} indicates the minimum fraction of nodes one typically needs to perturb in order to destroy the collective state where all elements are in the same well. We find that stronger coupling yields larger f_{crit}. For instance, $f_{crit} \approx 0.02$ for $C = 0.5$ and $f_{crit} \approx 0.04$ for $C = 1$. So for stronger coupling, the bulk of the elements are capable of pulling the perturbed nodes back to original well, increasing the resilience of the network.

Due to the structure of the ring, the stability of the system with respect to localized perturbations depends on whether the perturbed nodes are contiguous and occur in a cluster (cf. the case in Fig. 4.4, 4.6) or randomly spread over the ring, where the locations of the perturbed nodes are uncorrelated. Fig 4.5 shows the multi-node basin stability when nodes perturbed are chosen randomly for different values of coupling. We observe that the system is more stable here, as compared to the case when nodes are perturbed in cluster, namely *perturbations at random locations in a ring allows the system to recover its original dynamical more readily than perturbations on a cluster of contiguous nodes.*

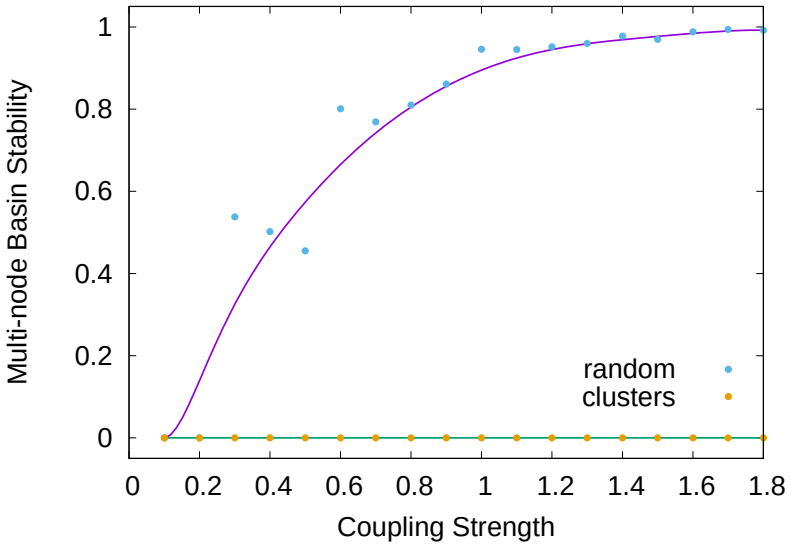

Figure 4.5: Dependence of Multi-Node Basin Stability on coupling strength, for a ring of bistable elements given by Eqn. 4.1, with the number of perturbed nodes. Here the size of the ring is $N = 100$, and size of the coupling neighbourhood is $k = 2$, namely each site couples to its two nearest neighbours. Figure shows the multi-node basin stability for the case of perturbations on randomly located nodes, for $f = 0.08$. The case of perturbation in clusters (orange) is also shown for reference, for the same fraction of perturbed nodes.

Further, Fig. 4.7 shows the dependence of multi-node basin stability on the fraction of perturbed nodes f for different system sizes N. We find that $f_{crit} \sim \frac{C}{N}$, implying that $f_{crit} \to 0$ as system size $N \to \infty$. This indicates that in a very large Ring, even the smallest finite fraction of perturbed nodes can disturb the Ring from its original steady state. So one can conclude that the synchronized state in the Ring is very susceptible to destruction, as only very few nodes in the system need to be perturbed in order to push the system out of the original state. Namely, in a ring of bi-stable elements, *the collective state where all elements are in the same well, is a very fragile state.*

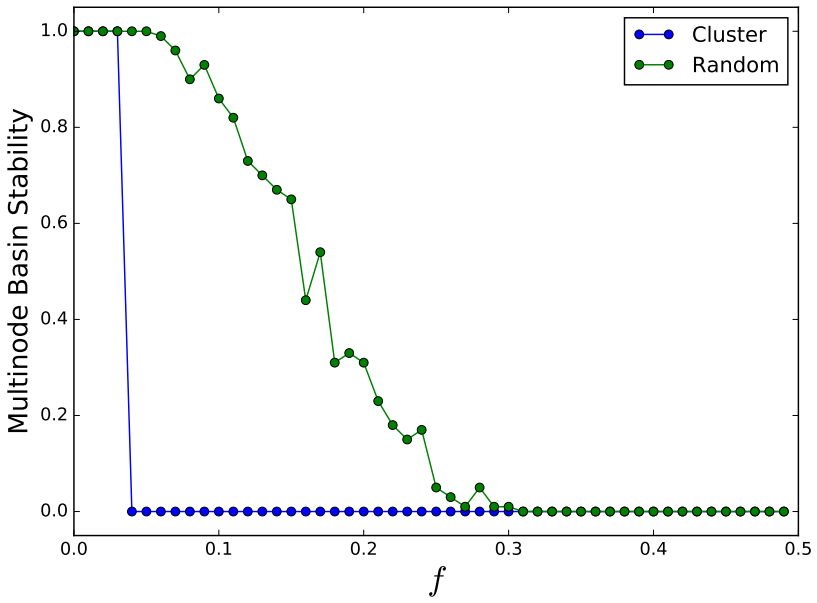

Figure 4.6: Dependence of Multi-Node Basin Stability on fraction of nodes perturbed, for a ring of bistable elements given by Eqn. 4.1. Here the size of the ring is $N = 100$, and size of the coupling neighbourhood is $k = 2$, namely each site couples to its two nearest neighbours. Figure shows the multi-node basin stability for the case of perturbations on randomly located nodes, for $C = 1$. The case of perturbation in clusters is also shown for reference, for the same coupling values.

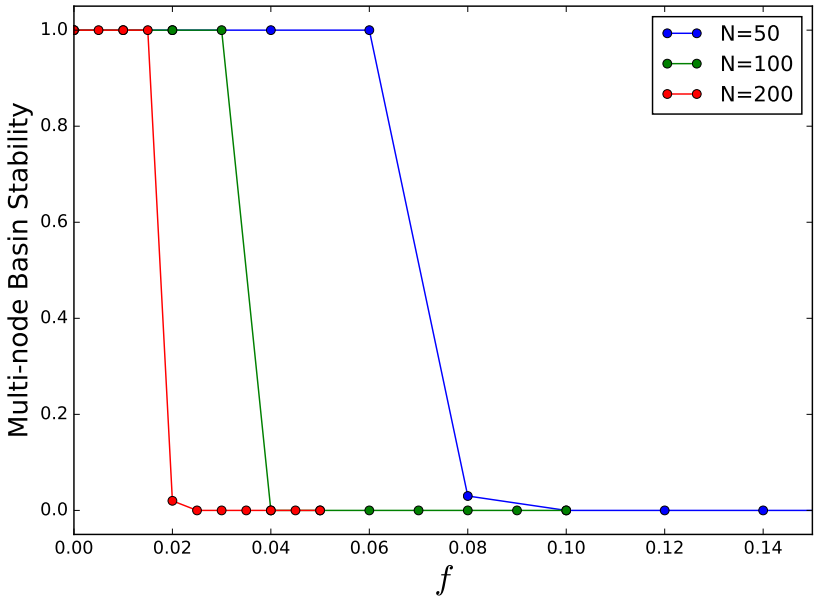

Figure 4.7: Dependence of Multi-Node Basin Stability on coupling strength, for a ring of bistable elements given by Eqn. 4.1, with the number of perturbed nodes f for different system sizes N, for $C = 1$. Here the size of the coupling neighbourhood is $k = 2$, namely each site couples to its two nearest neighbours.

4.4 Dynamics of a Star Network of Bistable Systems

Now we study the spatiotemporal evolution of bistable elements connected in a star configuration. Here the central hub node has the maximum degree, betweenness and closeness centrality, while the rest of the nodes, namely the peripheral leaf nodes have very low degree, betweenness and closeness centrality. Namely, in this network the difference in degree, closeness and betweenness centrality of the hub and the peripheral nodes is extremely large. So this network offers a good test-bed to investigate the correlation between specific properties of a node and the resilience of the network to large localized perturbations at such nodes.

Figs. 4.8a-b display the dynamics for two illustrative cases. In Fig. 4.8(a), *only the hub node is perturbed* in the star network consisting of 100 elements. We notice, that this *single* perturbed node pulls *all* the other nodes of the network away from its original state. So the star network is *extremely vulnerable to perturbations at the hub*, and cannot typically recover from disturbances to the state of the hub, even if all the other nodes are unperturbed. On the other hand, Fig. 4.8(b), shows what ensues when a *large number of peripheral nodes are perturbed*. Now, even when as many as 90% of the peripheral nodes in the network experience a disturbance in their state, the entire network still manages to recover to its original state. This dramatic difference in the outcome of perturbations clearly illustrates how sensitively the robustness of a dynamical state depends on the degree, closeness and betweenness centrality of the perturbed node.

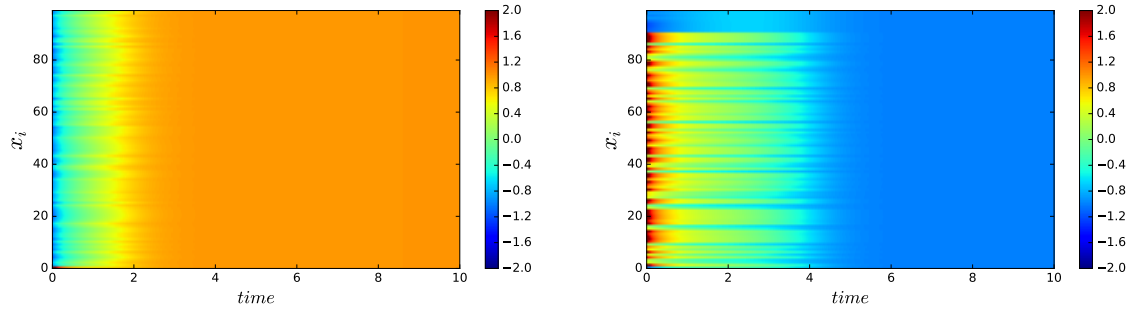

(a) (b)

Figure 4.8: Time evolution of 100 bistable elements coupled in star configuration, given by Eqn. 4.1, with coupling strength $C = 1$. In (a) only the hub node is perturbed; in (b) 90 peripheral nodes are perturbed.

Next we examine the multi-node basin stability of the network, for fraction f of perturbed nodes ranging from $1/N$ (namely single node in Fig. 4.9(a)) to $f \sim 1$, namely the case where nearly all nodes in the system are perturbed. As evident from Fig. 4.9

(b), when only the peripheral nodes are perturbed, even for values of f as high as 0.7, there is no discernable difference in the basin stability, which remains close to 1. This implies that even when more than half the nodes in the network are perturbed the entire system almost always recovers to the original state. In contrast, in Fig. 4.9(a) shows the single-node basin stability for the case of the hub node being perturbed, where the basin stability is clearly drastically reduced and approaches zero very quickly. It is clear that just a *single* node is enough to destroy the stability of the network, if that node has very high degree, closeness and betweenness centrality, such as the hub node. These quantitative results are consistent with the qualitative spatiotemporal patterns observed in Fig. 4.8.

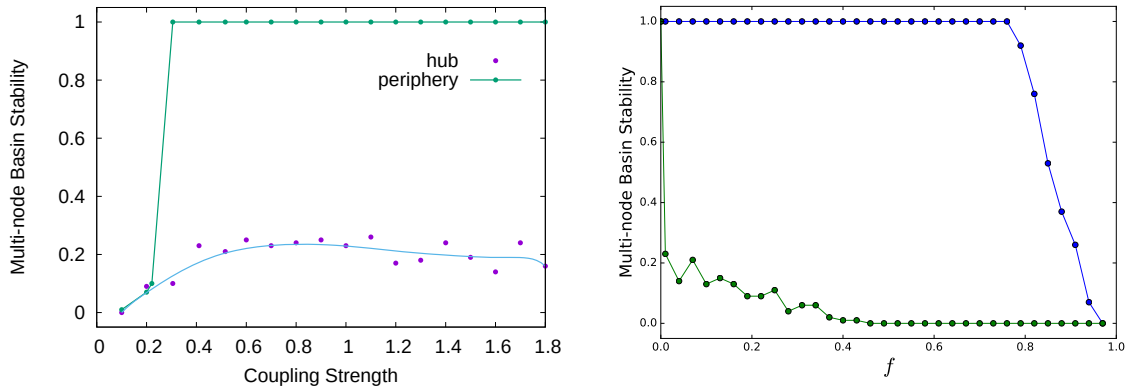

(a) (b)

Figure 4.9: (a) Multi-node Basin Stability vs coupling strength for a Star network of size $N = 100$, where the hub node is perturbed (blue) and a single peripheral node is perturbed (green); (b) Multi-node Basin Stability vs number of nodes perturbed in the Star network of bistable elements. Here the size of the network $N = 100$ and coupling strength $C = 1$. The blue curve represents the case where only peripheral nodes are perturbed, while green represents the case where the hub is perturbed along with peripheral nodes.

Further Fig. 4.9(b) shows the decline in Multi-node Basin Stability with increasing fraction of perturbed nodes f. Interestingly, when only the peripheral nodes are perturbed, Basin Stability is close to one even when a very large fraction of nodes in the system are perturbed, and $f_{crit} \approx 0.7$. So when only peripheral nodes are perturbed, the perturbed nodes manage to return to their original state, *even when a majority of nodes in the system have been pushed to the basin of attraction of the other state.* However when the perturbed nodes include the central hub node, the basin stability declines rapidly with increasing f, and $f_{crit} \approx 1/N$. So our analysis reveals how significant the

degree, closeness and betweenness of nodes are in determining the resilience of the network. In fact, very clearly, the *hub node holds the key to the maintenance of the collective state* [1].

4.4.1 Analysis

We will now rationalize the above results by analyzing the dynamical equations of star networks under large perturbations, and attempt to provide an explanation of why nodes with high centrality measure impact the basin stability to such a high extent. We give the equations for the dynamics at the nodes of the star network explicitly below.

For the hub node ($i = 0$):

$$\dot{x_0} = F(x_0) + \epsilon(\frac{\sum_{j=1}^{N-1} x_j}{(N-1)} - x_0) \tag{4.2}$$

For peripheral nodes ($i = 1, \ldots N-1$):

$$\dot{x_i} = F(x_i) + \epsilon(x_0 - x_i) \tag{4.3}$$

With no loss of generality, we consider the specific case of $F(x_i) = x_i - x_i^3$, with the initial state of all nodes at the negative fixed point $x_i = -1$ (where $F(x_i) = 0$) for all i. When fraction f of the nodes in the network are strongly perturbed, their state is pushed to the positive well, and thus go to values around $+1$. We consider the perturbed nodes to be $i = 1, \ldots, fN$, with no loss of generality. We also consider coupling strength ϵ to be of $O(1)$.

1. First consider the case when fraction f of peripheral nodes are perturbed to the other well. The dynamics of the hub right after the perturbation, is governed by

[1] Note that in a network modeling power grids in Ref. [42] it had been observed that higher degree nodes which are not adjacent to the end-nodes show higher resilience to perturbations, while perturbations to the end-nodes rendered the network more vulnerable to desynchronization. In the Star network the high degree hub node is adjacent to the end-nodes, and the network is significantly *more vulnerable to attacks on the hub*. So we can infer that high degree nodes adjacent to end-nodes display very different response to perturbation, vis-a-vis high degree nodes occurring at some distance from the periphery.

the equation:

$$\dot{x_0} \approx \epsilon(\frac{\sum_{N-1-fN}(-1) + \sum_{fN}(+1)}{N-1} - (-1))$$
$$\implies \dot{x_0} \approx \epsilon(\frac{2fN}{N-1})$$

For large network size N, the above is approximately $2\epsilon f$

For peripheral nodes undergoing perturbation ($i = 1, \ldots, fN$), the dynamics is given approximately by:

$$\dot{x_i} = \epsilon((-1) - (+1))$$
$$\implies \dot{x_i} \approx -2\epsilon$$

For the rest of the peripheral nodes ($i = fN + 1, \ldots, N - 1$) the dynamics after perturbation is governed by the equation:

$$\dot{x_i} = \epsilon((-1) - (-1))$$
$$\implies \dot{x_i} \approx 0$$

So the coupling term is significant *only* for the perturbed nodes, and not for any of the other peripheral nodes. It is also clearly evident from the above equations that the magnitude of the coupling term for the hub node (i.e. $2\epsilon f$) is significant (i.e. of order $O(1)$) only when $f > \frac{1}{2}$. So more than half the peripheral nodes need to be strongly perturbed in order to have impact on the system. This is consistent with our numerical results, which suggest that $f \sim 0.7$ to destroy the stability of the network. That is, remarkably, even when as many as 70% of the peripheral nodes are perturbed, the network still manages to return to its original state.

2. Secondly, consider the case where *only* the hub node is perturbed to other well, that is $x_0 \approx 1$ and $x_i \approx -1$ $\forall i = 1, \ldots, N-1$. The dynamical equations right after perturbation, for the hub and peripheral nodes is given below.
   For the perturbed hub ($i = 0$)

$$\dot{x_0} \approx \epsilon(\frac{\sum(-1)}{N-1} - 1)$$
$$\implies \dot{x_0} \approx -2\epsilon$$

For all peripheral nodes ($i = 1, \ldots N-1$):

$$\dot{x_i} \approx \epsilon((+1) - (-1))$$
$$\implies \dot{x_i} \approx 2\epsilon$$

So in contrast to the case of perturbations on peripheral nodes, here the coupling term is large *for all nodes* ($\sim O(1)$), even though only *one* node is perturbed. This indicates why there is such a dramatic difference between localized perturbations on the hub and on the peripheral nodes, as clearly observed in the numerical simulations as well.

4.5 Dynamics of a Random Scale-Free Network of Bistable Systems

We will now go on to explore Random Scale-Free (RSF) Networks of bi-stable dynamical elements. In particular, we construct these networks via the Barabasi-Albert preferential attachment algorithm, with the number of links of each new node denoted by parameter m [36](see fig. 4.10,4.11).

The network is characterised by a fat-tailed degree distribution. Specifically we will display results for networks of size $N = 100$, with $m = 1$ and $m = 2$. Figs. 4.12a-b shows two contrasting representative cases where (a) twenty nodes with highest betweenness centrality are perturbed, and (b) twenty nodes with the lowest betweenness centrality were perturbed. It is observed that perturbation on nodes with high betweenness centrality destabilises the entire network, and the perturbed nodes rapidly drag all the other nodes to a different well. This is evident from the switched colors of the asymptotic state in Fig. 4.12a. On the other hand, when the perturbed nodes have low betweenness centrality, the network recovers quickly from the perturbation and reverts to the original well, as clearly seen in Fig.4.12b. These completely different outcomes occur even though the *number of perturbed nodes is the same* in both cases, thereby clearly illustrating that nodes with high betweenness-centrality have much stronger influence on the global stability of the system and that the network is very sensitive to perturbations on nodes with high betweenness centrality.

We will now present the dependence of the global stability of the collective dynamics on different centrality measures in this heterogeneous network, quantitatively, through

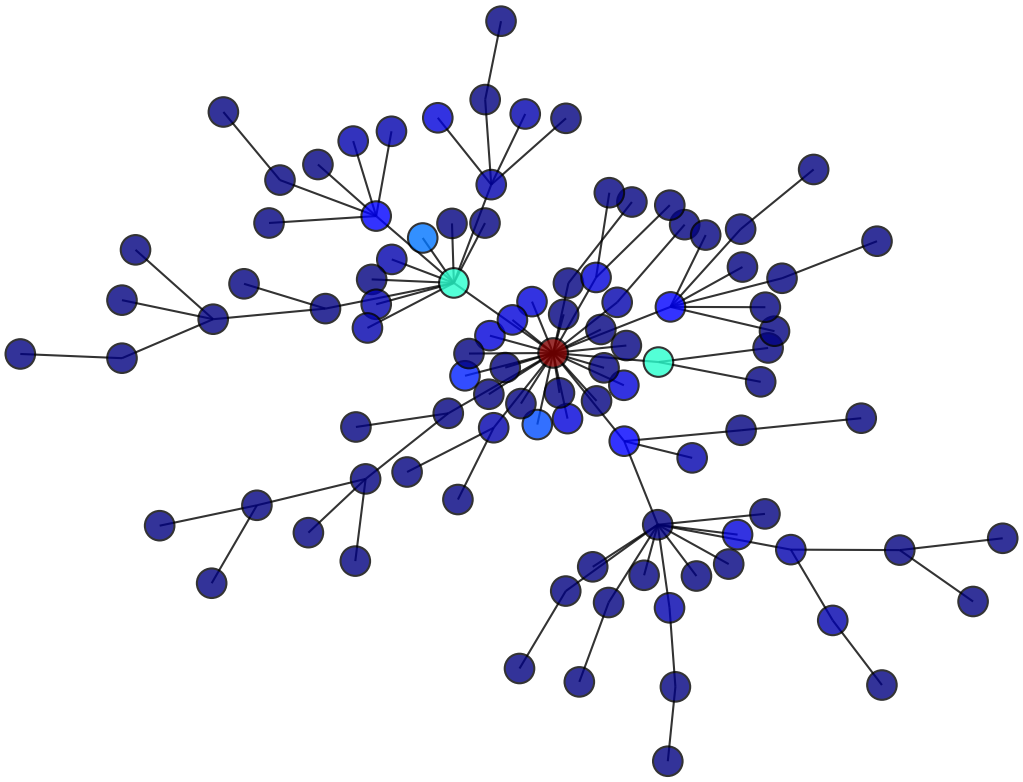

Figure 4.10: Construction of a Scale-Free Network (adapted from Ref. [36]) of size $N = 100$ with $m = 1$.

multi-node basin stability measures. In particular, in order to explore the correlation between a given centrality measure of the nodes and the resilience of the system, we will estimate the multi-node basin stability under perturbations on sub-sets of nodes with increasing (or decreasing) values of the centrality under consideration. That is, we order the nodes according to the centrality we are probing, and consider the effect of perturbations on fraction f of nodes with the highest (or lowest) centrality.

The influence of perturbations on nodes with the highest and lowest betweenness, closeness and degree centrality in a Random Scale-Free network are displayed in Figs. 4.13a-c. The broad trends are similar for all three centrality measures, and it is clearly evident that when nodes with the highest betweenness, closeness and degree centrality are perturbed, multi-node basin stability falls drastically. On the other hand, perturbing the same number of nodes of low centrality leaves the basin stability virtually unchanged. Further, when nodes of low centrality are perturbed, for sufficiently high coupling strengths, the network almost always recovers to its original state, yielding a basin stability of 1.

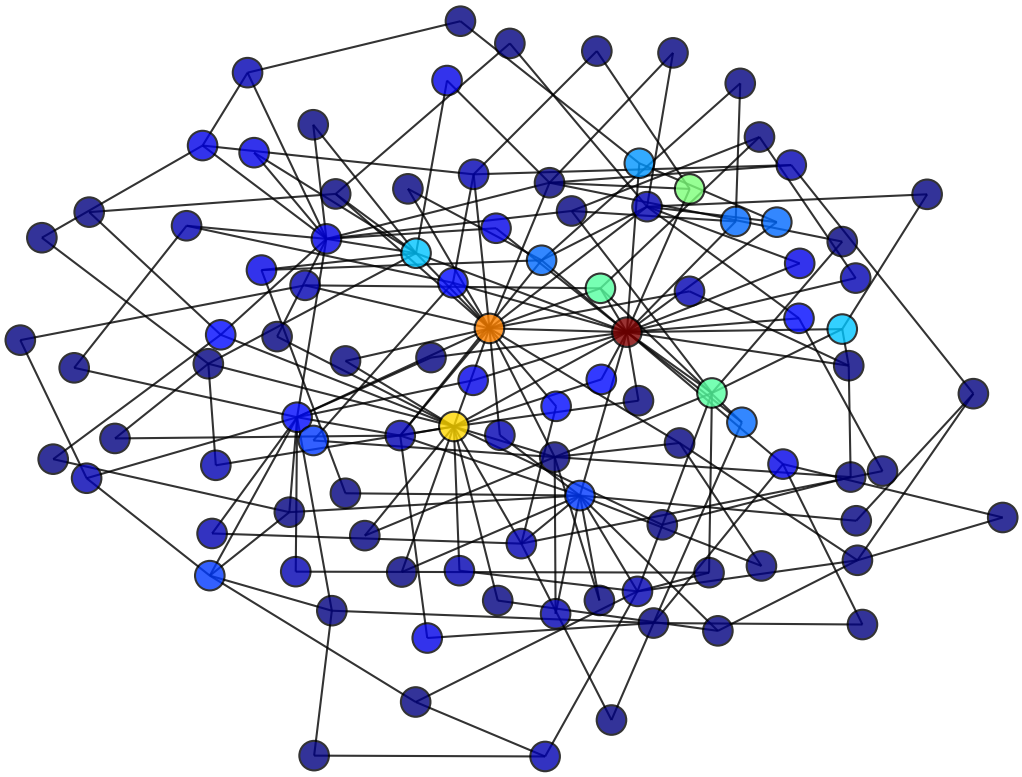

Figure 4.11: Construction of a Scale-Free Network (adapted from Ref. [36]) of size $N = 100$ with $m = 2$.

So one can conclude that perturbing nodes with high betweenness, closeness and degree centrality destroys the synchronized state readily, while perturbing nodes of low centrality allows the perturbed nodes to return to the original state, thereby restoring the synchronized state. For reference, Fig. 4.13 also shows the basin stability of a network where the perturbed nodes are randomly chosen, corresponding to *random attacks* on a subset of nodes. Clearly, a *targeted attack* on nodes with high centrality can destroy the collective dynamics much more efficiently than random attacks.

Further we observe(from fig. 4.13 top panels) that the response to perturbations on random nodes is closer to that obtained from perturbing nodes of low centrality. This can be rationalized by noting that the probability to draw a node of low centrality in a Random Scale-Free network is significantly larger than that for a node with high centrality. So a randomly chosen node is more likely to have low centrality. However, when there is a *targetted attack* on the nodes, the extreme sensitivity of the network to perturbations on nodes of high centrality will be most pertinent.

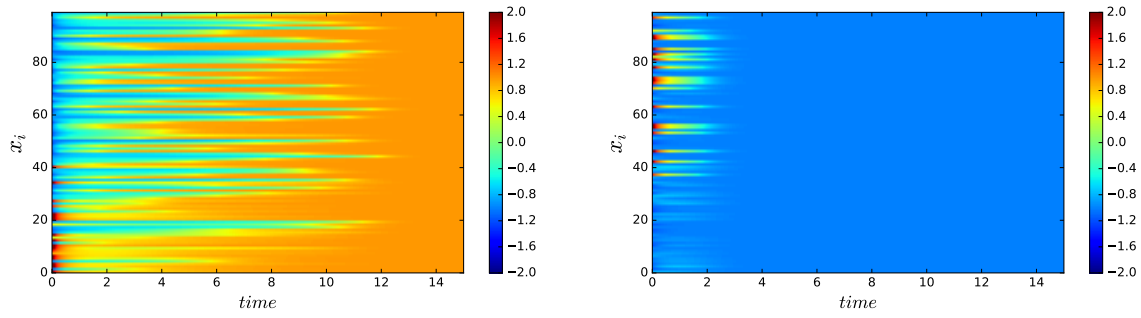

(a) (b)

Figure 4.12: Time evolution of 100 bistable elements coupled in a Random Scale-Free network with $m = 2$, given by Eqn. 4.1, with coupling strength $C = 1$. In (a) 20 nodes of highest betweenness centrality are perturbed; in (b) 20 nodes of lowest betweenness centrality are perturbed. Here the original state of the networks has all nodes in the negative well, i.e. all $x_i < 0$ at $t = 0$.

Now we investigate which centrality measure is most crucial in determining the global robustness of collective behaviour in the network. We do this through the following numerical experiment: we compare the basin stability of the collective dynamics of Random Scale-Free networks with $m = 1$ and $m = 2$. Interestingly, the distribution of the betweenness centrality, closeness centrality and degree of the nodes in RSF networks with $m = 1$ and $m = 2$ are significantly different, as evident in Fig. 4.14 (top panels). It is clear that for $m = 1$ the distribution of the degree and closeness centrality of the nodes in the network is shifted towards lower k and c values as compared to RSF networks with $m = 2$, while the distribution of betweenness centrality shifts towards higher values in RSF networks with $m = 1$ vis-a-vis the distribution of the betweenness centrality in RSF networks with $m = 2$.

So in RSF networks with $m = 1$ the nodes with the highest betweenness centrality typically have significantly higher b than in RSF networks with $m = 2$ of the same size. On the other hand, since the tail of the probability distribution of degree and closeness centrality of the nodes in a RSF network with $m = 2$ extends further than that in a RSF network with $m = 1$, the nodes with the highest degree and closeness centrality typically have lower k and c in RSF networks with $m = 1$ compared to RSF networks with $m = 2$. So these networks can potentially *provide a test-bed for determining which of the centrality properties most crucially influence dynamical robustness.* Note that it was not possible to use the Ring to probe this issue, as all nodes there have identical centrality properties. Nor did the Star network offer a system where one could distinguish between the effects of different centrality measures on dynamical robustness, as the nodes there split into two classes, the single hub and the periphery, with all the peripheral

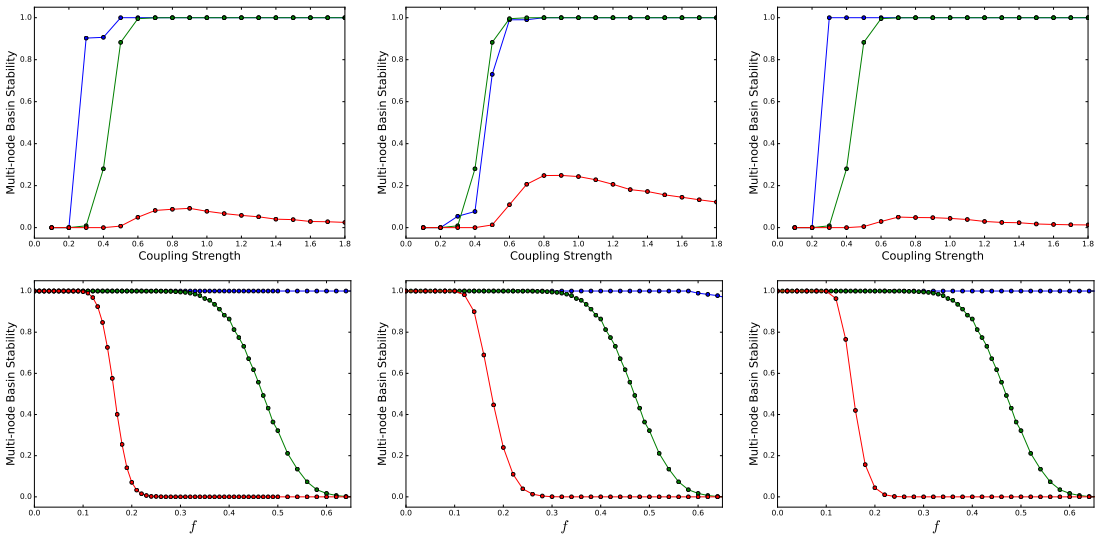

(a) (b) (c)

Figure 4.13: (a) Dependence of the Multi-node Basin Stability of Random Scale-Free networks of size $N = 100$, with $m = 2$, on coupling strength C, with $f = 0.2$ (top panels) and fraction f of perturbed nodes, with $C = 1$ (bottom panels). In the panels, three cases are shown. In the first case, the perturbed nodes are chosen at random (green curves). In the second case (red curves) the perturbed nodes are chosen in descending order of (a) betweenness centrality, (b) closeness centrality and (c) degree (i.e. the perturbed nodes are the ones with the highest b, c or k centrality measures). In the third case (blue curves) the perturbed nodes are chosen in ascending order of (a) betweenness centrality, (b) closeness centrality and (c) degree (i.e. the perturbed nodes are the ones with the lowest b, c or k centrality measures).

nodes having identical betweenness, closeness and degree. However, one can compare the response of Random Scale-Free networks with different m to probe which nodal property renders a heterogeneous network most vulnerable to large localized perturbations. This implies that if we consider nodes with the highest betweenness in the network with $m = 1$ with $m = 2$, we will typically have nodes with higher betweenness, and lower degree and closeness centrality, than the $m = 2$ network.

Fig. 4.14 (bottom panels) displays the dependence of the multi-node Basin stability on the fraction of perturbed nodes f in the Random Scale-Free network with $m = 1$ and $m = 2$. A feature to be observed is that nodes with high betweenness centrality are more influential in determining the basin stability of Random scale free network than closeness centrality. As number of nodes perturbed increases, the multi-node basin stability falls significantly for RSF networks with $m = 1$, while RSF networks with $m = 2$ remains robust up to a critical fraction f_{crit} of perturbed nodes, with $f_{crit} \sim 0.2$. One can rationalize this, by noting the difference in the typical values of betweenness centrality at

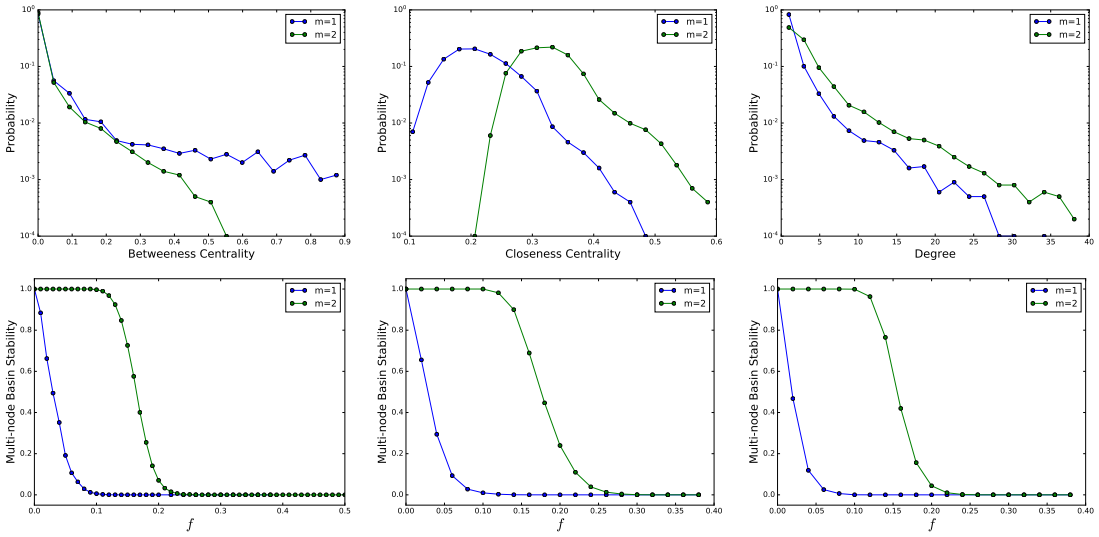

(a) (b) (c)

Figure 4.14: Top panel: Probability distribution of the (a) betweenness centrality, (b) closeness centrality and (c) degree of the nodes in a Random Scale-Free network of size $N = 100$, with $m = 1$ (blue) and $m = 2$ (green). Bottom panel: Multi-node basin Stability vs fraction f of nodes perturbed, for Random Scale-Free network of size $N = 100$, coupling strength $C = 1$, with $m = 1$ and $m = 2$, where the perturbed nodes are chosen in descending order of (a) betweenness centrality, (b) closeness centrality and (c) degree (i.e. the perturbed nodes are the ones with the highest b, c or k centrality measures).

the highest end in the RSF network with $m = 1$ and $m = 2$. For instance, if one considers 10% of nodes with the highest betweenness centrality in these networks of size $N = 100$, typically b lies between 0.1 to 0.9 for $m = 1$ and between 0.01 and 0.5 for $m = 2$. So the marked difference in the sensitivity of the global stability to perturbations in Random Scale-Free networks with $m = 1$ and $m = 2$ stems from the higher betweenness centrality of the nodes in the former network.

Now when nodes of the highest closeness centrality and degree are perturbed we observe the same trend as above. This occurs inspite of the tail of the distribution of closeness centrality and degree extending to higher values for RSF networks with $m = 2$ as compared to RSF networks with $m = 1$, implying that the nodes with highest degree and closeness centrality for the $m = 2$ case will have a larger value of k and c, as compared to the $m = 1$ case. So one may have expected that the RSF network with $m = 2$ would be less stable than the RSF network with $m = 1$. However, the observations are contrary to this expectation and this surprising result stems from the following: the set of nodes with the highest betweenness centrality, closeness centrality and degree, overlap to a very large extent. So for instance, for $f = 0.1$ in a network of size $N = 100$, the set of 10

nodes with the highest betweenness centralities, is practically the same as the set of nodes with the highest closeness centralities and highest degrees. However, in the RSF network with $m = 1$ these nodes have higher betweenness centrality, while having lower closeness centrality and degree, than the corresponding set in the RSF network with $m = 2$. Now higher betweenness centrality should inhibit stability, while lower closeness and degree should aid the stability of the collective state. So the comparative influence of these two opposing trends will determine the comparative global stability of these two classes of networks. If the betweenness centrality of the perturbed nodes is more crucial for stability, the multi-node Basin Stability of the network with $m = 1$ will go to zero faster than the network with $m = 2$. On the other hand if closeness centrality (and/or degree) of the perturbed nodes dictates global stability rather than betweenness centrality, the network with $m = 2$ will lose global stability faster than the one with $m = 1$. Now, since we find that network with $m = 1$ always loses stability faster than the network with $m = 2$, we can conclude that the *effect of betweenness centrality on the global stability is more dominant than the effect of the closeness centrality and degree of the perturbed nodes.*

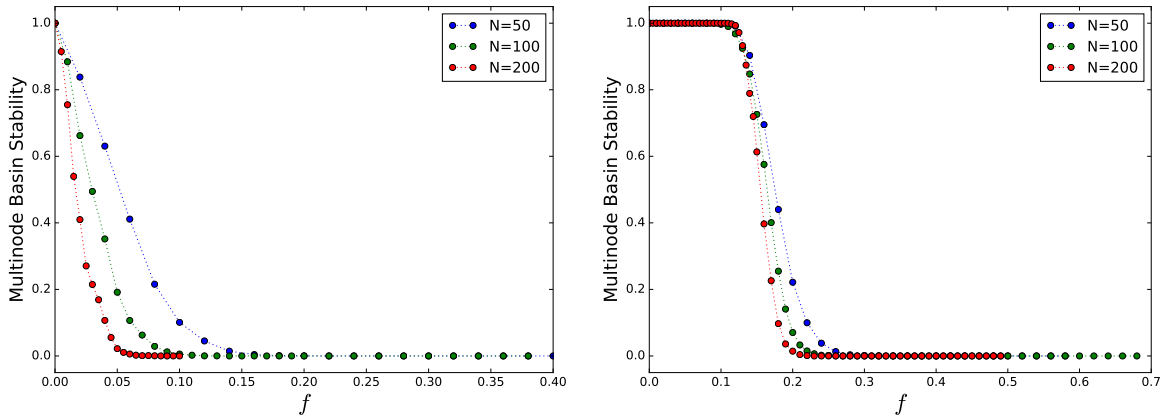

Figure 4.15: Multi-node basin Stability vs fraction f of nodes perturbed, for Random Scale-Free network of size $N = 50$ (blue), 100 (green), 200 (red) for $m = 2$ and $m = 1$.

Lastly, we study the effect of system size on multi-node basin stability, perturbing nodes in decreasing order of betweenness centrality. Figs. 4.15a-b shows the results for networks sizes ranging from 50 to 200. We have found an appropriate finite-size scaling that allows data collapse (cf. Fig. 4.16), and this indicates the value f_{crit} in the limit of large network size. We observe that a Random Scale-Free network with $m = 1$ yields $f_{crit} \to 0$ (i.e. the smallest fraction of perturbed nodes destroy the collective state), while $f_{crit} \sim 0.13$ for the case of $m = 2$(also see fig. 4.17). So a RSF network with $m = 2$ is more robust to localized perturbations than a RSF network with $m = 1$, as in the $m = 2$

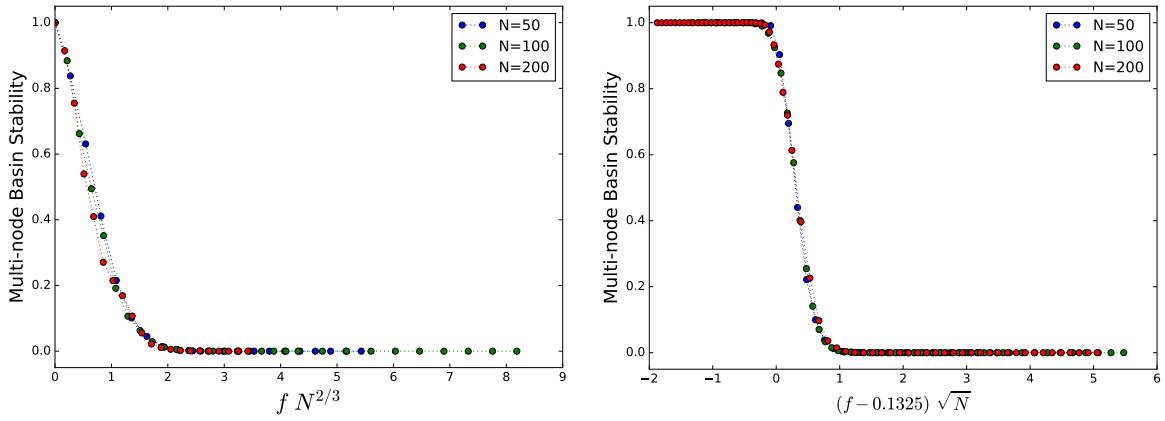

(a) (b)

Figure 4.16: Scaling resulting in data collapse, for the case of $m = 1$(a) and $m = 2$(b). The nodes perturbed are the ones with highest value of betweenness centrality.

case, even when nearly 13% of the nodes of the highest betweenness centrality are perturbed the entire network still manages to return to the original state. This compelling difference again arises due to the fact that the highest betweenness centrality found in the RSF network with $m = 1$ is significantly higher on an average than that in RSF networks of the same size with $m = 2$. This again corroborates the results in Fig. 4.14, and highlights the profound influence of betweenness centrality on global stability.

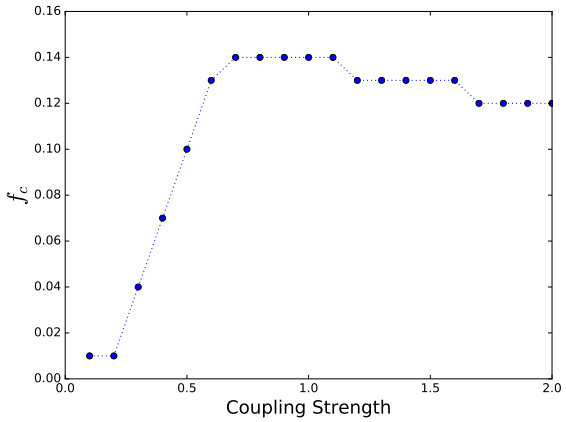

Figure 4.17: f_{crit} vs coupling for random scale free network with size N=100 and m=2. Here the nodes with highest betweenness centrality were perturbed. The threshold value of basin stability here is taken to be 90% probability.

4.6 Robustness of the phenomena:

In order to ascertain the generality of our observations, we have considered different nonlinear functions $F(x)$ in Eq.(1). For example, we explored a system of considerable biological interest, namely, a system of coupled synthetic gene networks. We used the quantitative model, developed in [18, 19, 20], describing the regulation of the operator region of λ phase, whose promoter region consists of three operator sites. The chemical reactions describing this network, given by suitable re-scaling yields [18, 19, 20]

$$F_{gene}(x) = \frac{m(1 + x^2 + \alpha\sigma_1 x^4)}{1 + x^2 + \sigma_1 x^4 + \sigma_1\sigma_2 x^6} - \gamma_x x \tag{4.4}$$

where x is the concentration of the repressor. The non linearity in this $F_{gene}(x)$ leads to a double well potential, and different γ introduces varying degrees of asymmetry in the potential. We studied a system of coupled genetic oscillators given by: $\dot{x_i} = F_{gene}(x_i) + C(\langle x_i^{nbhd}\rangle - x_i)$, where C is the coupling strength and $\langle x_i^{nbhd}\rangle$ is the local mean field generated by the set of neighbours of site i. Fig 4.18-4.21 shows some of the representative results.

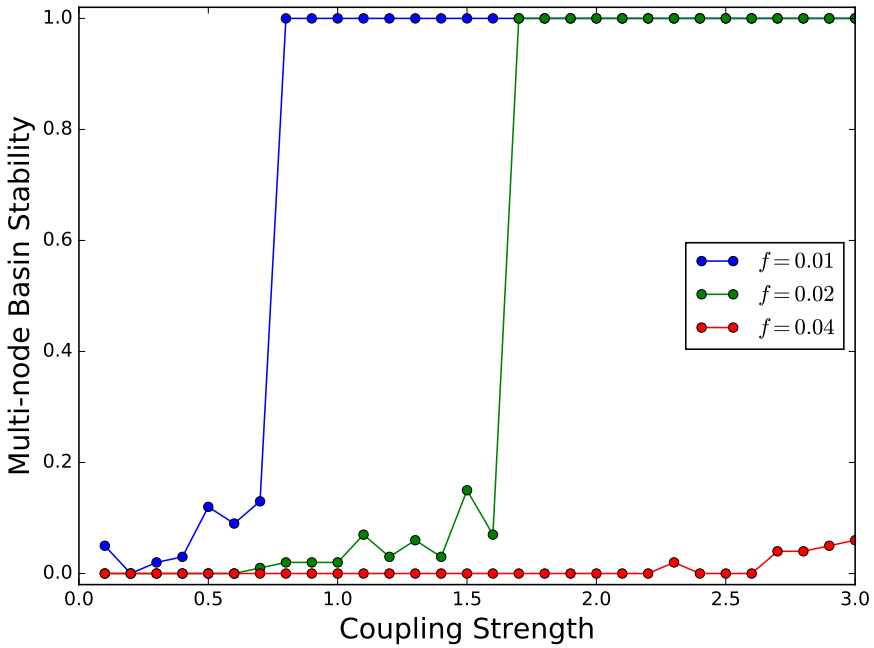

Figure 4.18: Dependence of Multi-Node Basin Stability on coupling strength, for a ring of bistable elements given by Eqn. 4.4, with the number of perturbed nodes(nodes perturbed in clusters). Here the size of the ring is $N = 100$, and size of the coupling neighbourhood is $k = 2$, namely each site couples to its two nearest neighbours.

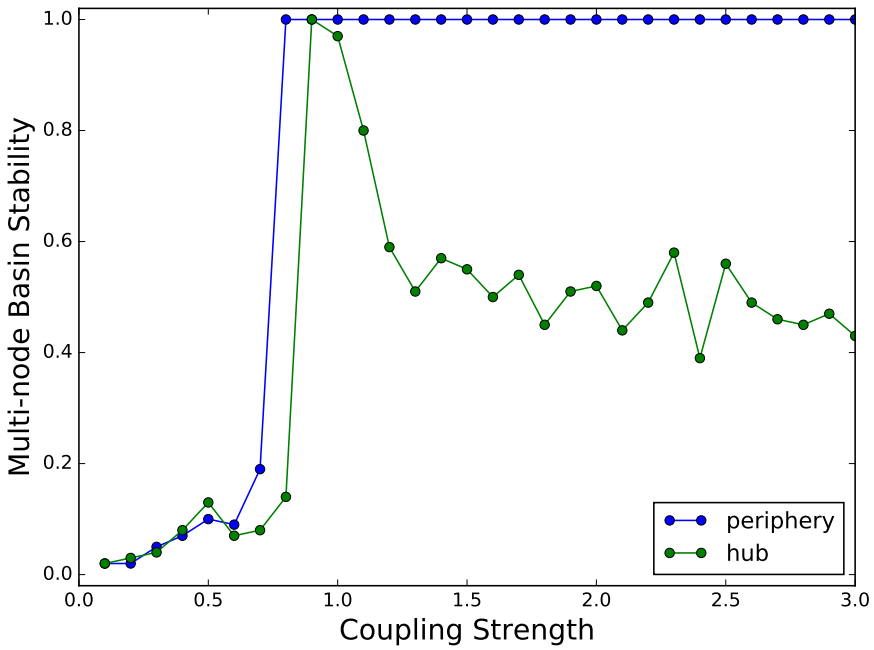

Figure 4.19: Dependence of Multi-Node Basin Stability on coupling strength, for a ring of bistable elements given by Eqn. 4.4, with the number of perturbed nodes(nodes perturbed in clusters). Here the size of the ring is $N = 100$, and size of the coupling neighbourhood is $k = 2$, namely each site couples to its two nearest neighbours.

Further we studied different networks of a piece-wise linear bi-stable system, that can be realised efficiently in electronic circuits [39], given by:

$$F(x) = \begin{cases} \beta x_l^* - \alpha x & \text{if } x < x_l^* \\ (\beta - \alpha)x & \text{if } x_l^* \leq x \leq x_u^* \\ \beta x_u^* - \alpha x & \text{if } x > x_u^* \end{cases} \tag{4.5}$$

where x_u^* and x_l^* are the upper and lower thresholds respectively

We simulated the coupled dynamics of these two bi-stable systems for different network topologies as well. We find that the qualitative trends in both these bi-stable systems is similar to that described above, indicating the generality of the central results presented here. Fig 4.22-4.25 shows some of the representative results.

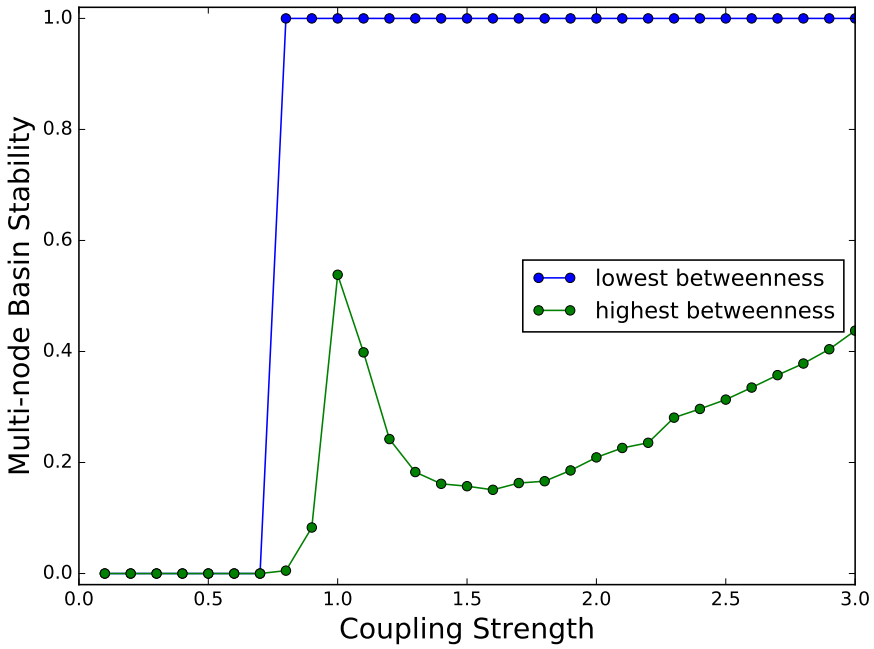

Figure 4.20: Dependence of Multi-Node Basin Stability on coupling strength, for a ring of bistable elements given by Eqn. 4.4, with the number of perturbed nodes(nodes perturbed in clusters). Here the size of the ring is $N = 100$, and size of the coupling neighbourhood is $k = 2$, namely each site couples to its two nearest neighbours.

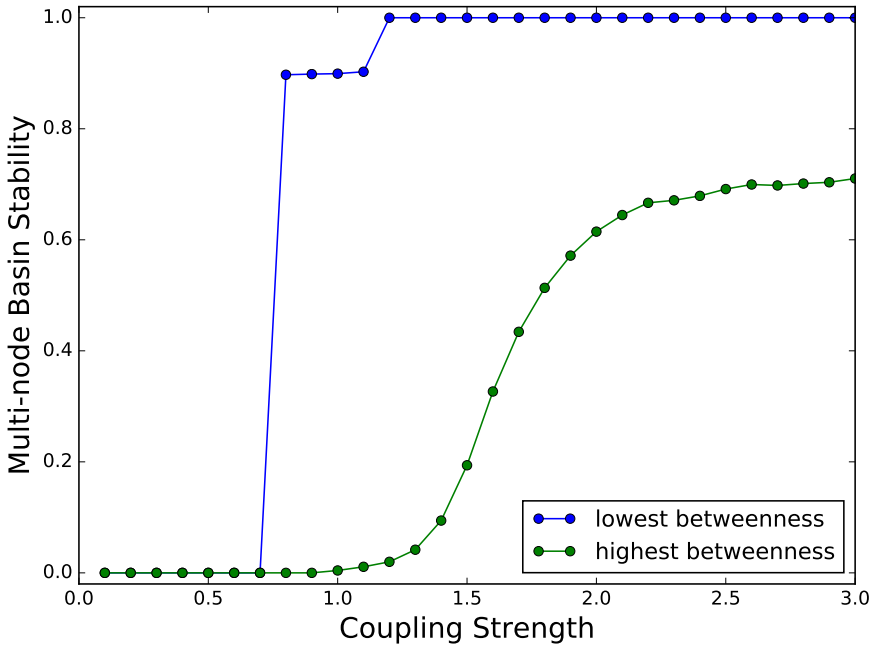

Figure 4.21: Dependence of Multi-Node Basin Stability on coupling strength, for a ring of bistable elements given by Eqn. 4.4, with the number of perturbed nodes(nodes perturbed in clusters). Here the size of the ring is $N = 100$, and size of the coupling neighbourhood is $k = 2$, namely each site couples to its two nearest neighbours.

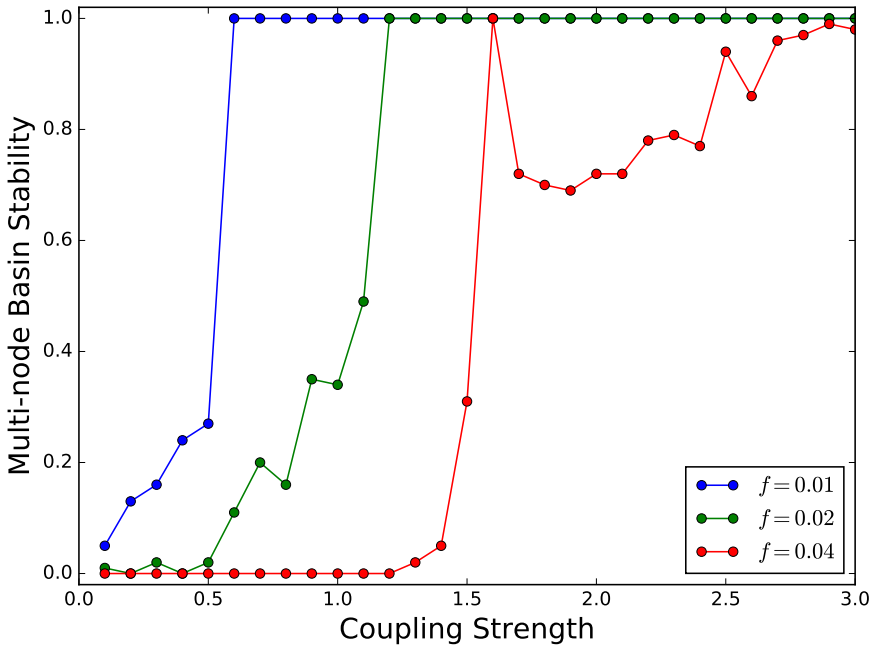

Figure 4.22: Dependence of Multi-Node Basin Stability on coupling strength, for a ring of bistable elements given by Eqn. 4.5, with the number of perturbed nodes(nodes perturbed in clusters). Here the size of the ring is $N = 100$, and size of the coupling neighbourhood is $k = 2$, namely each site couples to its two nearest neighbours.

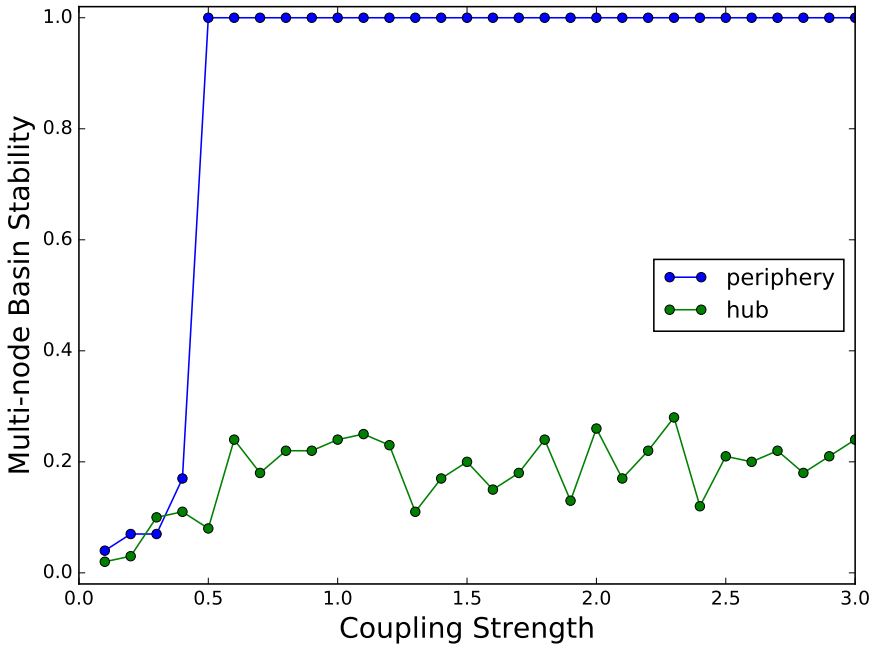

Figure 4.23: Dependence of Multi-Node Basin Stability on coupling strength, for a ring of bistable elements given by Eqn. 4.5, with the number of perturbed nodes(nodes perturbed in clusters). Here the size of the ring is $N = 100$, and size of the coupling neighbourhood is $k = 2$, namely each site couples to its two nearest neighbours.

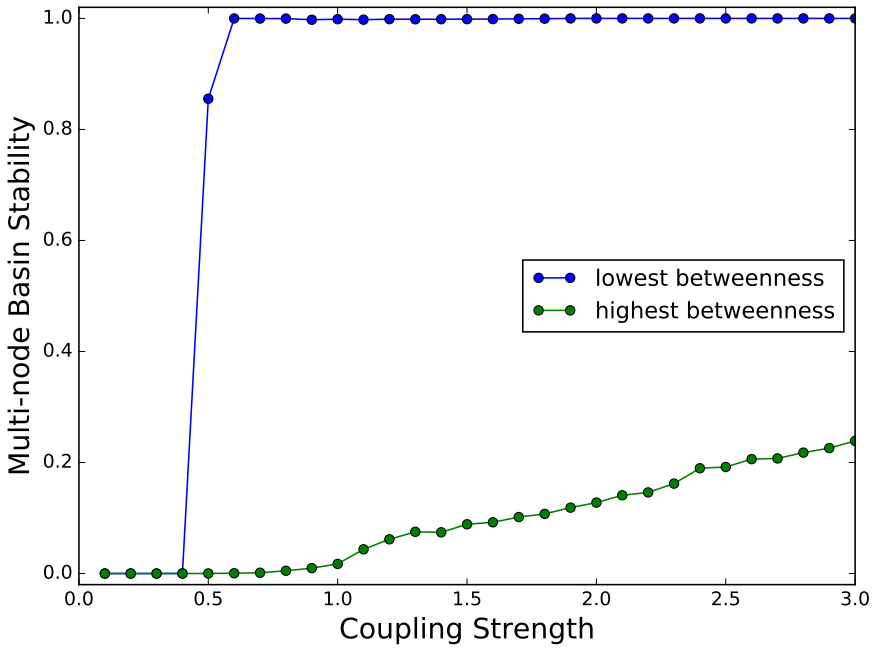

Figure 4.24: Dependence of Multi-Node Basin Stability on coupling strength, for a ring of bistable elements given by Eqn. 4.5, with the number of perturbed nodes(nodes perturbed in clusters). Here the size of the ring is $N = 100$, and size of the coupling neighbourhood is $k = 2$, namely each site couples to its two nearest neighbours.

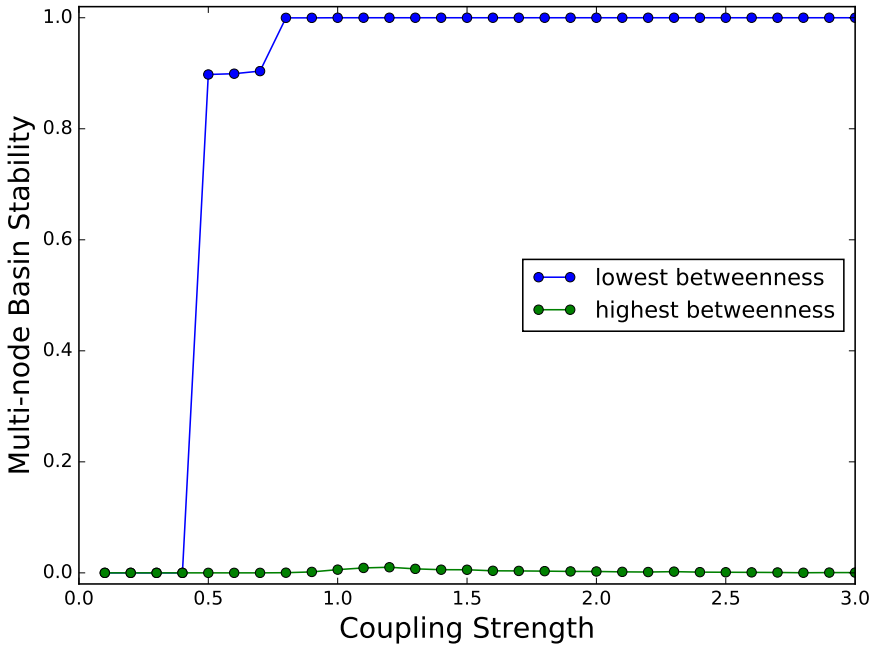

Figure 4.25: Dependence of Multi-Node Basin Stability on coupling strength, for a ring of bistable elements given by Eqn. 4.5, with the number of perturbed nodes(nodes perturbed in clusters). Here the size of the ring is $N = 100$, and size of the coupling neighbourhood is $k = 2$, namely each site couples to its two nearest neighbours.

4.7 Conclusions

In conclusion, we have introduced a variant of multi-node basin stability to obtain a measure reflecting the response of the network to localized perturbations. This provides a quantity that can clearly indicate which nodes have the greatest influence on the robustness of the dynamical state of the network, and allowed us to find which particular characteristic of the perturbed nodes significantly affects the capacity of the system to return to its original state.

We have investigated the collective dynamics of bi-stable elements connected in different network topologies, ranging from rings and small-world networks, to scale-free networks and stars. Our focus was a question of utmost relevance: identification of the properties of the nodes of a network that crucially impact collective dynamics. This approach enables us to address the important reverse question: perturbation of what class of nodes in the network have the most significant effect on the resilience of the network? Understanding this potentially allows us to determine which nodes render the network most susceptible to external influences. Alternately, it suggests which nodes to protect more stringently from perturbations in order to protect the dynamical robustness of the entire network.

Specifically, we estimated the dynamical robustness of such networks by introducing a variant of the concept of multi-node basin stability which allowed us to gauge the global stability of the dynamics of the network in response to local perturbations affecting particular nodes of a system. We show that perturbing nodes with high closeness and betweenness-centrality significantly reduces the capacity of the system to return to the desired stable state. This effect is very pronounced for a star network which has one hub node with significantly different closeness/betweenness-centrality than the peripheral nodes. Considering such a network with all nodes in one well, if one perturbs the hub to another well, this *single* perturbed node drags the entire system to its well, thereby preventing the network from recovering its dynamical state. In contrast, even when *all* peripheral nodes are kicked to the other well, the hub manages to restore the entire system back to the original well. Lastly we explore explore Random Scale-Free Networks of bi-stable dynamical elements. Since the distribution of betweenness centralities, closeness centralities and degrees of the nodes is significantly different for Random Scale-Free Networks with $m = 1$ and $m = 2$, these networks have the potential to provide a test-bed for determining which of these centrality properties most influences the robustness of the collective dynamics. The comparison between the global stability of these two classes of

networks provides clear indications that the *betweenness centrality of the perturbed node is more crucial for dynamical robustness, than closeness centrality or degree of the node.* This result is important in deciding which nodes to safeguard in order to maintain the collective state of this network against targeted localized attacks.

Chapter 5

Conclusion

The work in this thesis focussed on synchronization in networks of bistable elements, with the coupling ranging over different scales and connection topologies. Currently, there is no well established mathematical framework which addresses the broad question of the stability of the synchronized state in its entirety. The only available solutions are linear stability approaches which fail to capture the global picture (as discussed in chapter3). Thus we attempted to estimate the global stability of the collective synchronized state through concepts such as Basin Stability and drew conclusions from our numerics which are statistically very relevant. As indicated by probability theory, our results might fail in a particular realization of a network, but the analysis holds on an average and offers indications of the typical outcome that may be expected in classes of networks.

At the nodal level, the networks considered here have bistable systems, with coexisting fixed point attractors. Such systems are commonly found in a variety of fields, ranging from relaxation oscillators and multi-vibrators, to light switches and Schmitt triggers. An important application of bistable elements is in digital electronics, where data stored is binary. Our focus is on the spatiotemporal properties of networks of such bistable systems. These networks exhibit very interesting phenomena, that range from hypersensitivity to heterogeneity (cf. Chapter 2), to robustness under generic large perturbations or large targetted perturbations (cf. Chapter 4 and 3 respectively).

In the first part, we explored the role of heterogeneity in the emergent spatio-temporal patterns in small-world networks of bistable elements. We demonstrated that under certain conditions *all* the elements in the system evolved to the stable state of the *minority* population, i.e. the entire system was driven to the natural state of the set with a much smaller number of elements. Further it was observed that for suitable parameters this

system could be made *ultra-sensitive* to heterogeneity in the system. It was found that in certain systems, even a *single* element with a different local parameter, could lead the entire system to its attracting state. Thus, in these conditions the collective field of the system is any extremely sensitive detector of non-homogeneity in the system.

In the second part, we considered the collective dynamics of a group of bi-stable elements connected in different network topologies, ranging from regular rings and small-world networks on one hand, to deterministic scale-free and random scale-free networks on the other. The basic question we addressed was the following: are there features of the underlying connection network that provide *consistent markers* for the emergence of *complete synchronization* and the robustness of the synchronized state? We focussed on the correlation between network properties and global synchronization features. Our central result was that, while networks properties can provide indicators of synchronization within a network class, they failed to provide consistent indicators across network classes. This suggests that local properties determined by the connection network does not provide a complete picture of global measures of synchronization. Our observations then have potential applications. For instance, if one needs to achieve synchronization in a network of bi-stable elements, such as electronic circuits, constrained by certain connection properties, our analysis can guide the choice of preferred topology [33]. More importantly, in the context of the general understanding of dynamical networks, our observations suggest important caveats to correlating network features to global dynamical phenomena.

In the third part, we attempted to identify the nodal property that most significantly influences the global stability of the network. We again explored bi-stable elements, connected in different network topologies, ranging from regular rings to random scale-free and star networks. We focussed now on the response of this network to localized perturbations on a sub-set of nodes. The central question we investigated here was the following: *what characteristics of the nodes (if any) significantly affect the global stability?*. We considered three properties of the nodes: degree, betweenness centrality and closeness centrality and studied the propagation of perturbations emanating from these nodes.

We showed that perturbing nodes with high closeness and betweenness-centrality significantly reduces the capacity of the system to return to the desired stable state. This effect is very pronounced for a star network which has one hub node with significantly different closeness/betweenness-centrality than the peripheral nodes. The comparison between the global stability of these two classes of networks, namely Random Scale-Free Networks with $m = 1$ and $m = 2$,, provides clear indications that the *betweenness*

centrality of the perturbed node is more crucial for dynamical robustness, than closeness centrality or degree of the node. This result is important in deciding which nodes to safeguard in order to maintain the collective state of this network against targeted localized attacks.

Studying these broad classes of networks has the advantage that many naturally occurring or human-engineered networks in the real world are very likely to lie in one of these classes. On the other hand there are special classes of networks which have not been considered in this thesis. These can then form the basis of future work.

Further, this thesis has considered bistable systems. The generality of the results here need to be verified in the context of multi-stable systems, with more than two co-existing attractors. Exploring this aspect, by studying networks of different multi-stable systems at the nodal level, can offer yet another avenue of promising new research.

Lastly, an important direction for future investigations involves the study of networks of systems exhibiting multi-stable chaotic dynamics, namely systems that have co-existing chaotic attractors. Our results here will then form the basis for what to expect in those networks. It would be exciting to see what broad similarities or significant differences emerge when we enter the realm of chaos. In summary, the results in this thesis shed light on the collective behaviour of networks of coupled bistable systems in particular, and has potential relevance for networks of multi-stable dynamical elements in general.

Bibliography

[1] Kunihiko Kaneko. Overview of coupled map lattices. *Chaos: An Interdisciplinary Journal of Nonlinear Science*, 2(3):279–282, 1992.

[2] Claudio J Tessone, Claudio R Mirasso, Raúl Toral, and James D Gunton. Diversity-induced resonance. *Physical review letters*, 97(19):194101, 2006.

[3] Jierui Xie, Sameet Sreenivasan, Gyorgy Korniss, Weituo Zhang, Chjan Lim, and Boleslaw K Szymanski. Social consensus through the influence of committed minorities. *Physical Review E*, 84(1):011130, 2011.

[4] Kamal P Singh, Rajeev Kapri, and Sudeshna Sinha. Scalable ultra-sensitive detection of heterogeneity via coupled bistable dynamics. *EPL (Europhysics Letters)*, 98(6):60004, 2012.

[5] V Kohar, A Choudhary, Kamal P Singh, and S Sinha. Verification of scalable ultra-sensitive detection of heterogeneity in an electronic circuit. *The European Physical Journal Special Topics*, 222(3-4):721–728, 2013.

[6] Duncan J Watts and Steven H Strogatz. Collective dynamics of small-worldnetworks. *nature*, 393(6684):440–442, 1998.

[7] Sudeshna Sinha. Random coupling of chaotic maps leads to spatiotemporal synchronization. *Physical Review E*, 66(1):016209, 2002.

[8] Arghya Mondal, Sudeshna Sinha, and Juergen Kurths. Rapidly switched random links enhance spatiotemporal regularity. *Physical Review E*, 78(6):066209, 2008.

[9] Anshul Choudhary, Vivek Kohar, and Sudeshna Sinha. Preventing catastrophes in spatially extended systems through dynamic switching of random interactions. *Pramana*, 84(2):217–228, 2015.

[10] A Choudhary, V Kohar, and S Sinha. Taming explosive growth through dynamic random links. *Scientific reports*, 4:4308–4308, 2013.

[11] Igor V Belykh, Vladimir N Belykh, and Martin Hasler. Blinking model and synchronization in small-world networks with a time-varying coupling. *Physica D: Nonlinear Phenomena*, 195(1):188–206, 2004.

[12] RE Amritkar and Chin-Kun Hu. Synchronized state of coupled dynamics on time-varying networks. *Chaos: An Interdisciplinary Journal of Nonlinear Science*, 16(1):015117, 2006.

[13] Vivek Kohar and Sudeshna Sinha. Emergence of epidemics in rapidly varying networks. *Chaos, Solitons & Fractals*, 54:127–134, 2013.

[14] Maurizio Porfiri. Stochastic synchronization in blinking networks of chaotic maps. *Physical Review E*, 85(5):056114, 2012.

[15] A Pikovsky, M Rosenblum, and J Kurths. Synchronization cambridge university press. *Cambridge, England*, 2001.

[16] Alex Arenas, Albert Díaz-Guilera, Jurgen Kurths, Yamir Moreno, and Changsong Zhou. Synchronization in complex networks. *Physics reports*, 469(3):93–153, 2008.

[17] Vivek Kohar, Peng Ji, Anshul Choudhary, Sudeshna Sinha, and Jüergen Kurths. Synchronization in time-varying networks. *Physical Review E*, 90(2):022812, 2014.

[18] Jeff Hasty, Farren Isaacs, Milos Dolnik, David McMillen, and James J Collins. Designer gene networks: Towards fundamental cellular control. *Chaos: An Interdisciplinary Journal of Nonlinear Science*, 11(1):207–220, 2001.

[19] Hiroyasu Ando, Sudeshna Sinha, Remo Storni, and Kazuyuki Aihara. Synthetic gene networks as potential flexible parallel logic gates. *EPL (Europhysics Letters)*, 93(5):50001, 2011.

[20] Edward H Hellen, Syamal K Dana, Jürgen Kurths, Elizabeth Kehler, and Sudeshna Sinha. Noise-aided logic in an electronic analog of synthetic genetic networks. *Plos one*, 8(10):e76032, 2013.

[21] Marten Scheffer. Complex systems: foreseeing tipping points. *Nature*, 467(7314):411–412, 2010.

[22] I Mahboob, E Flurin, K Nishiguchi, A Fujiwara, and H Yamaguchi. Interconnect-free parallel logic circuits in a single mechanical resonator. *Nature communications*, 2:198, 2011.

[23] Seung-Bo Shim, Matthias Imboden, and Pritiraj Mohanty. Synchronized oscillation in coupled nanomechanical oscillators. *Science*, 316(5821):95–99, 2007.

[24] Micha Nixon, Moti Friedman, Eitan Ronen, Asher A Friesem, Nir Davidson, and Ido Kanter. Synchronized cluster formation in coupled laser networks. *Physical review letters*, 106(22):223901, 2011.

[25] Grigory V Osipov, Jürgen Kurths, and Changsong Zhou. *Synchronization in oscillatory networks*. Springer Science & Business Media, 2007.

[26] Arthur T Winfree. Biological rhythms and the behavior of populations of coupled oscillators. *Journal of theoretical biology*, 16(1):15–42, 1967.

[27] Takashi Nishikawa and Adilson E Motter. Network synchronization landscape reveals compensatory structures, quantization, and the positive effect of negative interactions. *Proceedings of the National Academy of Sciences*, 107(23):10342–10347, 2010.

[28] Fatihcan M Atay, Tuerker Biyikoglu, and Jürgen Jost. Synchronization of networks with prescribed degree distributions. *IEEE Transactions on Circuits and Systems I: Regular Papers*, 53(1):92–98, 2006.

[29] Zhisheng Duan, Guanrong Chen, and Lin Huang. Complex network synchronizability: Analysis and control. *Physical Review E*, 76(5):056103, 2007.

[30] Takashi Nishikawa, Adilson E Motter, Ying-Cheng Lai, and Frank C Hoppensteadt. Heterogeneity in oscillator networks: Are smaller worlds easier to synchronize? *Physical review letters*, 91(1):014101, 2003.

[31] H Hong, Beom Jun Kim, MY Choi, and Hyunggyu Park. Factors that predict better synchronizability on complex networks. *Physical Review E*, 69(6):067105, 2004.

[32] Chai Wah Wu. Synchronizability of networks of chaotic systems coupled via a graph with a prescribed degree sequence. *Physics Letters A*, 346(4):281–287, 2005.

[33] AN Pisarchik, R Jaimes-Reátegui, JR Villalobos-Salazar, JH Garcia-Lopez, and S Boccaletti. Synchronization of chaotic systems with coexisting attractors. *Physical review letters*, 96(24):244102, 2006.

[34] Peter J Menck, Jobst Heitzig, Norbert Marwan, and Jürgen Kurths. How basin stability complements the linear-stability paradigm. *Nature Physics*, 9(2):89, 2013.

[35] Chiranjit Mitra, Anshul Choudhary, Sudeshna Sinha, Jürgen Kurths, and Reik V. Donner. Multiple-node basin stability in complex dynamical networks. *Phys. Rev. E*, 95:032317, Mar 2017.

[36] Albert-László Barabási and Réka Albert. Emergence of scaling in random networks. *science*, 286(5439):509–512, 1999.

[37] Albert-László Barabási, Erzsebet Ravasz, and Tamas Vicsek. Deterministic scale-free networks. *Physica A: Statistical Mechanics and its Applications*, 299(3):559–564, 2001.

[38] Louis M Pecora and Thomas L Carroll. Master stability functions for synchronized coupled systems. *Physical review letters*, 80(10):2109, 1998.

[39] K Murali, Sudeshna Sinha, William L Ditto, and Adi R Bulsara. Reliable logic circuit elements that exploit nonlinearity in the presence of a noise floor. *Physical review letters*, 102(10):104101, 2009.

[40] Heetae Kim, Sang Hoon Lee, and Petter Holme. Community consistency determines the stability transition window of power-grid nodes. *New Journal of Physics*, 17(11):113005, 2015.

[41] Chiranjit Mitra, Jürgen Kurths, and Reik V Donner. Rewiring hierarchical scale-free networks: Influence on synchronizability and topology. *EPL (Europhysics Letters)*, 119(3):30002, 2017.

[42] Peter J Menck, Jobst Heitzig, Jürgen Kurths, and Hans Joachim Schellnhuber. How dead ends undermine power grid stability. *Nature communications*, 5:3969, 2014.

[43] Chiranjit Mitra, Tim Kittel, Anshul Choudhary, Jürgen Kurths, and Reik V Donner. Recovery time after localized perturbations in complex dynamical networks. *New Journal of Physics*, 19(10):103004, 2017.

[44] Luca Donetti, Pablo I. Hurtado, and Miguel A. Muñoz. Entangled networks, synchronization, and optimal network topology. *Phys. Rev. Lett.*, 95:188701, Oct 2005.

[45] Pranay Deep Rungta, Anshul Choudhary, Chandrakala Meena, and Sudeshna Sinha. Are network properties consistent indicators of synchronization? *EPL (Europhysics Letters)*, 117(2):20003, 2017.